Doctoral School of Geosciences

SCALE FORMATION AND TREATMENT PLAN IN INDONESIAN GEOTHERMAL WELLS

Ph.D. Dissertation

Author

AKHMAD SOFYAN

Supervisor

Dr. János Szanyi

University of Szeged (SZTE), Faculty of Science and Informatics, Department of Geology

Co-Supervisor

Dr. Gábor Bozsó

University of Szeged (SZTE), Faculty of Science and Informatics, Department of Geology

University of Szeged (SZTE),

Faculty of Science and Informatics

Department of Geology

2025

SZEGED

DEDICATION

To my beloved wife, ***Drg. Rini Retnowati,***

Your love, strength, and faith in me have always been my greatest support. and someday we will be together again

(Akhmad, 2025)

DECLARATION OF THE SUPERVISOR

We, Dr. **János Szanyi**; the supervisor and Dr. **Gábor Bozsó,** the co-supervisor of **Akhmad Sofyan,** declare that the doctoral thesis entitled "*Scale Formation and Treatment Plan in Indonesian Geothermal Wells*", is based on the independent work of the candidate. He had a significant role in achieving the research results presented in the dissertation. The content of the dissertation is scientifically sound; thus, I fully support its submission for review and acceptance.

Szeged (Hungary), 18th July 2025

Dr. János Szanyi,
PhD Supervisor

Dr. Gábor Bozsó
PhD Co-Supervisor

Preface

The doctoral thesis results and main findings are primarily derived from the following publications. My thesis is mainly based on the first three listed published papers. Additionally, other research papers, and conference proceedings had been completed during my PhD study period and are listed as publications 1-10 and conferences 11-16.

List of Publications in Scopus and Web of Science Indexed Journals

1. **Sofyan, A.**, Wiharti, S., Szanyi, J., Suranta, B.Y., Njeru, R. (2023). Determination of Scaling Zone and Scaling Type in Slotted Liner Based on the Fluid Flow Pattern in the Geothermal Well "X". International Journal of Renewable Energy Research, 28 March 2023. https://doi.org/10.20508/ijrer.v13i1.13603.g8681
2. **Sofyan, A.**, Szanyi, J., Aka, H.S. (2023). Investigation of Zone and Type of Scaling Based on the Fluid Flow Pattern in the Geothermal Well "X" at the Salak Geothermal Field -- Indonesia. International Journal of Renewable Energy Research, 16 July 2023. https://doi.org/10.20508/ijrer.v14i1.14254.g8879
3. **Sofyan, A.**, Jaya, R., Susanto, H., Njeru, R.M., Bozsó, G., Szanyi, J. (2025). Scale Treatment Planning Using Broaching Method in a Vapor-Dominated Geothermal Well X at Kamojang Geothermal Field. Eng publisher, April 2025. https://doi.org/10.3390/eng6040067
4. **Sofyan, A.**, Bujang, Y.D.G., Suranta, B.Y. (2023). Heat Loss Effect Analysis by Using JIWAFlow Wellbore Simulation in Geothermal Field Well-Y. American Institute of Physics (AIP), 8 May 2023. http://dx.doi.org/10.1063/5.0120544
5. Suranta, B.Y., **Sofyan, A.**, Khoiriarta, F., Handaja, S. (2023). Selection of Drilling Bit for the 12 ¼" Holes in The Geothermal Wells at The Company of XYZ. International Journal of Renewable Energy Research, 11 September 2023. https://doi.org/10.20508/ijrer.v14i4.14417.g8946
6. Suranta, B.Y., **Sofyan, A.**, Wicaksono, B.A. (2023). Pore pressure prediction as the anticipation of abnormal pressure in well X and Y. American Institute of Physics (AIP), 8 May 2023. https://doi.org/10.1063/5.0120746
7. Rosiani, D., Walay, M.G., Rahalintar, P., Candra, A.D., **Sofyan, A.**, Haratua, Y.A. (2023). Application of Artificial Intelligence in Predicting Oil Production Based on Water Injection Rate. International Journal on Advanced Science, Engineering and Information Technology, November 2023. https://doi.org/10.18517/ijaseit.13.6.19399
8. Suranta, B.Y., et al., **Sofyan, A.** (2023). Best Practices to Achieve Optimal Geothermal Drilling Performance in A Cost-Effective Manner: Case Study of the Fastest Geothermal Well Drilling in Java and Sumatra. Scientific Contributions Oil and Gas, 26 December 2023. https://doi.org/10.29017/SCOG.46.3.1591

9. Njeru, R.M., **Sofyan, A.**, Halisch, M., Kóbor, B., Szanyi, J. (2024). Optimizing Micro-CT Resolution for Geothermal Reservoir Characterization in the Pannonian Basin. Energies. https://doi.org/10.3390/en17133081

10. Rosiani, D., Zulfan, Suranta, B.Y., **Sofyan, A.** (2025). Machine Learning Classifies Data for Early Warning of Stuck Pipe Detection in Geothermal Drilling. International Journal on Advanced Science, Engineering and Information Technology, January 2025. https://doi.org/10.18517/ijaseit.15.1.20333

List of Conferences

11. **Sofyan, A.**, Muqtadir A., Aka H.S. Bujang, Y.D.G., Suranta, B.Y. (2021). Heat Loss Effect Analysis by Using JIWAFlow Wellbore Simulation in Geothermal Field Well-Y. 3rd Borobudur International Symposium of Science and Technology, Indonesia.

12. **Sofyan, A.**, Wiharti, S. (2022). The Analysis of Horizontal Lip Pressure Production Test Method in Well X. European Geothermal PhD Day, Aachen, Germany.

13. **Sofyan, A.** (2022). The Effect of Casing Design on Well X Production in Geothermal Y Field Using JIWA Flow. 1st International Conference in Earth Sciences and Energy Transition, Muscat, Oman.

14. **Sofyan, A.**, Wiharti, S., Szanyi, J., Suranta, B.Y., Njeru, R. (2023). Scaling Type and Scaling Zone Determination in Slotted Liner Based on the Fluid Flow Pattern in Geothermal Well X. European Geothermal PhD Day, Glasgow, UK.

15. **Sofyan, A.**, Jaya, R.,. Njeru, R.M., Bozsó, G., Szanyi, J. (2024). Scaling Mitigation in Well X Using Broaching Method at the Vapour Dominated Geothermal Field. European Geothermal PhD Day, Delft, Netherlands.

16. **Sofyan, A.** (2025). Scale Formation and Treatment in Indonesian Geothermal Wells: A Multi-Field Comparative Analysis. European Geothermal PhD Day, Szeged, Hungary

Table of Contents

Abstract

This study examines scale formation mechanisms, detection methodologies, and treatment strategies in production wells across Patuha, Salak, and Kamojang geothermal fields in Indonesia. The comprehensive methodology integrated Hewitt-Robert flow pattern mapping, PTS survey analysis, geochemical sampling, PHREEQC thermodynamic modeling, and XRD mineral characterization to evaluate scaling phenomena. Results revealed that annular flow consistently correlates with scale precipitation at flashing zones, typically occurring at casing diameter transitions. This study identified distinct scale compositions characteristic to each field: calcite predominates in Patuha, amorphous silica in Salak, and quartz with magnetite in Kamojang. In Patuha and Salak, and predicted scale accumulation locations by analyzing PTS (Pressure-Temperature-Spinner) data to identify flashing zones at depths of 1458.27 m and 4600 ft respectively. Meanwhile, well integrity testing at Kamojang using Go-Devil operations and sample catchers precisely located scale accumulation at depths of 900.74 m. Economic evaluation demonstrated the broaching method cost-effectiveness for silica scaling in systems with deviation angles below 50°, requiring only $42,690 compared to conventional methods ($628,147-$1,195,339). This approach restored production from 28.71 to 31.50 tons/hour with a 3.3-month payback period at Kamojang, significantly outperforming alternative treatments requiring 4-10 years for cost recovery. This research challenges assumptions that vapor-dominated systems like Kamojang are less susceptible to scaling and establishes a methodological framework applicable across diverse geothermal fields with different reservoir characteristics. The findings provide evidence-based guidance for treatment selection based on scale characteristics, well geometry, and economic considerations across all three fields, demonstrating how strategic scale management extends well productivity while reducing operational costs, thus enhancing sustainable geothermal resource development in Indonesia's premier geothermal assets.

List of Figures

List of Tables

List Of Abbreviations and Acronyms

a.s.l.	Above Sea Level
Ar	Argon
ASTM	American Society for Testing and Materials
B	Boron
Ca	Calcium
$CaCO_3$	Calcium Carbonate
CF	Capacity Factor
CH_4	Methane
Cl	Chloride
CO_2	Carbon Dioxide
CO_3^{2-}	Carbonate Ion
CSI	Calcite Saturation Index
EGS	Enhanced Geothermal Systems
ESDM	Energi dan Sumber Daya Mineral (Ministry of Energy and Mineral Resources of Indonesia)
F	Fluoride
GFF	Geothermal Fund Facility
GPP	Geothermal Power Plant
GWh	Gigawatt-hour
H_2	Hydrogen
H_2S	Hydrogen Sulfide
HCO_3^-	Bicarbonate Ion
ICP-OES	Inductively Coupled Plasma Optical Emission Spectroscopy
IGA	International Geothermal Association
IRENA	International Renewable Energy Agency
JIWAFlow	Java Integrated Well Analysis Flow
K	Potassium
kph	Kilopound per hour
Ksp	Solubility Product Constant
Li	Lithium
MD	Measured Depth
Mg	Magnesium
MW	Megawatt
MWe	Megawatt electric
Na	Sodium
N_2	Nitrogen
NCG	Non-Condensable Gases
NH_3	Ammonia
OES	Optical Emission Spectrometry
ORC	Organic Rankine Cycle
pH	Power of Hydrogen
PHREEQC	Program for PH-REE-dox-Equilibrium Calculations

ppm	Parts Per Million
PGE	Pertamina Geothermal Energy
POOH	Pull-Out-Of-Hole
PPF	Pounds Per Foot
PTS	Pressure, Temperature, and Spinner (survey)
QPA	Quantitative Phase Analysis
RIH	Run-In-Hole
SI	Saturation Index
SiO_2	Silicon Dioxide (Silica)
SO_4	Sulfate
SSI	Silica Saturation Index
SZTE	Szegedi Tudományegyetem (University of Szeged, Hungary)
TDS	Total Dissolved Solids
TFS	Total Flow Steam
TVD	True Vertical Depth
USD	United States Dollar
WHP	Wellhead Pressure
XRD	X-Ray Diffraction

Research Aims and Objectives

This dissertation aims to develop a comprehensive, systematic framework for the management of scaling in geothermal production wells across different geothermal systems. By building upon three foundational studies conducted in Indonesia's Patuha, Salak, and Kamojang geothermal fields, this research seeks to enhance operational efficiency, extend well longevity, and improve the economic viability of geothermal energy production through effective scale identification, characterization, and treatment. The significance of this work is magnified by Indonesia's position as home to approximately 40% of the world's geothermal (S. W. Yudha et al., 2022), of which only 4.5% has been utilized, largely due to operational challenges such as mineral scaling.

This research has five primary objectives. Firstly, this research aims to establish predictive models for scale formation based on fluid flow patterns, These models can be used to identify how different flow regimes influence the type, location, and severity of scaling in both vapor-dominated and liquid-dominated geothermal systems. These models were developed based directly on findings from the Patuha field study, which revealed correlations between annular flow patterns and calcite scaling in slotted liners.

Secondly, this research aims to develop an integrated methodological approach for the accurate identification of scaling zones by combining multiple diagnostic techniques, including PTS surveys, well integrity testing, and geochemical analysis. The Salak field study demonstrated the efficacy of combining PTS data with flow pattern analysis to locate scaling accumulation zones. This dissertation seeks to develop these detection methods, enabling operators to pinpoint incipient scaling with greater precision and reliability across different well configurations.

Thirdly, this research aims to develop an integrated method for scale characterization incorporating field sampling, laboratory analysis, and geochemical modeling to determine scale composition and formation mechanisms across different geothermal environments. Based on the successful application of XRD analysis in the Kamojang study to identify specific scale components in vapor-dominated systems, this research aims to establish robust characterization protocols that can differentiate between scale types and their formation conditions, essential knowledge for the effective treatment selection of treatment method.

Fourthly, this research aims to formulate a decision-making framework for selecting optimal scale treatment methods based on well conditions, scale characteristics, and economic considerations, Particular emphasis is placed on on cost-effectiveness and production recovery. The Kamojang field study provided compelling evidence for the improvement of economic performance of the broaching method compared to conventional treatments.

Fifthly, this research aims to design a scale management system that integrates identification, characterization, treatment selection, implementation, and monitoring processes adaptable to diverse geothermal field conditions. This combined approach brings together methods and findings of all three key studies to build a single management system that can be used in different types of geothermal field.

These objectives address significant knowledge gaps in understanding scaling phenomena, particularly in vapor-dominated fields. They, aim to provide practical solutions for geothermal operators facing scaling challenges, ultimately contributing to more sustainable utilization of geothermal resources globally. By achieving of these aims, this dissertation will advance both theoretical understanding and the practical management strategies for addressing one of the most significant operational challenges in geothermal energy production. This could unlock a greater portion of Indonesia's vast geothermal potential and contribute to global renewable energy goals.

CHAPTER I

1. Introduction

1.1. Global Geothermal Power Development: Current Status and Technological Distribution

The global geothermal power landscape has demonstrated consistent and substantial growth over recent decades, as comprehensively documented by Gutiérrez-Negrín (2024). Figure 1 provides a compelling visual representation of geothermal power's development trajectory from 1980 to 2023, tracking both installed capacity expansion and generation growth during this 43-year period. Figure 1 illustrates how installed capacity has grown from 2,110 MW in 1980 to 16,318 MW in 2023—a nearly eightfold increase—while annual electricity generation has risen from approximately 13,100 GWh to 96,552 GWh over the same timeframe. The parallel growth curves seen in Figure 1 demonstrate how the addition of capacity has resulted in a proportional increase in generation, with only minor fluctuations in the overall capacity factor over four decades of development (Gutiérrez-Negrín, 2024; Huttrer, 2020).

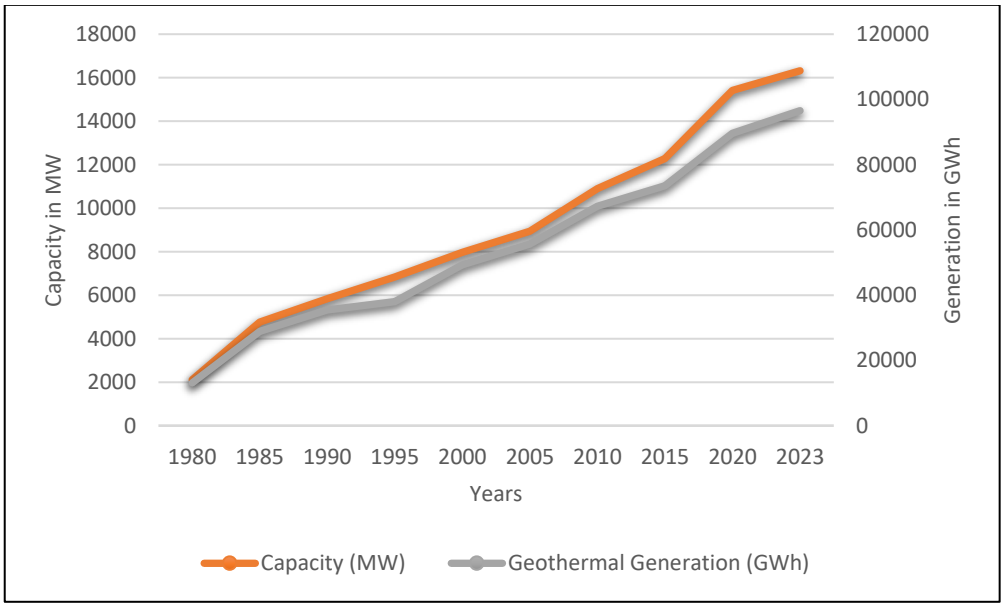

Figure 1. World geothermal capacity and electric generation between 1980 and 2023. Electric generation in 1980 and 1985 is estimated. Modified from Gutiérrez-Negrín, 2024.

Looking deeper into this visualization, several distinct development phases become apparent. The period of 1980-1990 shows moderate growth, with capacity increasing from 2,110 MW to 5,834 MW, corresponding to early geothermal developments in the United States, Philippines, and Italy (Bertani, 2016; DiPippo, 2005). The 1990-2010 timeframe exhibits a more gradual expansion rate, reflecting the technological and economic challenges of the era, with capacity reaching 10,898 MW in 2010 (Bertani, 2012). From 2010 onward, the slope steepens noticeably as Indonesia, Turkey, and Kenya accelerated their geothermal development

programs, bringing online substantial new capacity (Fridleifsson et al., 2017; IRENA, 2023). This visualization effectively communicates geothermal steady rather than fluctuating growth pattern, characterized by incremental capacity additions across multiple countries rather than explosive expansion in single markets.

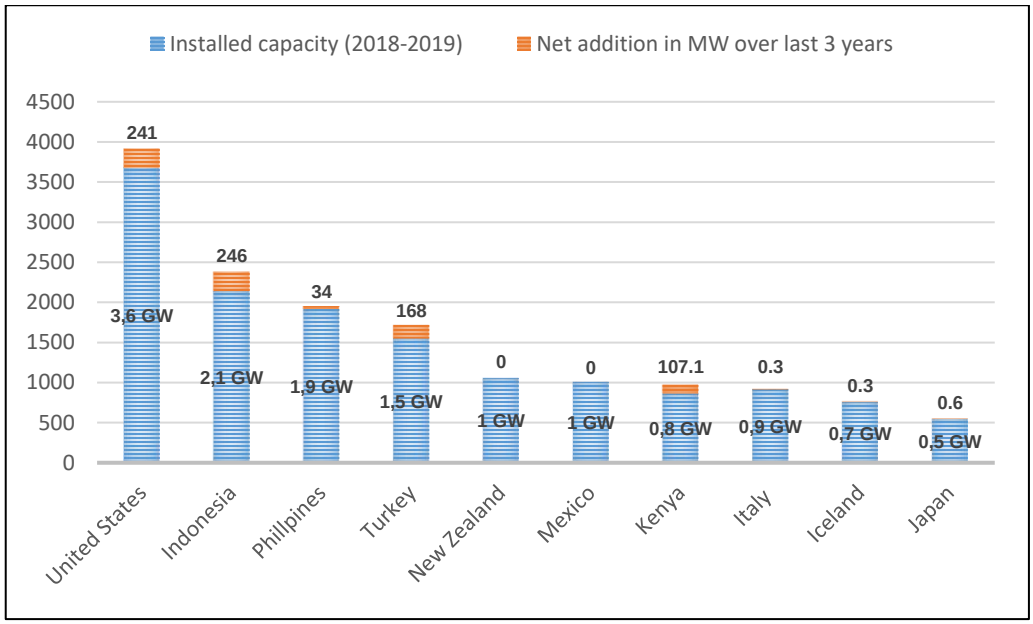

Figure 2. Top Ten Countries with the Highest geothermal Installed capacity in 2020-2021, and net additions in MW over the last 3 years. Modified from Gutiérrez-Negrín, 2024.

Indonesia's contribution to the global geothermal landscape is particularly significant, emerging as the second-largest producer with 2,384 MW of installed capacity by 2023. The acceleration of the development of installed geothermal capacity in Indonesia (see, Figure 2) follows crucial policy reforms including the Geothermal Law No. 21/2014, which reclassified geothermal from "mining" to "renewable energy" activities (CELIOS-WALHI, 2024). Indonesia has developed approximately 15 geothermal fields across the islands of Java, Sumatra, Sulawesi, and Bali, predominantly using flash technology that aligns with the global technological distribution shown in Table 6 (ESDM, 2023; IRENA, 2023).

Despite this progress, Indonesia has developed less than 10% of its estimated 28.5 GW potential—the largest theoretical geothermal resource worldwide—highlighting significant future expansion opportunities that could substantially reshape the global capacity distribution depicted in Table 1 (Setiawan et al., 2019; Sobhi et al., 2022).

Geothermal power technologies vary worldwide in their deployment and productivity. Flash steam plants constitute only 36.7% of global installations yet produce over half of the world's geothermal capacity and generation. This disproportionate contribution stems from their deployment in large, high-temperature fields, enabling greater power output per facility (DiPippo, 2015). Binary ORC plants make up 43% of units, but contribute just 21.7% of capacity and 21% of generation, since they are smaller and work with lower-temperature resources (S. J. Zarrouk & Moon, 2014). Dry steam plants are only 8.9% of units but provide 17.8% of capacity, as they are found in a few highly productive fields such as The Geysers and Larderello (Bertani, 2016). The remaining 11.4% use hybrid or combined systems. Therefore, it is clear that technology choices depend on the type of geothermal resource, not a single standard approach (Gutiérrez-Negrín, 2024). This paper will not address the uptake of petrothermal (fluid-added) enhanced geothermal systems or closed-loop deep heat exchanger systems, as they are currently negligible, although its role could be significantly enhanced in the future.

Table 1. Worldwide installed capacity, generation, and annual capacity factor in 2021-2022. Modified from Gutiérrez-Negrín, 2024

No	Country	Capacity (MW)	Generation (GWh)	C.F. (%)
1	United States	3919,40	18702,20	54,50
2	Indonesia	2384,40	16588,00	79,40
3	Philippines	1951,80	11670,00	68,30
4	Turkey	1717,30	10840,00	72,1
5	New Zealand	1054,80	7820,00	84,60
6	Mexico	1001,90	4511,50	51,40
7	Kenya	972,50	5590,00	65,60
8	Italy	915,80	5917,00	73,80
9	Iceland	755,30	5788,40	87,5
10	Japan	545,70	2660,80	55,70
11	Costa Rica	252,50	1599,00	72,30
12	El Salvador	204,40	1575,00	88,00
13	Nicaragua	165,40	780,00	53,80
14	Russia	81,90	440,70	61,40
15	Chile	81,00	600,00	84,60
16	Papua-New guinea	50,00	118,30	27,00
17	Germany	47,00	207,70	50,40
18	Guatemala	46,50	310,00	7,1

19	China	45,10	131,20	33,20
20	Honduras	35,00	297,00	96,90
21	Portugal	31,80	158,9	57,00
22	France	17,20	127,00	84,30
23	Croatia	16,50	74,70	51,60
24	Ethiopia	7,30	0,00	0,00
25	Taiwan	6,60	25,00	43,30
26	Canada	6,30	0,00	0,00
27	Hungary	3,00	18,1	69,00
28	Austria	1,20	0,50	4,80
29	Australia	0,30	0,00	0,00
30	Thailand	0,30	0,20	7,60
31	Colombia	0,10	0,00	0,00
32	Romania	0,10	0,80	91,30
	Total	**16318,40**	**96552,00**	**67,50**

Geothermal power's global footprint encompasses 32 countries utilizing approximately 198 geothermal fields through 673 individual power units (Gutiérrez-Negrín, 2024). Table 1 presents a comprehensive country-by-country breakdown of this deployment, ranking nations by installed capacity while also providing generation and capacity factor data (Gutiérrez-Negrín, 2024). Table 1 reveals significant concentration in the geothermal market, with the United States (3,919 MW), Indonesia (2,384 MW), the Philippines (1,951 MW), and Türkiye (1,717 MW) collectively accounting for over 61% of global capacity. However, Table 1 highlights geothermal disproportionate impact in specific national contexts, with Kenya (45%), Iceland (30%), and El Salvador (24%) deriving substantial portions of their electricity generation from this resource despite having modest absolute capacity figures (Fridleifsson et al., 2017; IRENA, 2023).

1.2. Classifications of Geothermal Energy Sources

Geothermal energy resources are remarkably diverse in their physical characteristics, temperature profiles, and methods of utilization. To effectively manage and develop these resources, systematic classification frameworks are essential, as they guide resource assessment, technology selection, and project planning. One of the most fundamental approaches is to classify geothermal resources by reservoir temperature, as outlined in Table 2. This method directly links temperature to thermodynamic potential and the choice of suitable conversion technologies. High-enthalpy resources with temperatures above 220°C, typically found in volcanic or tectonically active regions, are most suitable for flash steam and dry steam power

plants, offering conversion efficiencies of 15–25% (Kaya et al., 2023). Medium-enthalpy resources, ranging from 100 to 220°C, are usually developed using binary cycle technologies that operate efficiently at moderate temperatures (Kurnia et al., 2022). Low-enthalpy resources below 100°C have historically been used for direct heating, but technological advances have lowered the minimum temperature for viable electricity generation to around 80°C (Astolfi et al., 2020). For very low-enthalpy resources at a temperature below 30°C, ground-source heat pumps are commonly used to, achieve high coefficients of performance, especially in heating and cooling applications (Lund & Toth, 2021).

Table 2. Temperature-based classification of geothermal resources with typical applications and conversion technologies. Adapted from Kaya et al., 2023; Liu et al., 2022.

Classification	Temperature Range	Primary Applications	Conversion Technologies	Efficiency Range	Example Locations
High-Enthalpy	>220°C	Electricity Generation	Flash steam, dry steam	15-25%	Larderello (Italy), Kamojang (Indonesia)
Medium-Enthalpy	100-200°C	Electricity Generation, Industrial Processes	Binary cycle	10-17%	Olkaria (Kenya), Saffon Sea (USA)
Low-Enthalpy	30-100°C	Direct Heating	Advanced binary cycle, direct use	7-12%	Paris Basin (France), Beijing (China)
Very low-Enthalpy	<30°C	Space Heating/Cooling	Ground source heat pumps	COP > 4.0	Widespread global distribution

In addition to temperature, geothermal systems can be classified by their geological context and heat transfer mechanisms, as illustrated in Table 3. This framework distinguishes between convection-dominated systems (where heat is transported primarily by fluid movement, such as in magmatic or fault-controlled settings) and conduction-dominated systems (where heat moves through rock without significant fluid flow) (Banwell, 1963; Wang et al., 2024). Examples include magmatic systems in volcanic regions like Kamojang, Indonesia, and conduction-dominated resources in sedimentary basins such as the EAVOR-Loop project at Geretsried in the Molasse Basin, Germany (Longfield et al., 2022).

Table 3. Geological classification of geothermal systems based on heat transfer mechanisms. Compiled from Banwell, 1963; Wang et al., 2023.

Heat Transfer Mechanism	System Type	Characteristic	Typical Temperature Range	Representative Fields
Convection-dominated	Magmatic	Associated with volcanism, high heat flow	200-350°C	Kamojang (Indonesia), Momotombo (Nicaragua)
	Fault-controlled	Structural permeability, deep circulation	100-200°C	Dixie Valley (USA), Kizildere (Turkey)
	Geopressured	Overpressure Sedimentary Basins	120-180°C	Gulf Coast (USA)
Conduction-dominated	Intracratonic basin	Sedimentary basin with insulating cap rock	60-120°C	Paris Basin (France), Pannonian Basin (Hungary)
	Crystalline basement	Radiogenic heat production	80-200°C	Cooper Basin (Australia), Soultz-sous-Forets (France)'Alpine systems, Himalayan Systems
	Orogenic belt	Residual heat from mountain-building	70-150°C	Alpine systems, Himalayan systems

From an engineering and utilization perspective, geothermal resources are further classified by their primary application, as summarized in Table 4. High- and intermediate-temperature resources are mainly used for electricity generation, while low temperature resources are suitable for direct thermal uses, such as district heating, agriculture, and industrial processes (Hsieh et al., 2021; Rubio-Maya et al., 2015).

Table 4. Classification of geothermal resources by utilization pathways. Synthesized from Baldi et al., 2022; Rubio-Maya et al., 2015.

Utilization Category	Temperature Requirements	Applications	Key Design Considerations	Example Locations
Electric Generation	>230°C	Power generation	Turbine scaling, H2S removal	Larderello (Italy), The Geysers (USA)
	>180°C	Power generation	Scaling Management, Brine Disposal	Olkaria (Kenya), Cerro Prietro (Mexico)
	80-180°C	Power generation	Working fluid selection, cooling system	Salton Sea (USA), Bavaria (Germany)
Direct Thermal Use	>100°C	Industrial Processing, Desalination	Heat exchanger materials, mineral scaling	Iceland, Tuscany (Italy)

	50-100℃	Direct heating, greenhouse agriculture	Distribution network design, season demand	Reykjavik (Iceland), Boise (USA)
	<50℃	Space heating, aquaculture	Cascaded use, thermal efficiency	Paris Basin (France), China

A notable category is Enhanced Geothermal Systems (EGS), which enable the extraction of heat from rocks that lack sufficient natural permeability through methods such as hydraulic stimulation. Emerging classification approaches now also recognize unconventional geothermal resources, including co-produced fluids from oil and gas operations, supercritical geothermal systems with temperatures and pressures above conventional limits, and the use of abandoned mines for thermal energy storage. In addition, hybrid systems are being developed by combining geothermal and other renewables, like solar energy, to increase efficiency and flexibility (Y. Li et al., 2020).

Altogether, these complementary classification systems—based on temperature, geological characteristics, and utilization pathways, as presented in Tables 1, 3, and 4—reflect the complex and evolving nature of geothermal resources. They provide a comprehensive foundation for technology selection and development strategies, ensuring geothermal energy continues to expand its role as a versatile and sustainable energy source (ESDM, 2020).

1.3. Geological Framework of Indonesia

Indonesia is one of Earth's most geologically active regions, situated where three major tectonic plates meet: Eurasia, India-Australia, and Pacific-Philippine Sea (Charlton, 2000). This island nation consists of over 18,000 islands stretching 5,000 kilometers across the equator, as shown in Figures 1. Indonesia formed over 300 million years as pieces of ancient continents came together, with most of its current features developing during the last 65 million years (Hall, 2019).

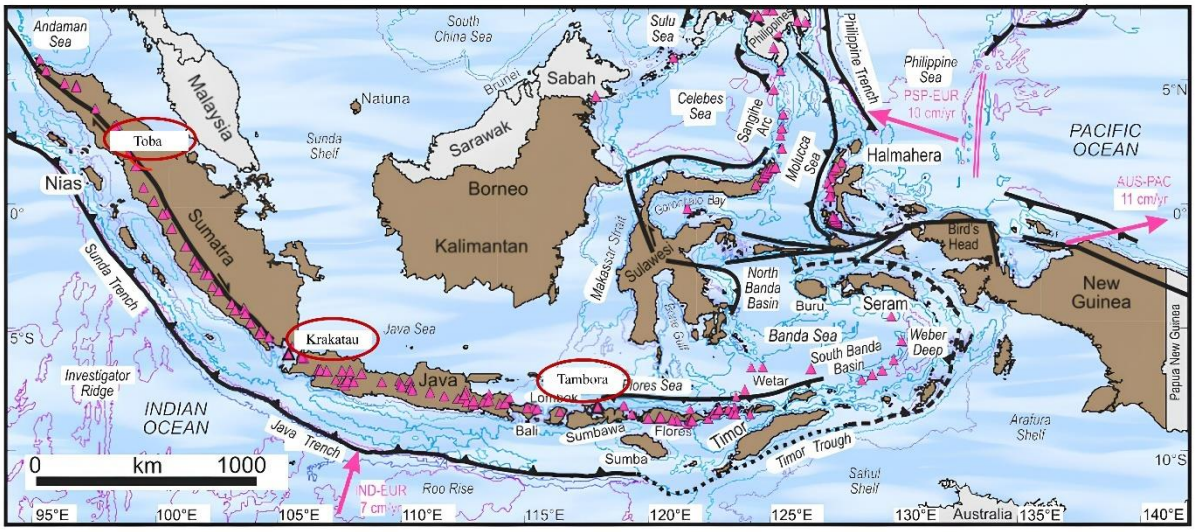

Figure 3. displays a map of Indonesia and its surrounding areas, highlighting current tectonic boundaries and volcanic centers. Indonesian territories appear in brown coloration, while adjacent countries are shown in light gray. Pink directional arrows indicate how tectonic plates are moving against each other, specifically showing movement vectors for the Indian plate (IND-EUR) and Philippine Sea plate (PSP-EUR) in relation to the Eurasian plate, as well as Australian plate motion relative to the Pacific plate (AUS-PAC). (modified from Hall 2019)

Looking at Figure 3, western Indonesia features the Sunda Trench, where the Indian plate slides beneath the Eurasian plate. Running through Sumatra is the Sumatran Fault, which allows for sideways movement between plates. East of Java, the geological picture becomes much more complex, with multiple smaller plates and subduction zones, including the Sorong Fault extending from New Guinea to Sulawesi. GPS measurements show these blocks move rapidly—several centimeters each year.

Indonesia's subduction zones create two notable features: earthquakes and volcanoes. Figure 4 shows earthquake activity extending 600 kilometers deep, while at least 95 volcanoes that have erupted since 1500-2019 in Indonesian. These volcanoes typically form 100-120 kilometers above where oceanic plates sink into the Earth. Indonesia has experienced some of history's most powerful eruptions, including Tambora in 1815 (marked in Figure 1), which caused the "year without summer" globally, and the ancient Toba eruption 74,000 years ago—Earth's largest known eruption in the past 2 million years (Hall, 2019).

In contrast, Indonesia's interior region—particularly the Java Sea, Sunda Shelf, and lower areas of Sumatra and Kalimantan—has little earthquake or volcanic activity, as shown in Figures 4. This stable region forms the continental core called Sundaland (Figure 5), which

extends to the Malay Peninsula and mainland Southeast Asia. During ice ages when sea levels were lower, much of this shallow area (less than 200 meters deep) was dry land.

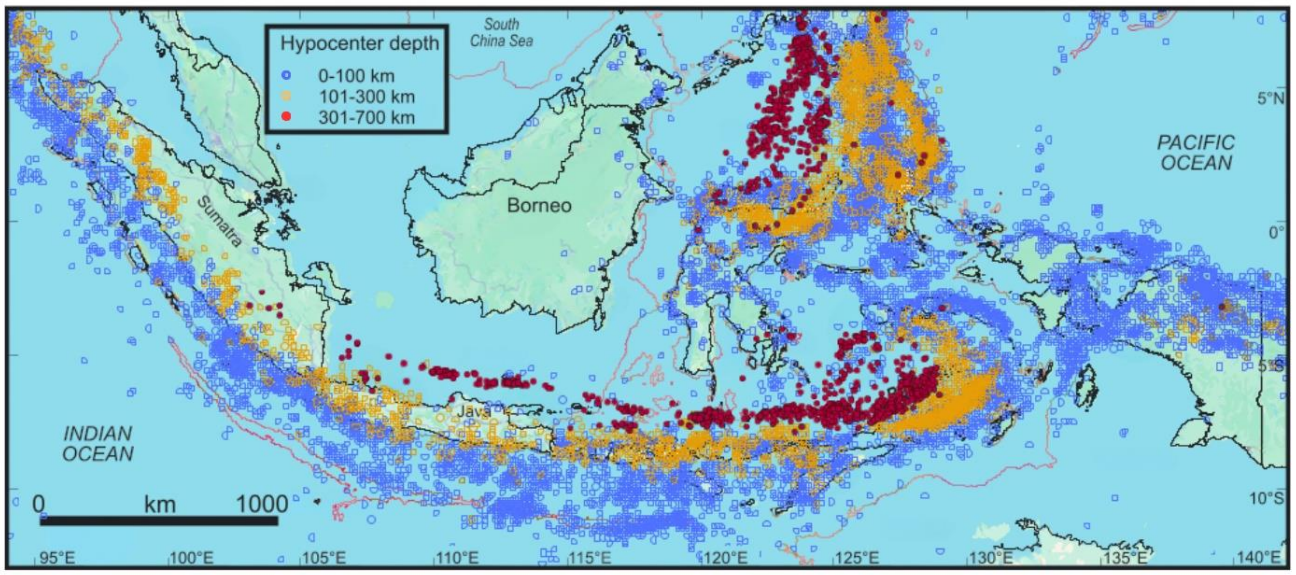

Figure 4. shows where earthquakes happened around Indonesia between 1964 and 2000, with lines marking shallow (200m) and deep (6000m) ocean floors (modified from Hall 2019)

Unlike older, stable continents, Sundaland has relatively thin, warm crust. This has allowed for significant changes over time, including the formation of deep basins and mountain ranges throughout Indonesia's history (Gao et al., 2024).

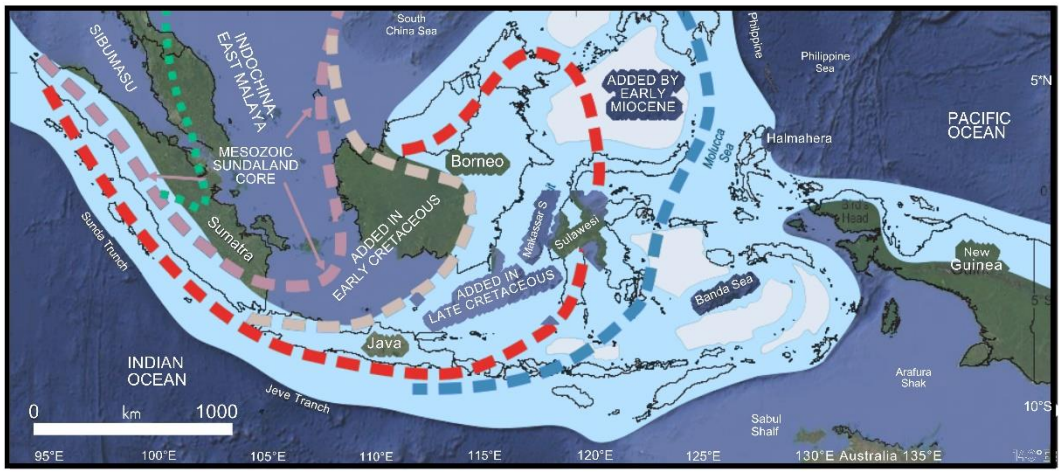

Figure 5. illustrates Indonesia's formation, showing the Triassic collision of ancient landmasses that created the Sundaland core, with later continental additions surrounding it. Blue light areas show current active deformation zones, while white sections indicated young ocean crust (modified from Hall 2019)

The oldest rocks in Indonesia are found in western regions, particularly Sumatra and Borneo. Sumatra contains rocks from the Carboniferous period (about 300-360 million years ago), with some possibly older (Katili, 1973). Western Sumatra's rocks originated from a piece of land called the Indochina–East Malaya block, while eastern Sumatra contains rocks from the Sibumasu block (shown in Figure 5). These two blocks collided about 250 million years ago, forming the foundation of western Indonesia (Metcalfe, 2017).

Borneo's southwestern region (visible in Figure 3) contains ancient metamorphic rocks intruded by younger granites in the Schwaner Mountains. Northwestern Kalimantan shows evidence of multiple collisions over time, accumulating various crustal fragments. During the Cretaceous period (66-145 million years ago), volcanic activity ran from Sumatra through Java and into Sulawesi (Hall, 2019).

Most of Indonesia is covered by younger rocks (less than 66 million years old) . About 45 million years ago, as Australia began moving rapidly northward, subduction resumed beneath Indonesia, creating widespread volcanic activity. At the same time, rifting throughout Sundaland created numerous deep basins. These basins, filled with sedimentary rocks, now contain important oil and gas resources in Sumatra, offshore Java, and eastern Kalimantan (Hall, 2019; Katili, 1975).

One significant rift separated Borneo from western Sulawesi, forming the Makassar Straits. This area became a deep-water environment about 30 million years ago. Today, these straits form a major pathway for water flowing between the Pacific and Indian Oceans and mark the Wallace Line—a famous boundary separating Asian and Australian animals.

About 23 million years ago, major collisions began between Australia and eastern Indonesia. These events brought pieces of oceanic crust onto land in Sulawesi and triggered mountain building in eastern Sulawesi and Borneo. As Australia continued northward, eastern Indonesia experienced stretching interrupted by collisions of smaller land fragments moving along strike-slip faults (Hall & Wilson, 2000).

Borneo's mountains grew higher, increasing erosion and delivering sediment to surrounding basins. Sulawesi underwent a complex sequence of compression, stretching, and strike-slip faulting, resulting in its distinctive K-shape with deep bays between its arms.

The curved Banda arc formed as oceanic crust within the Australian plate subducted northward. About 3-4 million years ago, this arc collided with Australia at Timor, causing thrusting and changing regional plate boundaries. New plate boundaries developed between Flores and Wetar (Figure 3).

Volcanic activity in Java and Sumatra decreased temporarily about 20 million years ago despite continued subduction, due to rotation of Borneo and Java caused by Australia's collision. Around 10 million years ago, volcanic activity resumed vigorously. Since then, compression has affected both Sumatra and Java, lifting them above sea level within the past few million years.

Indonesia's geology continues to change today, with ongoing plate movements creating one of Earth's most active regions. Figure 2 shows the pattern of earthquakes throughout Indonesia, reflecting this ongoing activity. The dynamic nature of Indonesia's geology has created remarkable diversity—from active volcanoes and deep ocean trenches to oil-rich basins and young mountain ranges—making it a natural laboratory for understanding how Earth's crust evolves over time

1.4. An Overview of Indonesian Geothermal Type, Potential, and Utilization

Indonesia’s location along the Pacific Ring of Fire provides a unique geological advantage, resulting in some of the world’s richest geothermal resources. The country’s volcanic arcs, formed by the tectonic collision of the Indo-Australian, Eurasian, and Pacific plates, stretch for roughly 7,000 kilometers and underpin an estimated geothermal potential of 23.9 GW across 331 identified prospects (Mohammadzadeh Bina et al., 2018). Despite this significant endowment, only about 2.3 GW of capacity had been installed by 2023, representing less than 10% of the total potential (IRENA, 2023). As detailed in Table 5, about 70% of Indonesia’s geothermal systems are categorized as high-enthalpy, volcano-hosted hydrothermal systems, commonly found along the Quaternary volcanic arc, with reservoir temperatures often exceeding 220°C and sometimes reaching beyond 300°C (Mohammadzadeh Bina et al., 2018). Other geothermal system types identified include fault-controlled systems (15%), sedimentary basin systems (8%), and mixed volcanic-sedimentary systems (7%), volcano-hosted systems like Kamojang and Darajat also classified as closely associated with active magmatic sources, whereas fault-controlled fields such as Sibayak rely on deep-seated fault structures for fluid flow (Mohammadzadeh Bina et al., 2018).

Table 5. Classification of Indonesian Geothermal Systems. Adapted from Mohammadzadeh Bina et al., 2018.

System Type	Proportion	Temperature Range	Key Characteristics	Example Fields
Volcano-hosted	70%	240-320℃	Central magmatic heat source, extensive hydrothermal alteration	Kamojang, Darajat (Indonesia)
Fault-controlled	15%	200-260℃	Deep fault zones for fluid circulation, no direct volcanic association	Sibayak (Indonesia)
Sedimentary basin	8%	120-200℃	Heat conduction through sedimentary formations	Areas in Central Java (Indonesia)
Mixed volcanic-sedimentary	7%	180-280℃	Combined characteristics	Dieng Complex (Indonesia)

Geochemical studies are increasingly revealing the complexity of Indonesia's geothermal provinces. Usman et al. (2022) describe three main geothermal fluid types, namely: neutral-pH chloride waters (predominant in volcanic settings; acid-sulfate fluids, typically found in vapor-dominated or near-vent zones); and bicarbonate waters (more often associated with peripheral or fault-controlled systems). These variations in fluid chemistry highlight differences in subsurface pathways, magmatic influences, and water-rock interactions. Geothermal potential is also unevenly distributed across major regions, as shown in Table 6. Sumatra possesses the largest share with approximately 9.5 GW of potential, followed by Java-Bali with 8.9 GW, Sulawesi with 2.5 GW, and the eastern islands—such as Flores and Sumba—providing about 3.0 GW (ESDM, 2020). Resource classification by exploration maturity, as proposed by Saputra et al. (2020), divides the national resource into speculative, probable, and proven categories. Technological advances like magnetotelluric surveys have recently expanded the inventory of high-potential prospects in areas such as Flores and Alor (Maryanto et al., 2017).

Table 6. Indonesian Geothermal Resources by Region and Development Status. Modified from ESDM, 2023.

Region	Potential (GW)	Installed Capacity (MW)	Development Ratio (%)	Major Fields
Sumatera	9,5	1030	10,8	Sarulla (330 MW), Sibayak (12 MW)
Java and Bali	8,9	1174	13,2	Salak (377 MW), Darajat (270 MW), Wayang Windu (227 MW)
Sulawesi	2,5	133	5,3	Lahendong (120 MW)

Eastern Island	3	13	0,4	Ulumbu (13 MW)
Total	**23,9**	**2350**	**29,7**	

By the end of 2023, Indonesia had become the world's second-largest geothermal power producer, with its 2.3 GW of installed capacity distributed over 15 operational fields. Table 6 indicates that, the leading developments include the Salak (377 MW), Sarulla (330 MW), Darajat (270 MW), and Wayang Windu (227 MW) fields, most of which utilize flash-steam technology (ESDM, 2023). The Sarulla plant stands out for integrating flash and binary cycle technologies, which enhances overall energy recovery. According to Sarjiya et al. (2020), Indonesian geothermal plants achieve energy conversion efficiencies in the range of 12–15%, with overall energy efficiency between 45–60%, matching international standards for high-enthalpy systems (Sarjiya et al., 2022). While electricity generation is the dominant application, direct-use projects remain limited to less than 0.3% of total utilization. Existing applications include agricultural drying, bathing, and district heating, as exemplified by the Lahendong project in North Sulawesi, where cascaded geothermal energy is used for agricultural processing downstream from power generation (Aloanis et al., 2023).

Indonesia's ambitious geothermal expansion faces persistent challenges. Nadhir et al. (2023) identify high exploration risks and upfront costs, environmental constraints—since over half of geothermal resources are in protected forests—limited remote infrastructure, and historically uncertain investment conditions as key barriers (Maryanto et al., 2017). Policy responses include the Geothermal Fund Facility (GFF) for risk mitigation and Presidential Regulation No. 109/2020, which streamlines permitting and shortens approval times (Richter, 2017). National targets aim to increase installed geothermal capacity to 7.2 GW by 2030 and 17.3 GW by 2050. Innovative strategies being pursued include small-scale modular geothermal plants for remote areas, integration of direct-use applications with power generation, and advanced exploration using artificial intelligence and geophysical modeling (Richter, 2017). As reflected in Tables 5 and 6, Indonesia's geothermal resources are notable for their scale, diversity, and regional distribution, requiring tailored approaches for different geological settings and development stages.

1.5. Scaling Problem in Geothermal Plant

Scaling represents one of the most persistent challenges in geothermal power production, impacting wellbore performance, equipment integrity, and generation efficiency across geothermal operations worldwide. This phenomenon occurs when dissolved minerals in geothermal fluids precipitate and form solid deposits on production equipment surfaces, typically triggered by physicochemical changes during production and utilization processes (S. J. Zarrouk & Moon, 2014). Such changes include pressure drops as fluids ascend from high-pressure reservoir conditions, temperature reductions during heat extraction, pH shifts arising from CO_2 degassing, and mixing of fluids that disrupt chemical equilibrium as fluids move from the reservoir to surface environments. The severity and progression of scaling are closely linked to operational parameters such as production rates, reinjection temperatures, and facility design configurations. The chemical composition of the geothermal scale varies considerably depending on reservoir fluid geochemistry, temperature-pressure conditions, and operational factors. Globally, the most common scaling compounds are calcium carbonate (calcite), amorphous silica and silica polymorphs, metal sulfides, and sulfates (S. J. Zarrouk & Moon, 2014). The distribution of scale types follows clear patterns: Silica scaling is dominant in high-temperature systems above 230°C, especially where significant temperature drops occur during energy extraction, while carbonate scaling is more prevalent in moderate-temperature systems with high dissolved CO_2 concentrations that experience pressure reduction during production (MØller et al., 1998). Sofyan et al. (2023) demonstrated that the annular flow pattern commonly seen in geothermal wells can further exacerbate scaling, particularly in zones where boiling occurs at the casing wall, which increases scale buildup (Sofyan, 2023).

The precipitation kinetics of scaling minerals also vary significantly, creating different challenges for prediction and mitigation. Silica scaling exhibits complex polymerization behavior, with an extended induction period followed by rapid precipitation, making it difficult to control using conventional chemical inhibitors (Yin et al., 2021). The formation process starts with monomeric silica that slowly forms polymers and colloids before eventually depositing as an amorphous silica scale, with kinetics strongly influenced by pH, temperature, and catalyzing ions. In contrast, calcite precipitation responds quickly to pressure changes and CO_2 degassing, with crystallization occurring within minutes under favorable conditions (S. J. Zarrouk & Moon, 2014).

Scaling's impacts are economically significant throughout the geothermal production chain. Near the reservoir, scale buildup in the wellbore can sharply reduce productivity by lowering permeability and restricting flow. Production wells may suffer from decreased flow rates, higher pumping requirements, and accelerated casing corrosion due to localized scaling. In surface facilities, even thin-scale layers in heat exchangers can reduce heat transfer efficiency by 40–50%, directly decreasing power output (Jarrahian et al., 2025). Scaling in reinjection wells can severely reduce injectivity, leading to operational constraints and unsustainable pressure increases. Unresolved scaling can lower overall plant efficiency by 10–20%, with heat exchangers being especially vulnerable (Penot et al., 2023; S. Zarrouk et al., 2014). These technical issues translate into increased operational costs, reduced power generation, frequent maintenance, and equipment replacement.

CHAPTER II

DETERMINATION OF SCALING ZONE AND SCALING TYPE IN SLOTTED LINER BASED ON THE FLUID FLOW PATTERN IN THE GEOTHERMAL WELL "X"

Akhmad Sofyan
[1]*Department of Mineralogy, Geochemistry and Petrology, Faculty of Earth Science, University of Szeged, 13 Dugonics Square Szeged 6722, Hungary;*
[2]*Politeknik energi dan mineral Akamigas, Jalan Gajahmada No.38 Cepu, 58315, Indonesia*

Syafira Wiharti
Politeknik energi dan mineral Akamigas, Jalan Gajahmada No.38 Cepu, 58315, Indonesia

János Szanyi
[1]*Department of Mineralogy, Geochemistry and Petrology, Faculty of Earth Science, University of Szeged, 13 Dugonics Square Szeged 6722, Hungary;*

Bambang Yudho Suranta
Politeknik energi dan mineral Akamigas, Jalan Gajahmada No.38 Cepu, 58315, Indonesia

Rita Njeru
[1]*Department of Mineralogy, Geochemistry and Petrology, Faculty of Earth Science, University of Szeged, 13 Dugonics Square Szeged 6722, Hungary;*

Bibliographic Data:
Sofyan, A., Syafira, W., János, S., Bambang, Y. S., & Rita, N. (2023). Determination of Scaling Zone and Scaling Type in Slotted Liner Based on the Fluid Flow Pattern in the Geothermal Well "X." *International Journal of Renewable Energy Research*, 13(1), 276–286.
http://doi.org/10.20508/ijrer.v13i1.13603.g8681

Abstract: A geothermal well can experience a decrease in the production of fluid (steam) due to the presence of scaling. The scaling usually is formed in the slotted liner hole. The purposes of this study were to determine the fluid flow pattern, the zone of scaling accumulation, and the scaling type in the well "X". This can be a reference to determine the next step to prevent and clean scaling problems in the wellbore. In determining the fluid flow pattern, the manual calculation using the Hewitt-Robert method and the simulation calculation using WellSim software were conducted. In determining the zone of scaling accumulation, the pressure, temperature, and spinner (PTS) survey data were utilized. In determining the scaling type, the geochemical analysis data were utilized. The results showed that the fluid flow pattern was annular flow based on the Hewitt-Robert method and mist flow based on WellSim software. There is no flow pattern type of mist in the grouping of flow patterns based on Hewitt-Robert. Because the characteristics of mist flow and annular flow are almost the same, the annular flow pattern can be considered similar to mist flow. Furthermore, the results were validated with PTS survey data so that the flashing zone was known at a depth of 1458.27 m from a total depth of 1700 m. Based on the geochemical analysis, it was known that the scaling type in the well "X" is of the calcite type.

Keywords *Flow Pattern, Geothermal, Production, Scaling, Slotted Liner*

1. Introduction

Geothermal energy is different from other natural energies such as oil, natural gas, minerals, and coal because it cannot be transported and can only be used for the development of production (Ghosh & Sanyal, 2021). This energy can only be produced at a given time, needs to be reserved, and is not available everywhere (Byrtus et al., 2022). However, The Geothermal energy is a replenished source and can be utilized all year round (Angumba et al., 2022). Because of that, the potential of geothermal energies is necessary to be investigated and discovered (Ilyas, 2021). In addition, the geothermal energy establishes an opportunity for fulfil the needs of future generations (Harrouz et al., 2018). In 2021, the total geothermal potential in Indonesia reaches 23,765.5-Megawatt equivalent (Mwe) or around 40% of the total geothermal potential in the world. Currently, geothermal potential in Indonesia has only been utilized at 4.5%, meaning that there is still around 95.5% of Indonesian geothermal potential that has not been utilized.

Therefore, the government has set a target to increase geothermal consumption to 23% by 2025 (Dewan Energi Nasional Republik Indonesia, 2022b). Along with the increasing energy consumption and demand due to changes in population growth and lifestyle (Shayan et al., 2021), the production of geothermal energy as alternative energy needs to be increased to full fill the national energy target in the year 2025. Several steps are carried out for the development of geothermal energy, namely the preliminary 3G survey (geology, geochemistry, geophysics), exploration 3G survey, exploration drilling, project review and planning, field development, power plant construction, commissioning, and operation (Association, 2014).

In utilizing geothermal energy, geothermal fluid that has been released to the surface of the earth contains heat energy which will be used to generate electrical energy. The fluid originates from the geothermal reservoir layer which is formed as a result of heat transfer from a heat source to its surroundings which occurs by conduction and convection (Saptadji, 2001). Each reservoir layer in the earth contains a variety of different characteristics such as fluid and rock content and rock hardness levels, so it is very important to research to find the right method to solve problems at each reservoir location. Some of the challenges faced when geothermal energy is produced from deep wells are the most common problems have been related to the chemistry of the geothermal fluids which sometimes contain quite considerable concentrations

of minerals and gases, which can cause scaling and corrosion in wells and surface installations which the geothermal fluids flow through (Gunnlaugsson et al., 2014).

Formation of scaling in geothermal wells is one of the main factors that can lead to a decrease in the quality and quantity of energy production because it can cause damage to pipes and reduce production speed. Scaling is deposits or solids in a reservoir or along a flow pipe of geothermal energy production which is formed due to changes in pressure, temperature, and pH in a liquid system. The type of scaling is affected by the chemical composition of the liquid in the system (Sapto & Salvius, 2001). The accumulation zone of scaling and the cause of scaling can be determined by analyzing the flow pattern and characteristics of the fluid (steam) in the geothermal wells.

Scaling usually occurs in the casing series. In a geothermal well" X", it is known that there is a blockage by scaling in the slotted liner hole which can reduce the amount of geothermal energy production. Therefore, the cause of the decline in geothermal energy production from the well "X" must be analyzed by determining the accumulation zone of scaling and the cause of scaling by determining the fluid flow pattern found in the well "X" (Agustinus et al., 2018). This can be a reference to determine the next step to prevent and clean scaling problems in the wellbore.

Research on determining fluid flow patterns was carried out in Banjarmasin in 2015 to examine the effect of salt concentration on the flow characteristics of two-phase fluid (gas-liquid fluid) using Hewitt-Robert calculation method for flow pattern mapping. The results showed that the flow pattern before flooding was annular and it during flooding was churn (Widodo et al., 2015). The other related research conducted by Flores Amenta in 2015 was about determining the flow pattern using WellSim software to establish the thermodynamic state of the fluid at any given depth to investigate the cause of decline production in the wellbore (Flores-Armenta & Alcalá, 2012). Furthermore, research conducted by Tolivia (1972) reported that by analyzing the flow pattern, the formation of scaling can be predicted in the well "Y". There are two types of scaling in the well, namely silica scaling and calcite scaling (Tolivia, 1972). The silica scaling dissolves in the high temperature well, evaporates from the liquid phase, and then settles on the casing wall of the well. At the same time, the calcite scaling, which does not dissolve in liquid, will lose carbon dioxide (CO2) and becomes calcium carbonate (CaCO3). This loss of carbon dioxide is caused by a decrease in pressure because the solubility of the gas

in the liquid is proportional to the pressure (Henry's Law). These two phenomena of scaling occur along the wellbore and in the annular flow zone where boiling of the fluid on the casing wall can increase the accumulation of the two scales (Tolivia, 1972).

However, the research conducted by Widodo et al. (2015) did not use data on actual conditions in the field (Widodo et al., 2015). Furthermore, research conducted by Widodo et al. (2015) and Tolivia (1972) did not perform simulations using the Wellsim software. Meanwhile, the research conducted by Flores Amenta can determine the flow pattern along the section of the well to differentiate separated (nonhomogeneous) flow from the homogenous flow but it was not related to determining the type of fluid flow pattern that has the potential to cause scaling (Flores Armenta et al., 2015). In year 2020, Zolfagharroshan and Khamehchi has conducted research to predicts scale precipitation and deposition during drilling in addition to modeling production conditions using two-phase fluid flow equations with HOLA software (Zolfagharroshan & Khamehchi, 2020). However, this research not determining the flow pattern that can cause the scaling in the wellbore (Tolivia, 1972) . Therefore, current research is important to do to cover the shortcomings in the previous studies.

This research used Hewitt-Robert calculation method to find out the fluid flow patterns that occur in the wellbore (the well "X") and was also validated using the Wellsim software. Wellsim is a geothermal wellbore simulator that can analyze the types of flow patterns at each wellbore depth. In addition to knowing the flashing zone that occurred in the wellbore, this study used the Pressure, Temperature, and Spinner (PTS) survey data obtained from the field. Furthermore, the object used in this research was the fluid from a geothermal reservoir (the well "X"). Meanwhile, the previous research used salt water as a research object and was carried out on the pipeline surface with the Dukler equation method (Tolivia, 1972). Therefore, this research is new and has not been conducted by other researchers yet.

The objectives of this study were (1) to determine the fluid flow pattern formed from the geothermal well "X", (2) to determine the accumulation zone of scaling in the well based on PTS survey data, (3) to determine the type of fluid flow pattern that has the potential to cause scaling, (4) to determine the type of scaling formed in the well.

2. Methods

The flow chart of this research is shown in detail in Figure.

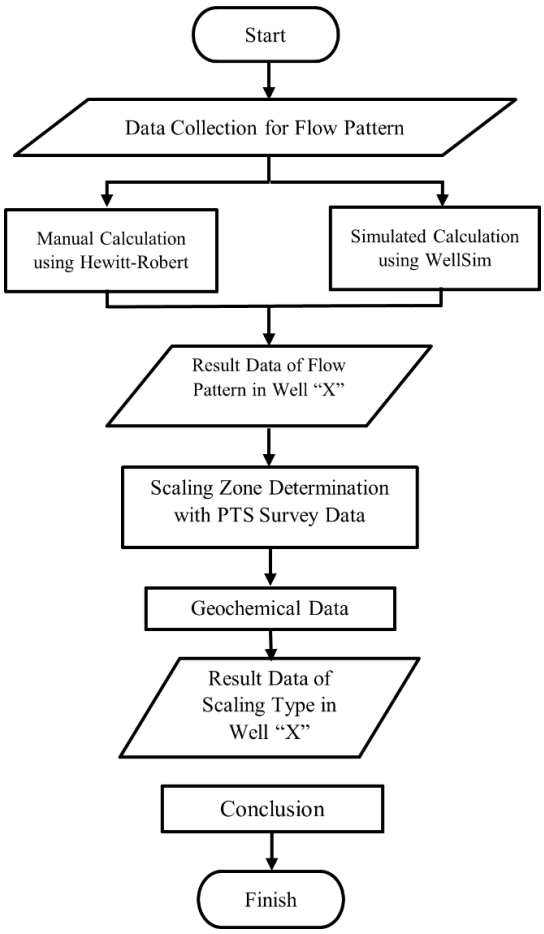

Figure 6. Flowchart of the research.

The data used in this research were real data collected from the real geothermal field from 3rd February 2022 to 3rd May 2022, as following: geochemical data, PTS data, well's head pressure data, well's production data, flow rate data, well's profile data, and casing summary data.

The data analysis process as shown in the Figure 19 was carried out after all the necessary data were collected. Then, the flow pattern was determined based on the coordinates of the calculation which was calculated manually using the Hewitt-Robert method. To validate the results obtained from the Hewitt-Robert method, the WellSim software was used to simulate the flow pattern, so that the results from the manual calculation and simulated calculation can be compared to determine the final type of fluid flow pattern in the well "X".

Furthermore, determining the depth of the flashing zone was carried out using the PTS survey data so the accumulation zone of scaling in the slotted liner in the well "X". By knowing the flashing zone in the well, scaling at a certain depth can be estimated because the fluid in the well "X" experiences change in pressure, temperature and pH.

After knowing the flashing zone, geochemical analysis was carried out to determine the type of scaling in the well "X". This was done to prove that there was scaling in the well "X" after knowing the flashing zone and flow pattern.

2.1. Manual Calculation Using Hewitt-Robert Method

Determination of the fluid flow pattern in the well "X" was manually carried out using the Hewitt-Robert method. This process requires some data, namely pressure, depth, flow rate, enthalpy, dryness pipe, and diameter. Then it is calculated by a formula based on the Hewitt-Robert method to get the cross-sectional area of the well "X". It is applied to get the coordinates of the x and y flow patterns. From these coordinates will determine the flow pattern in well "X".

2.2. Simulation Using WellSim Software

In the calculation process using WellSim, some data are needed, namely well deviation, casing configuration, geometry configuration, and feed zone. Then it starts the discharge simulation calculation to find the flow pattern results in well "X"

2.3. Geochemical Analysis

Water and gas from the geothermal well were analyzed and the samples were obtained from the downhole tube sampler with Klyen Methode. The cations and anions were analyzed using ion chromatography, ICP-OES, alkalimetric titration, and spectrophotometry, while isotopes were measured using a Liquid Water Isotope Analyzer (Idroes & Yusuf, 2019).

After the tube sampler returned to the surface and was cooled down, the gas and aqueous samples were separated into different containers. The gas sample was induced and stored in another pre vacuum stainless tube sampler, and the aqueous sample was separated into three distinct bottles, one for onsite measurement, one for anion analysis and one for cation analysis. The aqueous sample for cation analysis was acidified in the field with ultra-pure nitric acid to pH < 2. The temperature, pH value, redox potentials (Eh) and electrical conductivity (EC) of the aqueous sample were immediately measured in the field with the electrochemistry meter.

Alkalinity was also analyzed in situ by titration with hydrochloric acid. The gas and remaining aqueous samples were sent to laboratories for chemical analysis. The aqueous samples were analysed by ion chromatography for anion analysis and by induced coupled plasma-mass spectroscopy for cation analysis (Hsieh et al., 2021). The collected gas sample was then taken to the laboratory for analysis. Analysis of gas samples was carried out by two methods i.e. gas chromatography method for inactive gases (H2, Ar, N2, and CH4) and GC titration method for reactive gases (CO2, NH3, and H2S) (Widodo et al., 2015).

3. Result and Discussion

3.1. Profile of Well "X"

The well "X" is a steam-dominated well that has a depth of up to 1700 meters with an energy production capacity of 12 MW and a dryness of 98% located in Patuha. The well "X" has production casings of 20" and 13 3/8" and perforated liners of 10 3/4" and 7", which can be seen in Figure 20.

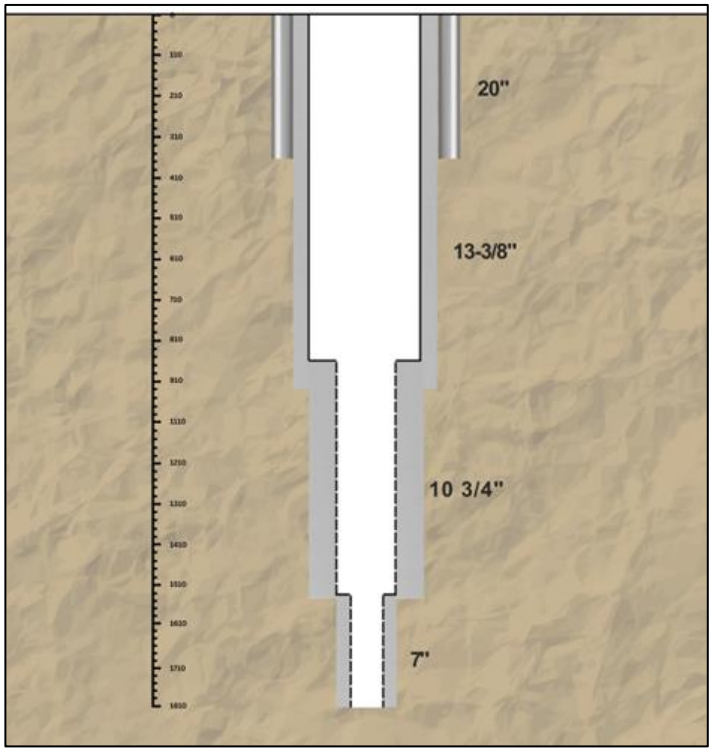

Figure 7. Schematic of the Well

3.2.Determination of Flow Pattern Using the Hewiitt-Robert Method

Determination of the vertical fluid flow pattern in the well “X” was conducted using Hewitt-Robert flow pattern mapping because the steam and hot water fluid flow upward (vertical up flow) with a pressure range of atmospheric pressure up to 1000 psi. The steps to determine the vertical flow pattern are as follows:

3.2.1.Determination of the Cross-Sectional Area of the Flow Pipe in the Well "X"

The cross-sectional area of the flow pipe in this analysis was the cross-sectional area of the entire casing in the well “X” from the surface to a depth of 1700 meters. Along the depth of the well, there were 20” and 13 3/8” production casings, then 10 3/4” and 7” perforated liners.

For example, the cross-sectional area of the flow pipe of the casing of 13 3/8" with an inner diameter of 12.415 in (1 in = 0.0254 m) can be calculated through the formulation below:

$$Ap = \pi \frac{di^2}{4} \qquad (1)$$

$$Ap = 3.14 \frac{(12.415\ x\ 0.0254)^2}{4}$$

$$\boldsymbol{Ap = 0.078\ m^2}$$

Where:

Ap, the cross-sectional area (m2); π, constants; *di*, diameter inside of the casing (m).

Based on the Figure 4, the calculation of the cross-sectional area of the flow pipe in the well “X” used the top casing first, namely the production casing of 13 3/8" with an inner diameter of 12.415 in, because the production casing of 20" was installed from the surface to a depth of 357 m while the production casing of 13 3/8" was installed from the surface to a depth of 919 m. In this case, the fluid was only through the production casing of 13 3/8". Hence, from the above calculation, a cross-sectional area was 0.078 m2.

3.2.2. Determination of the Coordinates of the Flow Pattern Map

The coordinates (x, y) of the flow pattern map were determined using equations 2 and 3. It was known that on the surface of the well "X" has a dryness (q) of 0.98, a total mass flow (Mtotal) of 23.75 kg/s, a cross-sectional area (Ap) of 0.078 m2, a water density (ρl) of 893.46 kg/m3 and a vapor density (ρg) of 4.50 kg/m3. The determination of the coordinates was conducted through equations 2 and 3 below (Nicholson, 1993):

$$X\ Axis = \frac{Gl^2}{\rho l} = \frac{\left((1-x)\frac{Mtotal}{Ap}\right)^2}{\rho l} \quad (2)$$

$$X\ Axis = \frac{Gl^2}{\rho l} = \frac{\left((1-0.98)\frac{23.75}{0.078}\right)^2}{893.46}$$

$$\boldsymbol{X\ Axis = 2.07\ kg/ms^2}$$

$$Y\ Axis = \frac{Gg^2}{\rho g} = \frac{\left((1-0.98)\frac{23.75}{0.078}\right)^2}{4.50} \quad (3)$$

$$\boldsymbol{Y\ Axis = 411.19\ kg/ms^2}$$

Where:

X-axis, horizontal axis (kg/(ms2)); *Y-axis*, vertical axis (kg/(ms2)); Gl, mass flux of liquid phase flowing alone in channel (kgm-2s-1) Gg, mass flux of gas phase flowing alone in channel (kgm-2s-1); ρl, liquid density (kg/m3); ρg, gas density (kg/m3); q, dryness; *Mtotal*, total mass (kg/s); *Ap*, the cross-sectional area (m2)

The results of complete calculations at various depths of the well "X" are displayed in full in Table 7. Then, the results of the x-axis and y-axis are plotted on the Hewitt-Robert flow pattern graph, shown in Figure 21.

Table 7. Calculation result using the Hewitt-Robert Method

Well Profile		Pressure (bar)	Enthalpy (kJ/kg)	Dryness	Ap	Massflow (kg/s)	Water		Steam	
Depth	Casing Size						Density (ρl)	x - axis $\left(\frac{Gl^2}{\rho l}\right)$	Density ρg	y-axis $\left(\frac{Gl^2}{\rho g}\right)$
0	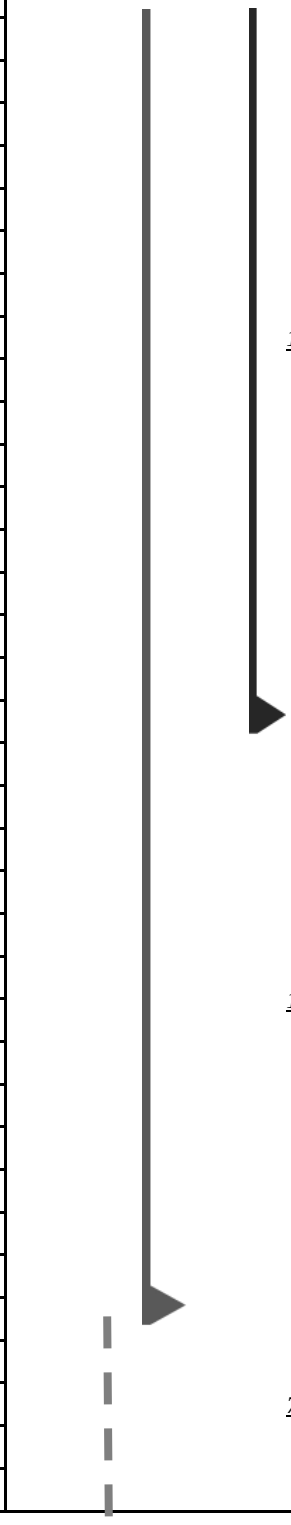	8,7	2730,8	0,98	0,078	23,75	893,5	2,07	4,5	411,2
50,86		8,7	2730,8	0,98	0,078	23,75	893,3	2,07	4,52	409,7
101,88		8,8	2730,8	0,98	0,078	23,75	893,1	2,07	4,53	408,2
152,91		8,8	2730,8	0,98	0,078	23,75	893,0	2,07	4,55	406,8
203,93		8,8	2730,8	0,98	0,078	23,75	892,8	2,07	4,57	405,3
254,95		8,9	2730,8	0,98	0,078	23,75	892,6	2,07	4,58	403,9
305,98		8,9	2730,8	0,98	0,078	23,75	892,5	2,07	4,6	402,5
357		8,9	2730,8	0,98	0,078	23,75	892,3	2,07	4,62	401,0
380,23	*13 3/8"*	8,9	2730,8	0,98	0,078	23,75	892,2	2,07	4,62	400,5
440,09		9,0	2730,8	0,98	0,078	23,75	892,1	2,07	4,64	399,1
499,95		9,0	2730,8	0,98	0,078	23,75	891,9	2,08	4,65	397,7
559,82		9,0	2730,8	0,98	0,078	23,75	891,7	2,08	4,67	396,3
619,68		9,1	2730,8	0,98	0,078	23,75	891,6	2,08	4,69	394,9
679,54		9,1	2730,8	0,98	0,078	23,75	891,4	2,08	4,7	393,5
739,41		9,1	2730,8	0,98	0,078	23,75	891,3	2,08	4,72	392,1
799,27		9,2	2730,8	0,98	0,078	23,75	891,1	2,08	4,74	390,8
859,14		9,2	2730,8	0,98	0,078	23,75	890,9	2,08	4,75	389,4
919		9,2	2730,8	0,98	0,048	23,75	890,8	5,44	4,77	1016,0
947		9,3	2730,8	0,98	0,048	23,35	890,7	5,26	4,78	980,6
1000,02		9,3	2730,8	0,98	0,048	23,35	890,6	5,26	4,79	977,8
1063,68		9,3	2730,8	0,98	0,048	23,35	890,4	5,26	4,81	974,4
1127,34		9,3	2730,8	0,98	0,048	23,35	890,2	5,26	4,82	971,1
1191		9,4	2730,8	0,98	0,048	22,95	890,1	5,08	4,84	934,9
1243,34		9,4	2730,8	0,98	0,048	22,95	889,9	5,08	4,85	932,3
1307	*10 3/4"*	9,4	2730,8	0,98	0,048	22,45	889,8	4,87	4,87	889,1
1343		9,5	2730,8	0,98	0,048	22,25	889,7	4,78	4,88	871,6
1359		9,5	2730,8	0,98	0,048	21,75	889,6	4,57	4,88	832,2
1371		9,5	2730,8	0,98	0,048	19,15	889,6	3,54	4,89	644,7
1385		9,5	2730,8	0,98	0,048	17,15	889,6	2,84	4,89	516,6
1389		9,5	2730,8	0,98	0,048	14,15	889,6	1,93	4,89	351,6
1415		9,5	2730,8	0,98	0,048	13,15	889,5	1,67	4,9	303,2
1436,7		9,5	2730,8	0,98	0,019	13,15	889,4	10,36	4,9	1879,0
1500,89		9,5	2730,8	0,98	0,019	13,15	889,3	10,36	4,92	1872,5
1567,26	*7"*	9,6	2730,8	0,98	0,019	13,15	889,1	10,37	4,94	1865,9
1633,63		9,6	2730,8	0,98	0,019	13,15	888,9	10,37	4,96	1859,3
1700		9,7	2730,8	0,98	0,019	13,15	888,8	10,37	4,97	1852,8

The Hewitt-Robert flow pattern graph can be used to determine the type of flow pattern using the x-axis and y-axis parameters. Based on the Figure 21, there are 6 types of flow pattern behavior in the geothermal wells, namely bubbly, bubbly slug, churn, annular, and wispy annular. Based on the plotting results of the x-axis and y-axis on the Hewitt-Robert flow pattern graph (Fig. 21), the intersection point of the x-y axis with the line of the annular flow pattern was obtained. Table 7 shows the types of flow patterns based on the results of the plotting shown in the Figure 21.

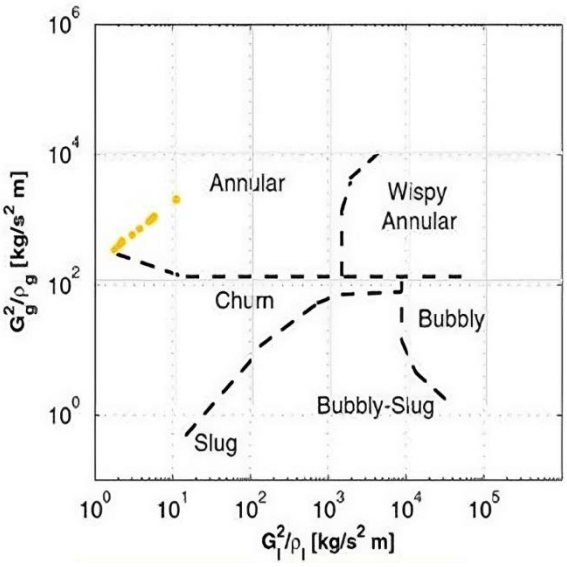

Figure 8. Plotting the x-axis and y-axis on the Hewitt-Robert Flow Pattern Graph

The results of determining the flow pattern in the well "X" with a range of depths for each casing series as shown in the Figure 3 and Table 2 show that the flow pattern formed was annular. An annular flow is a flow that flows in the internal perimeter of a channel with gas (or vapor) having a higher velocity in the center. This flow pattern is very stable and is the desired flow pattern in piping (Thome, 2016).

Table 8. Flow Patterns based on Hewitt-Robert graph plots

Well Profile			Water		Steam	
Depth	Flow Pattern	Casing Size	Density (ρl)	x - axis $\left(\frac{Gl^2}{\rho l}\right)$	Density ρg	y-axis $\left(\frac{Gl^2}{\rho g}\right)$
0	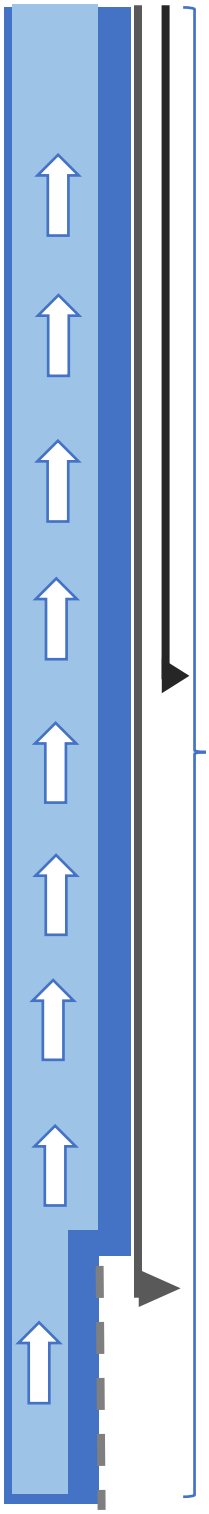		893,5	2,07	4,5	411,2
50,86			893,3	2,07	4,52	409,7
101,88			893,1	2,07	4,53	408,2
152,91			893,0	2,07	4,55	406,8
203,93			892,8	2,07	4,57	405,3
254,95			892,6	2,07	4,58	403,9
305,98			892,5	2,07	4,6	402,5
357			892,3	2,07	4,62	401,0
380,23		*13 3/8"*	892,2	2,07	4,62	400,5
440,09			892,1	2,07	4,64	399,1
499,95			891,9	2,08	4,65	397,7
559,82			891,7	2,08	4,67	396,3
619,68			891,6	2,08	4,69	394,9
679,54			891,4	2,08	4,7	393,5
739,41			891,3	2,08	4,72	392,1
799,27			891,1	2,08	4,74	390,8
859,14			890,9	2,08	4,75	389,4
919		**Annular Flow**	890,8	5,44	4,77	1016,0
947			890,7	5,26	4,78	980,6
1000,02			890,6	5,26	4,79	977,8
1063,68			890,4	5,26	4,81	974,4
1127,34			890,2	5,26	4,82	971,1
1191			890,1	5,08	4,84	934,9
1243,34			889,9	5,08	4,85	932,3
1307		*10 3/4"*	889,8	4,87	4,87	889,1
1343			889,7	4,78	4,88	871,6
1359			889,6	4,57	4,88	832,2
1371			889,6	3,54	4,89	644,7
1385			889,6	2,84	4,89	516,6
1389			889,6	1,93	4,89	351,6
1415			889,5	1,67	4,9	303,2
1436,7			889,4	10,36	4,9	1879,0
1500,89			889,3	10,36	4,92	1872,5
1567,26		*7"*	889,1	10,37	4,94	1865,9
1633,63			888,9	10,37	4,96	1859,3
1700			888,8	10,37	4,97	1852,8

From the calculation using the WellSim software, there was a mist flow pattern with dryness of 0.98, steam mass 23.26 of kg/s, and brine mass of 0.49 kg/s. A dryness of 0.98 is considered the same along the wellbore because at the time the measurement is only carried out on the surface. The flow pattern obtained should be annular flow because it only produces steam with a dryness of 0.98, which means it is considered a single-phase flow, but because the grouping of flow patterns based on Hewitt-Robert is only for annular flow patterns, the results of calculations and graph plots obtained are annular flow. This annular flow pattern can be thought of as similar to mist flow because it can be found at high vapor quality at the point where the annular flow is thinned by shearing of the gas core at the interface until it becomes unstable so that all the liquid is trapped as droplets in the continuous gas phase (Thome & Cioncolini, 2015) .

It can be concluded that based on the manual and software calculations, the well "X" has a vapor fraction of 100% and an annular flow pattern. This annular flow is a flow pattern that is in great demand because it has the highest vapor fraction so it can produce large amounts of steam. In addition, the annular flow is a fairly stable and safe flow, unlike the turbulent flow pattern which can cause large friction and irregular flow (Ganat & Hrairi, 2019). Meanwhile, the flow pattern that is avoided in geothermal wells is a slug flow pattern (Rahmandhika et al., 2020).

3.2.3. Flashing Zone Depth Based on PTS Survey Data

The pressure, temperature, and spinner (PTS) survey is one of the many monitoring activities of geothermal wells, that is routinely carried out on geothermal wells to describe the flow along the wellbore (Herianto, 2019).

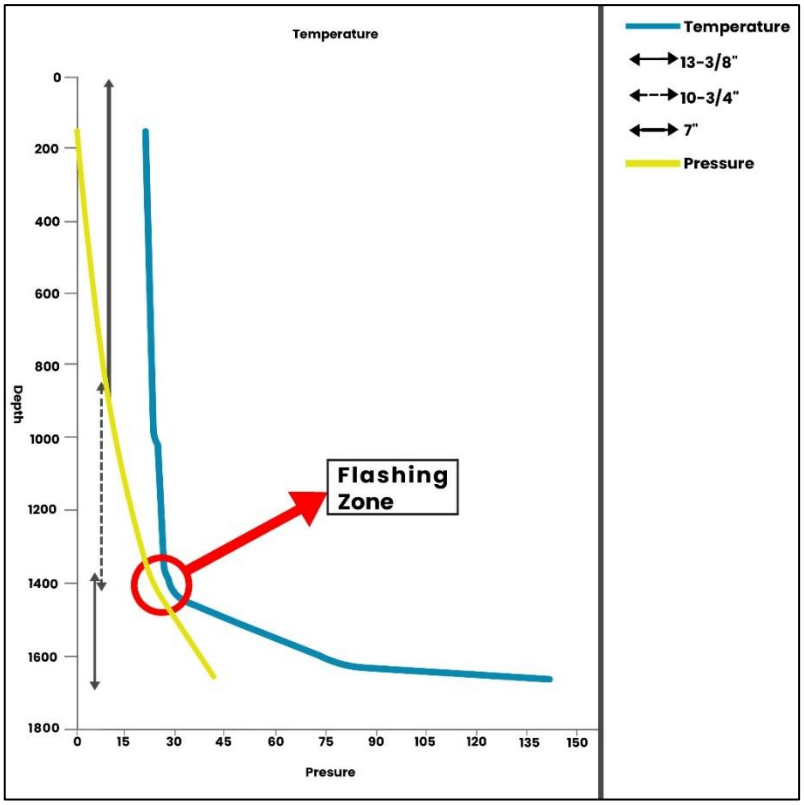

Figure 9. Graph of PTS injection data

From the flow pattern calculations, at a depth of 1458.27 meters to the surface, there is no brine because the flow pattern formed is annular based on the Hewitt-Robert classification. Based on the PTS injection data in the well "X", it can be seen that this well is a geothermal well that produces steam fluid. This can be seen in Figure 4 showing a constant increase in pressure which means that throughout the production casing from a depth of 1458.27 m to the surface no brine flow can increase pressure. While from a depth of 1458.27 m to 1658.27 m there is a brine flow, this can be seen from the sudden change in pressure and temperature at a certain depth. It can also be seen that the well "X" has a dryness of 0.98 so the well "X" can be called a well with single-phase flow or steam dominated.

The flashing zone is at a depth of about 1458.27 m, because at that depth there is a decrease in pressure from 135 bara to 44 bara due to a change in diameter between the 7" perforated liner which has a small diameter of 6.184" and the 10" perforated liner which has a larger diameter of 9.76". This decrease in pressure will cause steam to come out of the brine which is called flashing.

The flashing will affect the composition of the brine, namely the concentration of scaling is getting thicker due to the loss of some water which turns into steam due to a decrease in pressure and temperature, as well as the release of gases such as CO2 and H2S which will affect the pH of the brine. This phenomenon can increase pH and ion concentrations and result in the formation of scaling in the well "X" (Solenis, 2021).

$$CaCO_3 + H_2O \leftrightharpoons Ca^{2+} + HCO_3^- + OH^- \qquad (4)$$

This phenomenon results in scaling which is the emergence of a problem in the production process of geothermal energy sources in this flash steam system. Therefore, after the flashing area reaches the surface, the steam fluid will flow at a higher speed.

In the analysis of PTS injection data of the well "X", the fluid injection rate at the time of measurement was 75.8 kg/s or 1,200 gpm. Fluid velocity analysis was performed using the slope between the spinner and the cable speed. Figure 5 shows the profile of the slope.

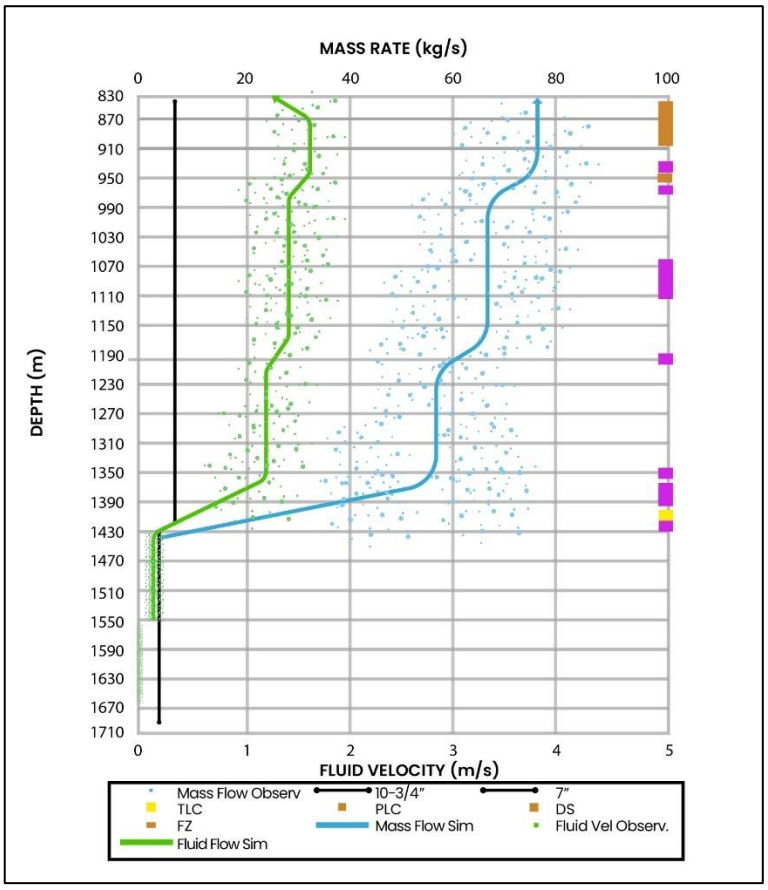

Figure 10. Graph of Data Velocity, Depth, and Mass Rate

Based on Figure 23, it is known that there are five feed zones, where the feed zone which is in the elevation range of 761-786 m or a depth of 1,389-1,421 m from the ground level has the largest contribution, which is 46%. This shows that the simulation results of mass rate and fluid flow are in accordance with the measurement data. However, the water column that is not formed perfectly causes the results of temperature and pressure measurements to be inconsistent with the measurement data.

3.2.4. Types of Scaling Based on Geochemical Data Analysis

After knowing the accumulation zone of scaling, it is necessary to validate the type of scaling found in the formation and around the liner so that the steam production from the well "X" does not decrease from time to time. From the PTS analysis, there is a flashing zone that can form a scale. This flashing zone results in the formation of steam originating from a decrease in temperature and pressure resulting in the release of H2S and CO2 which will affect the pH of the brine.

The geochemical analysis is carried out to determine the fluid content that causes the formation of scaling. Indications of the formation of scaling in the form of silica and calcite can be seen from the value of the saturation index of silica and calcite. If a chemical compound has an index value that exceeds its saturation value (> 1), it means that the scaling is formed in the well (Furqan, 2015).

The chemical content of the downhole sample from the well "X" obtained from the geochemical analysis is shown in Table 9.

Table 9. The geochemical analysis results using a downhole sample from the well "X"

Downhole Sampling		
pH Field	8.2	
pH Lab	6.52	
Temp.	254	Celcius
Li	0.029	Ppm
Na	43	Ppm
K	9	Ppm
Ca	52.2	Ppm
Mg	0.36	Ppm
SiO_2	204	Ppm
B	10	Ppm
Cl	6	Ppm
F	5	Ppm
SO_4	170	Ppm
HCO_3	56	Ppm
NH_4	0.1	Ppm
As	0.267	Ppm
Fe	0.165	Ppm

By using the geochemical analysis results (Table 9), the type of scaling in the well "X" can be determined by performing excel calculations on the content of calcite and amorphous silica. The Calcite Saturation Index (CSI) is calculated using a formula shown in Equation (5) [26].

$$\text{CSI} = log\,\frac{IAP}{Ksp} \qquad (5)$$

Where:

CSI, calcite Saturation Index; *IAP*, ion activity product; *Ksp*, solubility product

Before calculating the CSI, it is necessary to know the Ksp of CaCO3. The calculation of Ksp value takes the values of $Ca2^+$ and CO32- with mole units but the data that has been obtained is still in ppm units (Table 3). If the Ca2+ unit is converted from ppm to mol, the Ca2+ content of 52.2 ppm will be 0.001305 mol. Because the data obtained is HCO3 (Table 3), it is necessary to convert its unit from ppm to mol so the HCO3 of 56 ppm is equal to 0.000918033 mol. Furthermore, the mol of CO32- can be calculated using the mol of HCO3, molecular weight of HCO3, and molecular weight of CO3 with the formula shown in equation (6) (Furqan, 2015):

$$CO_3 = \text{Mol } HCO_3 \frac{Mr\ CO3}{Mr\ HCO3} \quad (6)$$

$$CO_3 = 0.000918033 \frac{60}{61}$$

$$\mathbf{CO_3 = 0.000902983}$$

Where:

Mr, molecule ratio

Furthermore, the Ksp CaCO3 is calculated using the following formula (Köhl et al., 2020):

$$Ksp(CaCO_3) = [Ca^{2+}] \,.\, [CO_3^{-2}]$$

$$Ksp\ (CaCO_3) = [0.001305] \,.\, [0.000902983] \quad (7)$$

$$\mathbf{Ksp\ (CaCO_3) = 3.3 \times 10^{-9}}$$

The solubility product (Ksp) for calcite at a temperature of 25oC is 3.36×10-9 mol2.L-2, where 25oC is the room temperature because the test was carried out in the laboratory at room temperature. More calcite will form with temperature. Then, the calculation of the ion activity product (IAP) was conducted with the formula below (Köhl et al., 2020):

$$Ion = HCO_3 \,.\, Ca$$

$$Ion = 0.000918033 \,.\, 0.001305 \quad (8)$$

$$\mathbf{Ion = 1.17839 \times 10^{-6}}$$

The ion activity product is the ion of the actual activity of Ca2+ and CO32- (Ganat & Hrairi, 2019). After getting the Ion and Ksp values, the Calcite Saturation Index (CSI) value can be calculated using the formula (5):

$$CSI = log \frac{IAP}{Ksp}$$

$$CSI = log \frac{1.17839\ x\ 10-6}{3.3\ x\ 10-9} \quad (9)$$

$$\mathbf{CSI = 2.54}$$

Where:

CSI, calcite Saturation Index; *IAP*, ion activity product; *Ksp*, solubility product

From these calculations, a CSI value of 2.54 was obtained. It can be said that the CSI value was above 1 which indicates that the scaling was formed from calcite in the well "X". The summary of the CSI calculations is shown in Table 10.

Table 10. Summary of the CSI calculations

Ca	0.001305
HCO_3	0.000918033
CO_3	0.000902983
Ion	1.17839E-06
Ksp	3.36E-09
CSI	2.544950842

To find out the solubility of amorphous silica formed in cbrine at vapor pressure, the equation that has been made by Fornier and Truesdell (1973) can be used (Köhl et al., 2020). The equation is shown in equation (9).

Silica Amorf (SiO_2): t(^oC)

$$\left(\frac{731}{(4.52-loglog\ SiO_2)}\right)-273.15 \quad (10)$$

Before calculating the Silica Saturation Index (SSI), it is necessary to calculate the log SiO_2 first. It is known that the reservoir temperature is 254^{o}C, then it was calculated by the formula (Fournier & Truesdell, 1973):

$$\text{Log } SiO_2 = 4.52-\left(\frac{751}{(Tres+273)}\right) \quad (11)$$

$$\text{Log } SiO_2 = 4.52-\left(\frac{751}{(254+273)}\right)$$

$$\text{Log } SiO_2 = 3.094952562$$

Where:
Tres, reservoir temperature (^{o}C)

After the log SiO_2 is known, then the Silica Saturation Index (SSI) calculation is immediately carried out using the formula (10), as follows (Tassew, 2001):

$$SSI = \left(\frac{731}{(4.52-loglog\ SiO2)}\right)-273.15 \quad (12)$$

$$SSI = \left(\frac{731}{(4.52-3.094}\right)-273.15$$

$$SSI = 0.850654368$$

From these calculations, the SSI value of 0.85 was obtained. It can be said that the SSI value is still below 1, which means that the silica content is not too saturated or even almost does not form in the X well. At lower temperatures, amorphous silica will be more easily formed than other types of silica. Therefore, amorphous silica is the dominant deposit in surface equipment and wastewater disposal sites (Tassew, 2001). The summary of the SSI calculations is shown in Table 11.

Table 11. Summary of the SSI calculations

SiO_2	204
log SiO_2	3.094952562
Silica Amorf	239.8153795
SSI	0.850654368

Based on the CSI and SSI calculations, it can be concluded that the scaling type in the well "X" is scaling from calcite. Based on our experiences, the type of calcite scaling is indeed commonly found in dry stream geothermal wells. The pictures of calcite scaling in the well "X" and the scale stuck in the check valve are shown in Figures 6 and 7, respectively (PT. Geodipa Energi Unit Patuha, 2021).

Figure 11. Calcite Sample in Well "X"

Figure 12. Trapped Sample in Check

In previous research by Zolfagharroshan and Khamehchi (Zolfagharroshan & Khamehchi, 2020). only investigate research to predict the scale deposition and modeling production conditions with HOLA software, there has been no detailed explanation regarding the flow pattern that related to scaling in in geothermal wells. However, in this study, we can accumulate zones of scaling and the cause of scaling can be determined by analyzing the flow pattern, characteristics of the fluid, and flashing zones in geothermal wells.

4. Conclusion

Based on the results of this research conducted by the author, it can be concluded that:

a) Based on Hewitt-Robert calculations, the flow pattern formed along the casing series of the well “X” starting from the casing slotted liner 10 " to the surface is an annular type flow pattern.
b) Based on the simulation results using the WellSim software, the flow pattern type in the well “X” is the mist type. This means that there are differences between the results of manual calculation (Hewitt-Robert method) and software calculation (WellSim software). The flow pattern obtained should be a mist flow because it only produces steam, but because the grouping of flow patterns based on Hewitt Robert is only for annular flow patterns, the mist flow is considered the same as annular because it is the closest.
c) According to the flow pattern that has been analyzed, the scaling is possible to be formed in the well “X”. Scaling can be formed along the wellbore and in the annular flow zone, which increases with the boiling of the fluid on the casing wall.
d) Based on the analysis using the PTS graph, the zone of accumulation of scaling is at a depth of 1458.27 m located between the casing shoe slotted liners of 7” and 10 3/4”.
e) The results of the geochemical analysis show that in the well “X”, scaling with calcite and silica types with saturation indexes of 2.54 and 0.85, respectively. It means that the scaling type in the well “X” is calcite scaling.
f) In this research we applied the data as following: geochemical data, PTS data, well’s head pressure data, well’s production data, flow rate data, well’s profile data, and casing summary data and the outcome of the research we can determine flow pattern

that can cause scaling and the flashing zone depth. In the future, in order to complete the study, there are some points that need to be research on how to prevent and clean the scaling in the wellbore and also from a financial and development perspective to provide effective and efficient results.

CHAPTER III

INVESTIGATION OF ZONE AND TYPE OF SCALING BASED ON THE FLUID FLOW PATTERN IN THE GEOTHERMAL WELL "X" AT THE SALAK GEOTHERMAL FIELD – INDONESIA

Akhmad Sofyan
[1]*Department of Mineralogy, Geochemistry and Petrology, Faculty of Earth Science, University of Szeged, 13 Dugonics Square Szeged 6722, Hungary;*
[2]*Polytechnic of Energy and Mineral Akamigas, Ministry of Energy and Mineral Resources (KESDM), Cepu, Central Java, Blora, 58315, Indonesia*

János Szanyi
Department of Mineralogy, Geochemistry and Petrology, Faculty of Earth Science, University of Szeged, 13 Dugonics Square Szeged 6722, Hungary

Hari Sumantri Aka
Polytechnic of Energy and Mineral Akamigas, Ministry of Energy and Mineral Resources (KESDM), Cepu, Central Java, Blora, 58315, Indonesia

Bibliographic Data:

Akhmad, S., Janos, S., & Hari, A. S. (2024). Investigation of Zone and Type of Scaling Based on the Fluid Flow Pattern in the Geothermal Well "X" at the Salak Geothermal Field - Indonesia. *International Journal Of Renewable Energy Research*, 14(1), 192–202.
http://doi.org/10.20508/ijrer.v14i1.14254.g8879

Abstract: Well "X" is one of the geothermal production wells, which produces two-phase fluids which are steam and brine. The pressure of fluid flow from the reservoir to the surface can decrease, so the fluid flow patterns can change. Determination of the flow pattern is very necessary to estimate the depth of the flashing zone where the condition of steam escapes from liquid and it can cause the scale precipitation which can be a major issue in the decline of the production rate. Concerning that, a continuous pressure drop will cause a slug flow and it will cause the fluid flow to become turbulent (irregular). The aim of the current research were to identify the fluid flow pattern, to estimate the scaling accumulation zone, and to determine the scaling type in the well. The current research can be used as a guide to decide what steps should be taken to avoid and eliminate scaling problems. The fluid flow pattern was determined using the Hewitt-Robert method. The scaling accumulation zone was estimated by using the PTS (pressure, temperature, and spinner) survey data. The scaling type was determined through chemical analysis of the scaling rock collected from the wellbore. The new finding in this research results indicated that the fluid flow pattern conformed to the annular flow category as established through the Hewitt-Robert method and it can promote scaling precipitation. The future research of developing the cleansing method can be conducted in this location. In addition, the flashing zone was estimated at a depth of 4600 ft from a total depth up to 5000 ft. Based on the scaling rock mineral analysis results, it was validated that the scaling type was amorphous silica.

Keywords: *Annular flow; Casing; Flashing Zone; Flow Pattern; Geothermal; Production.*

1. Introduction

Since being covered by the Ring of Fire, Indonesia country has geothermal potential as proven by the country's 117 active volcanoes which are spread among the islands of Sumatra, Java, Maluku, Nusa Tenggara, and Sulawesi (Nasruddin et al., 2016). Geothermal potential in Indonesia is estimated at around 29,51 MW. Nevertheless, just 4.5% of it is used for electricity in the nation. In this world, the highest geothermal energy potential is found in Indonesia, which accounts for around 40% of global potential (Sofyan et al., 2023). With a goal of 7.2 GW in 2025 and 17.6 GW in 2050, the government is still working to expand the geothermal power plants (Dewan Energi Nasional Republik Indonesia, 2022a).

Geothermal can be interpreted as energy generated from the earth, which is a combination of the Greek terms geo (earth) and thermal (heat). The energy is contained in geothermal fluids in the form of steam, liquid or both as a mixture (Nasruddin et al., 2016). The geothermal power plant produces electricity from geothermal energy. The geothermal power plant is called as a renewable, sustainable, and eco-friendly generator because of the characteristics of the geothermal energy (Holm et al., 2012).

In addition, Geothermal energy has its limitations, as Radek explains that it can only be produced at specific times, requires reservation, and is not universally available (Byrtus et al., 2022). In contrast, Pedro Angumba presents a more positive outlook, highlighting geothermal energy as a renewable source that remains accessible throughout the year (Angumba et al., 2022). Recognizing its potential, Syed Zafar emphasizes the need for comprehensive investigation and discovery of geothermal energies (Ilyas, 2021). Additionally, Abdelkader Harrouz highlighted that geothermal energy represents an opportunity to meet the needs of future generations (Harrouz et al., 2018).

Along with the rapid demand for energy consumption due to changes in lifestyle and population growth (Shayan et al., 2021), geothermal energy production, as one of the alternative energies, must be improved to meet the 2025 national energy target. Development of geothermal energy involves several processes, including (1) the preliminary survey of 3G (geology, geochemistry, and geophysics), (2) the exploration survey of 3G, (3) the exploration drilling, (4) the project review and planning, (5) the field development, (6) the power plant construction, (7) commissioning, and (8) operation (Association, 2014).

The process of utilizing geothermal energy involves the extraction of geothermal fluid from subsurface reservoirs which contains heat energy. Then the geothermal fluid is converted into electricity. This fluid comes from a layer of a geothermal reservoir, which is created when heat is transferred from a heat source to the surrounding rocks, facilitated by both conductive and convective processes (Saptadji, 2001). Given the unique composition and varying rock properties of each reservoir layer in the earth, it is imperative to conduct thorough research to identify effective strategies for addressing site-specific issues. In the context of extracting geothermal energy from deep wells, one of the most common challenges faced is the impact of the geothermal fluid's chemical properties. The fluid often contains minerals and gases in high concentrations, which can result in scaling and corrosion within the wells and surface infrastructure (Ármannsson H. Thorhallsson S. & E., n.d.).

Scaling is the process of deposit or solid formation along the flow pipe during the production of geothermal energy as a result of temperature, pH, and pressure changes in a liquid system. Meanwhile, the chemical composition of the liquid has a significant impact on the type of scaling. The scaling accumulation zone and its underlying cause can be estimated by examining the fluid flow pattern as well as the properties of the fluid and scaling rock obtained from the geothermal wells (Sapto & Salvius, 2001).

Scaling is a common issue in the casing series of geothermal wells. The blockages caused by scaling in the well can significantly impede the production of geothermal energy. Therefore, it is very important to conduct an in-depth analysis of the scaling accumulation zone and fluid flow patterns within the well to ascertain the root causes of the reduced geothermal energy production (Agustinus et al., 2018). The in-depth analysis can provide valuable insights for devising effective strategies to avoid and remediate scaling-related issues in the wells, thereby optimizing the efficiency and sustainability of geothermal energy production.

This study was conducted at the Salak field geothermal system, which is connected to multiple volcanic eruption centres near Indonesia's Mount Salak. The geothermal manifestations in the area are fumaroles and sulphate hot springs, which are strongly associated with the geothermal system, whereas bicarbonate hot springs and bicarbonatechloride mixed springs are found at lower elevations.

The Salak geothermal field has 110 wells including 77 production wells, 10 injection wells (condensate), 12 injection wells (brine), 6 abandon wells, and 5 monitoring wells, resulting in

an electricity capacity of 377 MW. The geothermal generation system used in the Salak geothermal field is a separated steam cycle consisting of Power Generation Facilities (PGF) and Resource Production Facilities (RPF) (Ganefianto et al., 2010).

In 2015, two studies were conducted to investigate different aspects of fluid flow patterns in geothermal wells. In the first study, which was carried out in Banjarmasin, the effects of salt concentrations on the two-phase fluid (gas liquid) flow were investigated. The Hewitt-Robert method was utilized for mapping the flow pattern. This first study aimed to determine the fluid flow patterns and found that the pattern was annular before flooding and churn during flooding (Widodo et al., 2015). Furthermore, In the second study, which was conducted by Flores Amenta in the same year, the WellSim software was utilized to investigate the thermodynamic state and flow pattern of the geothermal fluid at different depths in the wellbore. This second study aimed to investigate the causes of production decline and improve the efficiency of geothermal energy production (Flores Armenta et al., 2015). Furthermore, Tolivia's research in 1972 reported that flow pattern analysis can predict the scaling formation in geothermal wells since the scaling can significantly reduce production efficiency (Tolivia, 1972). Collectively, these studies demonstrate the importance of fluid flow pattern analysis in optimizing geothermal energy production and preventing scaling-related problems in the wellbore.

Scaling mainly can occur in a well in two forms which are silica scaling and calcite scaling. At high temperatures, the silica in the rock will dissolve in the liquid, then evaporate and then precipitate on the casing wall. However, calcite in the rock does not dissolve in liquid and instead loses carbon dioxide, converting to calcium carbonate due to a decrease in pressure. These scaling phenomena take place in the annular flow zone and along the wellbore. Previous studies by Widodo et al. in 2015 (Widodo et al., 2015) and Tolivia in 1972 (Tolivia, 1972) did not use field data and did not determine the specific flow pattern that can lead to scaling. Similarly, Flores Armenta et al. (2015) identified flow patterns but did not determine which patterns could cause scaling (Flores Armenta et al., 2015). In 2020, Zolfagharroshan and Khamehchi predicted scale precipitation and deposition during drilling but did not address the flow pattern responsible for scaling. Therefore, new research is necessary to fill these gaps in knowledge (Zolfagharroshan & Khamehchi, 2020).

This research had four main objectives which were (1) to identify the fluid flow patterns in the well “X” using the Hewitt-Robert calculation method, (2) to estimate the scaling

accumulation zone in the well through the analysis of the Pressure, Temperature, and Spinner (PTS) survey data, (3) to identify the specific fluid flow pattern that could cause scaling, (4) to validate the type of scaling in the well through the chemical analysis of scaling rock obtained from the geothermal wellbore of the well "X".

2. Geological Background

In the West Java province, Indonesia, near the Sunda Volcanic Arc, there is a geothermal field of Salak (also known as Awibengkok) (Fig.26). It is encircled by mountains which range in elevation of 950 - 1,500 metres above sea level. The distance of the Salak geothermal field from Jakarta (the capital city of Indonesia) is around 60 kilometres..

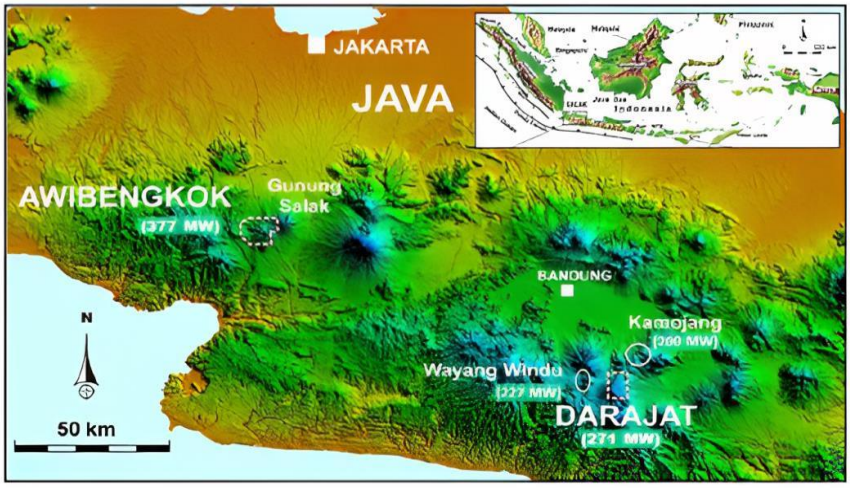

Figure 13. Position of the Awibengkok/Salak geothermal field [15].

The salak geothermal system is mostly liquid and has a fracture-controlled reservoir that has moderate to high temperatures ranging from 464°F to 600°F. The system contains benign fluids with moderate to low non-condensable gas. This geothermal reservoir is connected to recent volcanic activities and intrusions in the highland's region east of the Cianten caldera and west of Salak mountain (D. Yudha et al., 2015).

The recent volcanic vent systems are concentrated along the Cibeureum and Awi faults, which predominantly trend in a north-to-northeast direction with subsidiary northwest and east-west trends. The ancestral andesitic cone that created the edge of the Cianten Caldera

to the west was active around 1610 to 670 ka, while the significant peaks of the Salak area were formed between 860 and 180 ka (Fig. 27).

The Salak geothermal production region has andesite, rhyodacite and lavas that date back from 185 to 280 ka. These are overlain by lavas, rhyolitic domes, and related tephra sequences, which are primarily erupted along a fault trending in a north-northeast direction. The rhyolitic volcanism's age is between 120 and 40 ka based on K-Ar and 40Ar/39Ar dating. At the top, the system has an extensive tephra known as the "Orange Tuff" which dates back between 40,000 and 8400 years before the present (B.P.) according to Stimac et al. (2008). This is bracketed by 14C dates on underlying lahar and overlying hydrothermal breccia units.

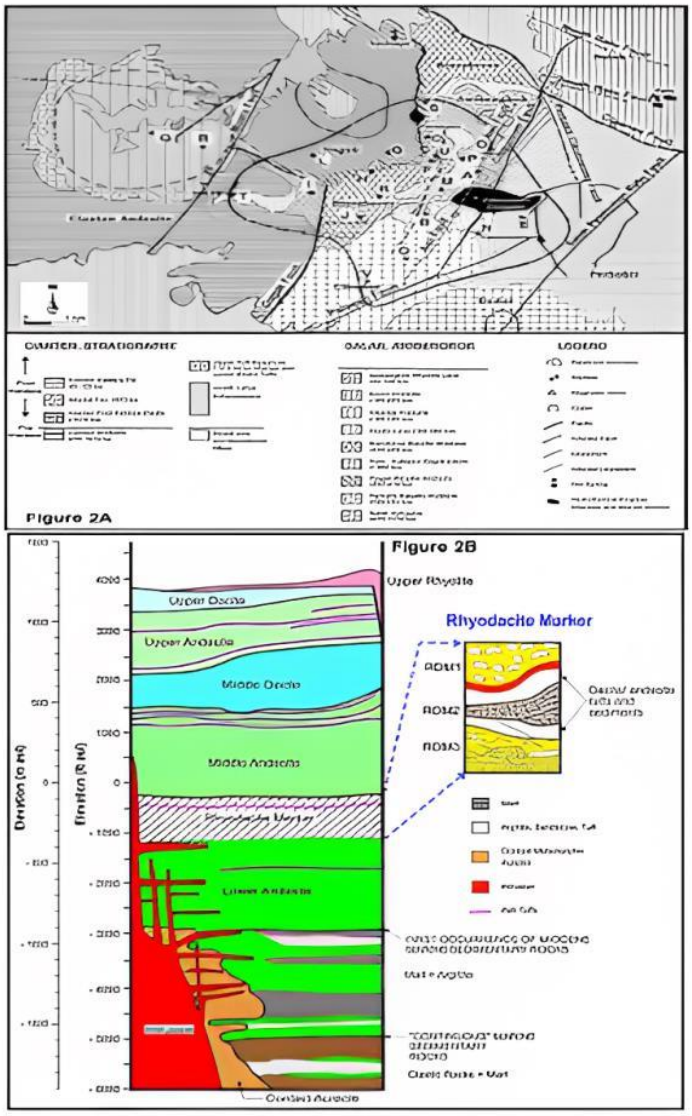

Figure 14. (a) Major rock types, prominent faults, altered ground, current reservoir boundary and well Pad locations of Surface geology of the Salak area, and (b) Representative stratigraphic column for the Awibengkok reservoir. Source: (D. Yudha et al., 2015).

The geothermal reservoir is mainly located within a sequence of volcanic rocks ranging from andesite to rhyodacite. These rocks are underlain by marine sedimentary rocks from the Miocene era, and both types of rocks have been intruded by igneous formations (Ganefianto et al., 2010). The stratigraphic section can be classified into four big formations that correspond to different stages in the evolution of the Sunda Volcanic Arc in western Java.

- The first formation is made up of shallow-marine carbonates and sedimentary rocks.
- The second formation is the Lower Volcanic Formation which consists of andesitic to basaltic volcanic rocks interbedded with sedimentary rocks.

- The third formation is the Middle Volcanic Formation which includes andesitic-to-dacitic lavas, tuffs, lahars, and debris flows. This formation represents the construction, collapse, and erosion of stratovolcanoes and lava dome complexes. This formation also contains silicic rock that represents a period of silicic volcanism and caldera formation.
- The fourth formation is the Upper Volcanic Formation which includes another andesitic sequence overlain by dacitic to rhyolitic rocks, including the surface deposits described earlier.

Each major volcanic formation can be divided into a lower andesitic section and an overlying rhyolitic or dacitic section, representing distinct or partially overlapping volcanic episodes that have become progressively more silicic over time (Fig. 2).

3. Method

The detailed flow chart of this research is presented in Fig. 3.

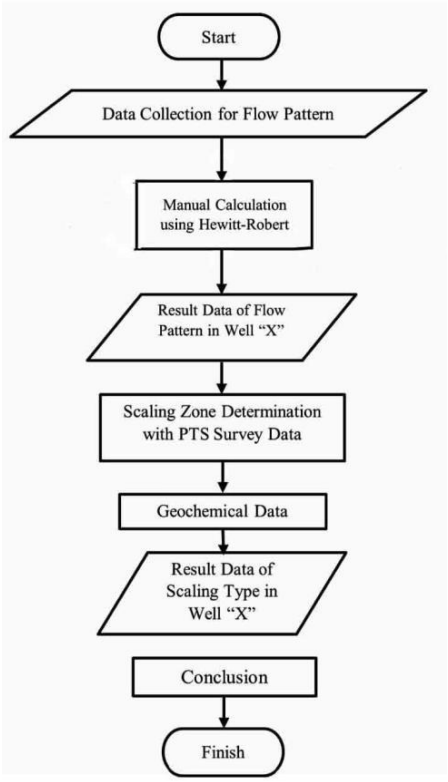

Figure 15. Flowchart of the research

The research utilized data which were collected from the well "X" in the Salak geothermal field. The data include chemical analysis results of the scaling rock, data of the PTS

survey, data of well production, data of wellhead pressure, data of well profile, data of flow rate, and data of casing/piping. After all necessary data had been collected, the data were then analysed to determine the flow pattern using the manual calculation following the Hewitt-Robert method. In addition, the PTS survey data were used to determine the flashing zone's depth, which provided insight into the accumulation zone of scaling in well production casing of well "X". By identifying the location of the flashing zone, it is possible to estimate the depth at which scaling occurs due to changes in temperature, pH, and pressure in the fluid (Sofyan, 2023b). After that, the chemical analysis of scaling rock was conducted to identify the type of scaling. This step was crucial in providing concrete evidence of scaling's existence in the well "X", as it confirmed that scaling was occurring in the specific flashing zone and flow pattern that had been identified earlier.

3.1. The Hewitt-Robert Method

Flow pattern or flow area is one of the important parameters for classifying two-phase fluid flow. Flow pattern specifications are based on the shape or type of flow distribution which generally occurs due to the effects of viscosity, density or surface tension. The determination of vertical flow patterns is currently accomplished through the widely accepted application of logarithmic graphs proposed by Fair (1960) and Hewitt and Roberts (1969) in the field (Thome, 2016).

The flow pattern of fluid in this study was determined manually through the Hewitt-Robert method. This calculation required several data including depth, pressure, enthalpy, flow rate, pipe dryness, and pipe diameter. The pipe cross-sectional area () of the well "X" was calculated using a formula according to the Hewitt-Robert method that include the parameter of constant (3.24) value and the diameter of the inside of the casing (m). The resulting coordinates of the X and Y flow patterns were then used to determine the actual flow pattern in the well "X".

3.2. The Collection and Chemical Analysis of Scaling Rock Sample

The Obstruction Identification were conducted to prove the scaling deposition in the wellbore using the Impression Block method. The tools were lowered down along the wellbore and stuck in the depth of 2,630 - 4,734 ft MD with a white stamp trace on the surface of the

Impression block. This sign indicated the occurrence of scaling deposition in the wellbore as shown in Fig. 29.

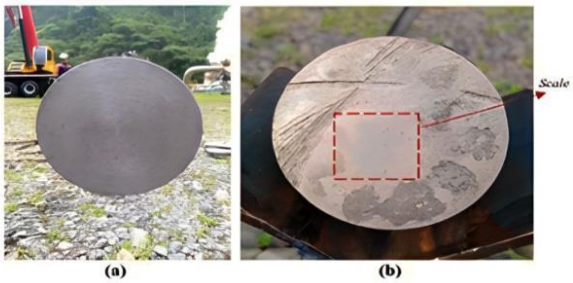

Figure 16. a) Impression block before use and (b) After use with white stamp.

The scaling rock sample was collected from the production liner casing using a sample catcher in the wellbore and then brought to the laboratory for the mineralogical composition analysis. The identification of the main and accessory mineral contents in the samples was carried out through X-ray powder diffraction (XRD) analysis using a Panalytical X'Pert Pro diffractometer with Cu-Kα radiation (λ = 1.54598 Å). Before analysis, the samples were milled in an agate mortar to create powders (Wanner et al., 2017). The powders were then treated with a 2N HCl solution to remove the carbonate fraction. Furthermore, the sample was suspended in ethanol and loaded onto silica plates. Then, the ethanol was evaporated. The XRD analysis was conducted repeatedly. The Panalytical software "High Score Plus" was used to analyses the diffractograms and identify the minerals.

4. Results and Discussion

4.1. The Well 'X' Profile

The well "X" is located in Salak geothermal field. The well is a water-dominated well having a depth up to 5000 ft and producing an energy capacity of 15 MW. As seen in Fig. 30, the well "X" has 20" and 13 3/8" production casings and 10 ¾ production liners.

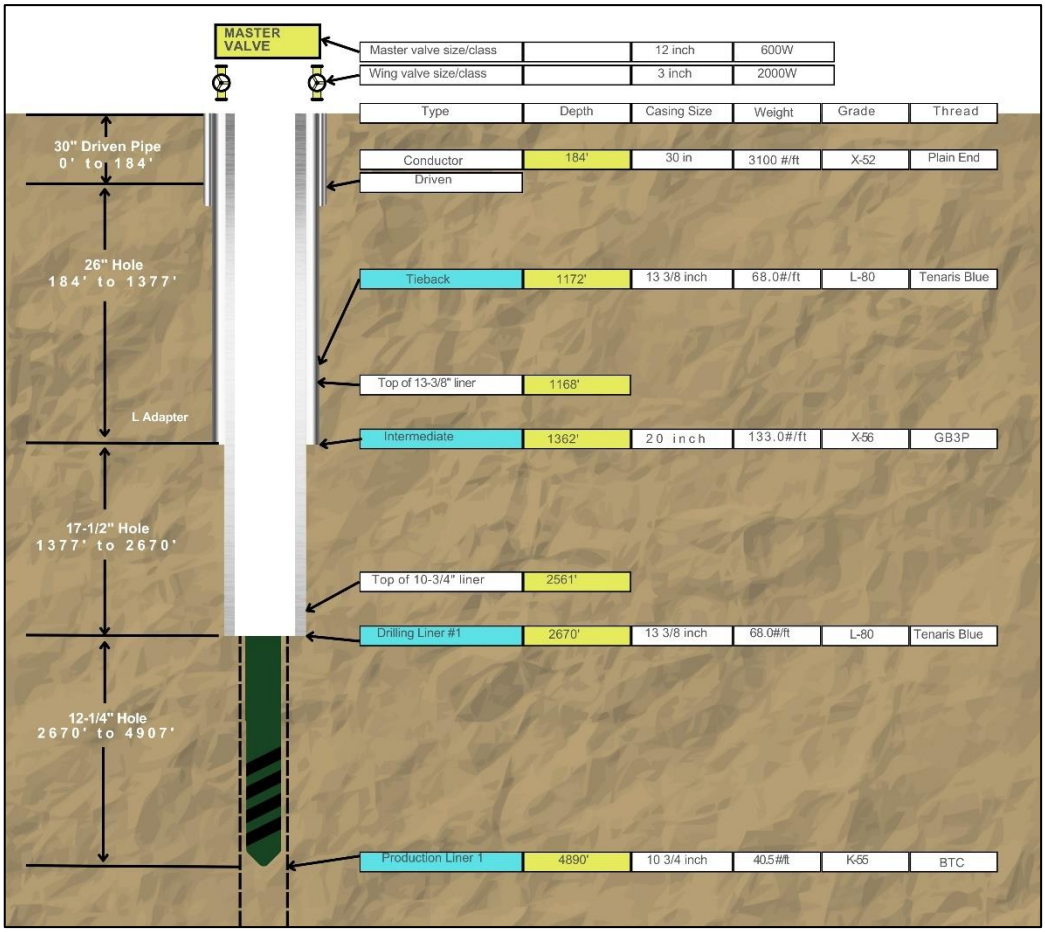

Figure 17. Profile of the Well "X"

4.2. Determination of Fluid Flow Pattern

The Hewitt-Robert calculation method was used to find the vertical fluid flow pattern in the well "X" because the hot water and steam fluid flows move upward (vertically up flow) having a pressure range from atmospheric pressure to 1000 psi (Sofyan, 2023b). The following are the procedures for determining the vertical flow pattern:

4.2.1. Calculation of the cross-sectional area

The cross-sectional area of the flow pipe () which is calculated in this sub-sub-section 4.2.1 is the cross-sectional area of the casing before the wellhead, which is the 13 3/8" production casing having an inner diameter of 7.025 inches. The was calculated through the Equation (1).

$$Ap = \pi \frac{di^2}{4}$$

$$Ap = 3.14 \frac{(7.025\ x\ 0.0254)^2}{4} \quad (1)$$

$$\boldsymbol{Ap = 0.025\ m^2}$$

Where:

Ap = the flow pipe's cross-sectional area (m2).

π = the constant (3.24)

di = The diameter of the inside of the casing (m)

Therefore, based on these calculations, the flow pipe's crosssectional area in the Well "X" was 0.025 m2.

4.2.2. Calculation of the coordinates of the flow pattern map

In this sub-sub-section 4.2.2, Equations (2) and (3) were used to determine the coordinates (X, Y) of the flow pattern map (Thome, 2016). For example, the surface of the well "X" was known to have a dryness (q) = 0.2309, a total mass flow (Mtotal) = 3.7295 kg/s, a cross-sectional area (Ap) = 0.025 m2, a water density (ρl) = 898.0645 kg/m3 and a vapour density (ρg) = 4.0656 kg/m3. Hence, the coordinates (X, Y) can be calculated by the following:

$$X\ Axis = \frac{Gl^2}{\rho l} = \frac{\left((1-x)\frac{Mtotal}{Ap}\right)^2}{\rho l}$$

$$X\ Axis = \frac{Gl^2}{\rho l} = \frac{\left((1-0.2309)\frac{3.7295}{0.025}\right)^2}{898.0645} \quad (2)$$

$$\boldsymbol{X\ Axis = 14.64\ kg/ms^2}$$

$$Y\ Axis = \frac{Gg^2}{\rho g} = \frac{\left((1 - 2309)\frac{3.7295}{0.025}\right)^2}{4.0656} \quad (3)$$

$$\boldsymbol{Y\ Axis = 291.3447\ kg/ms^2}$$

Where:

Y-axis	=	vertical axis (kg/(ms2))
X-axis	=	horizontal axis (kg/(ms2))
Gg	=	mass flux of gas phase flowing alone in the channel (kgm-2s-1)
Gl	=	mass flux of liquid phase flowing alone in the channel (kgm-2s-1)
ρg	=	gas density (kg/m3)
ρl	=	liquid density (kg/m3)
q	=	dryness
Ap	=	the cross-sectional area (m2)
Mtotal	=	total mass (kg/s)

By the same calculation way, the coordinates (X, Y) at various Wellhead pressures in the well "X" was determined and presented in Table 12.

Table 12. Results of Determination of the X and Y axis of the Hewwit-Robert's plot

WHP (Well Head Pressure)			**Wellhead Enthalpy**			**Wellhead**	**Mass Flow**		**Ap**	**Water**	**Steam**		
			Total (hWH)	**Liquid (hfWH)**	**Vapor (hgWH)**	**Dryness**	**Total**			**Density (ρl)**	**Axis X ($Gl^2/\rho l$)**	**Density (ρg)**	**Axis Y ($Gg^2/\rho g$)**
psig	psia	bara	kJ/kg	kJ/kg	kJ/kg	(xWH)	Ton/hour	kg/s	m^2	kg/m^3	$kg/(ms^2)$	kg/m^3	$kg/(ms^2)$
103	114,76	7,81	1190	716,59	2767,3	0,23	13,43	3,73	0,025	898,1	14,64	4,07	291,3
103	114,76	7,81	1190	716,59	2767,3	0,23	14,65	4,07	0,025	898,1	17,43	4,07	346,9
105	116,76	7,94	1190	719,72	2768,01	0,23	13,61	3,78	0,025	897,3	15,10	4,13	291,2
106	117,76	8,01	1190	721,26	2768,36	0,23	13,34	3,70	0,025	897,0	14,53	4,17	275,9
107	118,76	8,08	1190	722,8	2768,7	0,23	13,29	3,69	0,025	896,6	14,46	4,20	270,4
103	114,76	7,81	1190	716,59	2767,3	0,23	13,24	3,68	0,025	898,1	14,25	4,07	283,5
106	117,76	8,01	1190	721,26	2768,36	0,23	12,11	3,36	0,025	897,0	11,99	4,17	227,6
106	117,76	8,01	1190	721,26	2768,36	0,23	10,93	3,04	0,025	897,0	9,76	4,17	185,4
105	116,76	7,94	1190	719,72	2768,01	0,23	11,52	3,20	0,025	897,3	10,82	4,13	208,8
105	116,76	7,94	1190	719,72	2768,01	0,23	17,64	4,90	0,025	897,3	25,39	4,13	489,6

The Hewitt-Robert flow pattern mapping method is useful in determining the vertical flow pattern in well "X" by analyzing the behavior of steam and hot water moving upward under pressures ranging from atmospheric pressure up to 1000 psi. The Hewitt-Robert flow pattern graph provides a visual representation of the flow pattern type by plotting the X and Y-axis parameters. Six types of flow pattern behaviors frequently seen in geothermal wells are "annular", "wispy annular", "bubbly", "bubbly-slug", "slug", and "churn". By plotting the X-axis and Y-axis values (showed in Table 12) on the flow pattern graph, the point of intersection of the X-Y axis and the line of the annular flow pattern is discovered (see Fig. 31). Then, the type of flow patterns at various wellhead pressures is shown in Table 13.

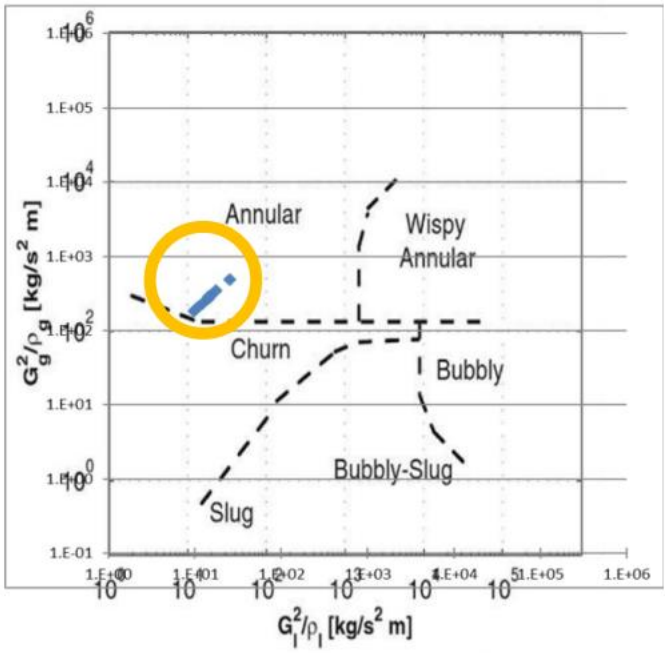

Figure 18. Plotting the coordinates values on the Hewitt-Robert Flow Pattern Graph

Table 13. The Type of Vertical Flow Patterns based on Hewwit Roberts Method

WHP (Well Head Pressure)			**X Axis (Gl2/ρl)**	**Y Axis (Gg2/ρg)**	**Flow Pattern**
psig	**psia**	**Bara**	**kg/(ms^2)**	**kg/(ms^2)**	
103	114.76	7.8068027	14.64107106	291.344736	(Annular)
103	114.76	7.8068027	17.4338968	346.9195691	(Annular)
105	116.76	7.9428571	15.10079162	291.2148845	(Annular)
106	117.76	8.0108844	14.53207693	275.9271044	(Annular)
107	118.76	8.0789116	14.46234854	270.3954626	(Annular)
103	114.76	7.8068027	14.24804011	283.5237579	(Annular)
106	117.76	8.0108844	11.98548328	227.5737811	(Annular)
106	117.76	8.0108844	9.764884544	185.4102706	(Annular)
105	116.76	7.9428571	10.82491858	208.7557721	(Annular)
105	116.76	7.9428571	25.38963209	489.6325282	(Annular)

Based on the analysis of the flow pattern in Well "X" at various wellhead pressures as shown in Fig. 31 and Table 13, it can be inferred that the flow pattern observed is an annular flow pattern, which leads to an increased vapor fraction for all types of wellhead pressures. An annular flow pattern is characterized by fluid flowing in the internal perimeter of the channel in which the gas or vapor has a higher velocity at the center. The annular flow pattern is regarded as the ideal flow pattern in piping systems since it is relatively stable (Thome, 2016). In well "X," the observed flow pattern is an annular flow pattern with a vapor fraction of 100%. This flow pattern is highly desirable as it results in the highest vapor fraction, making it capable of producing large amounts of steam. Moreover, annular flow is known for its stability and safety, making it a preferred choice compared to turbulent flow patterns that can cause irregular flow and significant friction (Ganat & Hrairi, 2019).

4.3. Determination of the Flashing Zone Depth

One of the various geothermal well monitoring procedures that are frequently used to describe the flow along the wellbore is the pressure, temperature, and spinner (PTS) survey (Herianto, 2019). Based on Fig. 32, it indicates that the well "X" is a production well that primarily produces steam fluid. The pressure (shown in blue colour) steadily increases throughout the production casings, from a depth of 4600 ft to the surface of the well “X” (Fig. 32). This indicates that there is no brine flow which could cause pressure fluctuations.

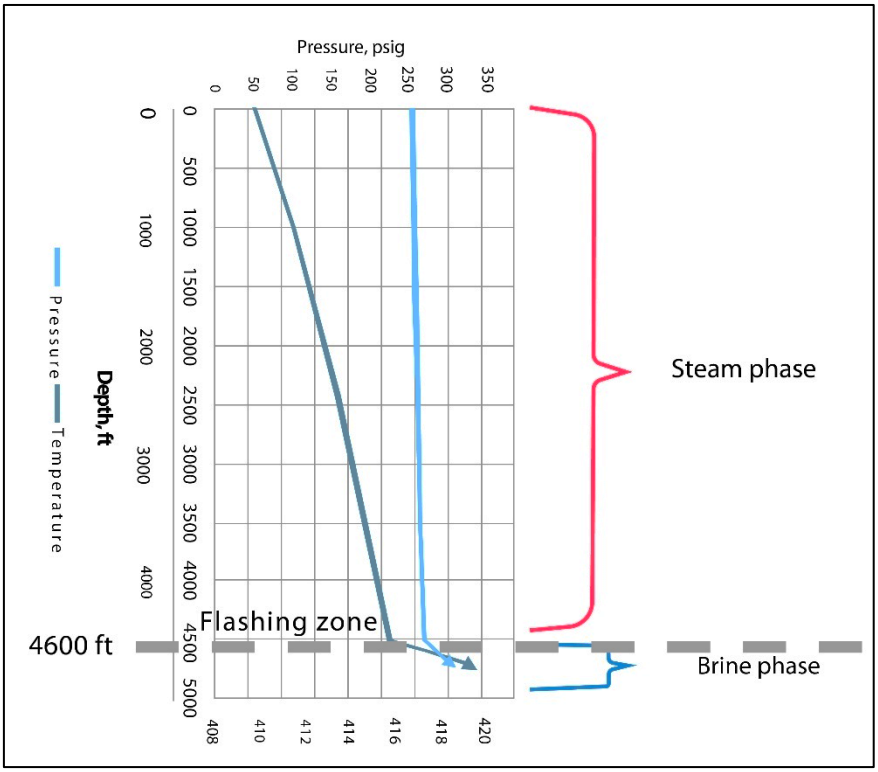

Figure 19. Pressure and Temperature Survey data at Well "X"

However, at depths of 4600 ft to 4800 ft, there is a sudden change in pressure and temperature (Fig. 32), indicating the presence of brine flow at these depths. The flashing zone is predicted to be at a depth of 4600 ft, where there is a pressure drop from 418.5 psig to 416.5 psig because of a difference in diameter of the perforated liner (having a smaller diameter of 7.025 inches) with that of the production casing (having a larger diameter of 13 3/8 inches). This pressure drop results in the release of steam from the brine, a phenomenon referred to as flashing. As a result, the steam fluid that reaches the surface has a high vapour fraction.

The process of flashing in the well "X" has a significant effect on the composition of the brine. When the pressure and temperature decrease during flashing, some of the water in the brine turns into steam, resulting in a higher concentration of scaling compounds. Additionally, the release of gases like CO2 and H2S alters the brine pH and increases ion concentrations. These changes can contribute to the scaling formation in the well “X”, which can negatively affect its productivity and longevity (Solenis, 2021). Therefore, the steam fluid will move more quickly after the flashing area reaches the surface (Sofyan, 2023b).

4.4. Determination of the Scaling Type

In order to ensure a sustained steam production from the well "X", identification of the type of scaling that is formed in the formation and around the liner is crucial. Based on the PTS analysis (sub-section 4.3), there is the presence of a flashing zone that can contribute to scaling. This is due to the drop in pressure and temperature, which results in the release of H2S and CO2 gases, thus affecting the pH of the brine. Therefore, it is essential to confirm the type of scaling formed in the well "X" to prevent a decrease in steam production over time.

Table 14. The results of the chemical analysis of the scaling sample obtained from the well "X"

Element	Well X
Quartz (SiO2)	10
Magnetite (Fe, Mg, Zn, Cu, Ni)(Fe, Al, Cr)2O4	12
Analcime (NaSi22AlO6.H2O)	25
Plagioclase feldspar (Na, Ca)Al(Si,Al)3O8	<3
K-Feldspar KASi3O8	<3
Pyrite FeS2	<5
Amorphous	>40
Unidentified	<5

The scaling sample was analysed in the laboratory to determine the mineralogical composition of the sample. The chemical compositions of the sample are presented in Table 14. Based on the chemical analysis results, the scaling in the well "X" contained primarily amorphous silica material with a weight percentage of greater than 40% (see Table 14). Amorphous silica will form more readily than other silica types at lower temperatures (Tassew, 2001).

A previous study by Zolfagharroshan and Khamehchi (Zolfagharroshan & Khamehchi, 2020) only focused on predicting the scale deposition and modelling the production of the energy using the HOLA software without providing a thorough explanation of the flow pattern associated with scaling in geothermal wells. This study, on the other hand, identified scaling zones and investigated the root causes of scaling by analysing the flow pattern, fluid characteristics, flashing zones, and chemical composition of the scaling rock in the well "X".

5. Conclusion

The conclusions derived from this research are outlined as follows:

a) The analysis of well "X" indicates that the flow pattern formed along the casing series is classified as annular, as determined by Hewitt-Robert calculations.
b) The potential for scaling in well "X" aligns with the identified flow pattern. In the annular flow zone, scaling may occur, with scaling accumulation increasing as the fluid boils on the casing wall.
c) The estimated scaling accumulation zone is located at a depth of 4600 ft, between the casing shoe slotted liners of 7" and 13 3/8".
d) Chemical analysis performed on the scaling sample obtained from well "X" confirms that the scaling type is amorphous silica.
e) This study focuses on determining the flow pattern responsible for scaling and estimating the depth of the
f) flashing zone. To further advance this research, future studies should prioritize the development of methods to
g) prevent and remove scaling within the wellbore.

Additionally, these methods should consider the financial and developmental aspects to achieve more effective and efficient results.

CHAPTER IV

SCALE TREATMENT PLANNING USING BROACHING METHOD IN A VAPOR-DOMINATED GEOTHERMAL WELL X AT KAMOJANG GEOTHERMAL FIELD

Akhmad Sofyan
[1]*Department of Geology, Faculty of Earth Science, University of Szeged, 13 Dugonics Square, 6720 Szeged, Hungary;*
[2]*Department of Oil and Gas Production Engineering Polytechnic of Energy and Mineral Akamigas, Ministry of Energy and Mineral Resources of Republic Indonesia, Jalan Gajahmada No. 38 Cepu, Jakarta 58315, Indonesia*

Rista Jaya
Department of Oil and Gas Production Engineering Polytechnic of Energy and Mineral Akamigas, Ministry of Energy and Mineral Resources of Republic Indonesia, Jalan Gajahmada No. 38 Cepu, Jakarta 58315, Indonesia

Hari Susanto
Pertamina Geothermal Energy Kamojang, Jalan Raya Kamojang Bandung, Garut 44151, Indonesia

Rita Mwendia Njeru
Department of Geology, Faculty of Earth Science, University of Szeged, 13 Dugonics Square, 6720 Szeged, Hungary;

Gábor Bozsó
Department of Geology, Faculty of Earth Science, University of Szeged, 13 Dugonics Square, 6720 Szeged, Hungary;

János Szanyi
Department of Geology, Faculty of Earth Science, University of Szeged, 13 Dugonics Square, 6720 Szeged, Hungary;

Bibliographic Data :
Sofyan, A., Jaya, R., Susanto, H., Njeru, R. M., Bozsó, G., & Szanyi, J. (2025). Scale Treatment Planning Using Broaching Method in a Vapor-Dominated Geothermal Well X at Kamojang Geothermal Field. *Eng*, 6(4), 67. https://doi.org/10.3390/eng6040067

Abstract: Scaling in geothermal production wells poses a critical challenge to sustainable energy production, particularly in vapor-dominated systems where scaling mechanisms are less understood. This study investigates scale treatment planning using the broaching method in Well X at Indonesia's Kamojang geothermal field. Through well integrity testing, geochemical analysis, and XRD characterization, silica (quartz) scale formations were identified in the production casing. Performance monitoring revealed gradual decreases in steam production and wellhead pressure over a three-year period. The selection of the broaching method was validated through analysis of scale characteristics, well geometry, and economic feasibility, offering a significantly more cost-effective solution compared

to conventional methods with a substantially shorter payback period. Broaching has effectively operated on multiple geothermal wells, restoring significant production capacity at approximately half the expense of conventional well workover methods. Our results challenge accepted assumptions on scaling in vapor-dominated systems and provide a methodical framework for scale treatment planning. This study demonstrates how strategic scale management can efficiently preserve well productivity while lowering operating costs, thus enabling sustainable geothermal resource development for operators worldwide.

Keywords: *broaching method; geothermal scaling; Kamojang field; scale treatment planning; vapor-dominated system; well integrity*

1. Introduction

Unconventional oil and gas resources and green energy such as geothermal energy are important energy sources for maintaining sustainable social development (Q. Li et al., 2025). Geothermal energy generation is widely acknowledged as an essential renewable resource, notably in Indonesia, which has substantial geothermal potential exceeding 23.9 GW (Sofyan et al., 2024). This potential, ranging from low to high enthalpy, extends along volcanic paths from Sumatra through Java, Bali, Nusa Tenggara Timur, Sulawesi, to Maluku. As of 2020, Indonesia's installed geothermal power plant (GPP) capacity reached 2130.7 MW, utilizing primarily imported technologies (Tjahjono et al., 2022). Although this clean energy source provides reliable power throughout the year, scaling in geothermal wells poses significant challenges that can impede efficiency and productivity (Boch et al., 2017). Effectively planning scale treatments becomes crucial for maintaining the long-term productivity and economic viability of geothermal operations (Sofyan et al., 2024).

Silica scaling is notably common in geothermal systems, arising when dissolved minerals precipitate as a result of fluctuations in pressure, temperature, and chemical conditions during extraction (Association, 2014; Fukuyama & Feiyang, 2021)bebe.

Research has consistently demonstrated that silica precipitation can markedly decrease the efficiency of geothermal-producing wells, resulting in reduced production rates and increasing operational expenses (Tranter et al., 2021). A study conducted by Setiawan et al. (2019) (Setiawan et al., 2019) demonstrated that the regulation of silica precipitation requires optimal pH and temperature conditions. To minimize scaling in cold re-injection systems, temperatures should be maintained at approximately 40 ◦C, and the pH should be 7 (Setiawan et al., 2019). An understanding of scale formation mechanisms is essential for formulating successful treatment strategies.

Additionally, Boersma emphasizes scale prevention with innovative materials such as glass-fiber-reinforced composites with epoxy or polyethylene inner surfaces, which provide improved scale resistance relative to conventional steel pipes (Boersma et al., 2023). Scale inhibitors, which act as an alternative approach to prevent cation aggregation, must be applied in precise dosing to avert by-product precipitation. Although initial expenses are increased, these sophisticated materials offer a more sustainable approach to scale management. Yet, creating effective inhibitors for silica and heavy-metal sulfides continues to pose difficulties (Kaypakoğlu et al., 2012).

Chemical and material-based strategies provide preventive measures for scaling problems, whilst mechanical interventions such as broaching have proven to be an effective corrective remedy. For example, broaching has effectively operated on 14 geothermal wells, restoring over 22 MW of production at around 50% of the expense of a conventional well workover. This illustrates broaching's capability to sustain operational efficiency while markedly decreasing maintenance expenses, corroborating its designation as a cost-effective option (Wilson et al., 2015).

However, the literature review reveals significant knowledge gaps in vapor-dominated geothermal systems, particularly in scale formation and treatment mechanisms (Vazquez et al., 2024). Despite substantial studies on liquid-dominated systems, there is a lack of comprehensive planning frameworks and economic evaluations for vapor-dominated fields, underscoring the necessity for systematic research that addresses both technical and economic dimensions of scale treatment.

This study identifies significant knowledge gaps and employs a thorough methodology for vapor-dominated systems, incorporating well integrity testing, XRD analysis, and economic assessment. In the case study of Well X at Kamojang, characterized by scale formation at a depth of 900.74 m, with a thickness of 252.7 mm (9.95 inches) and an inclination of 30◦, broaching techniques were optimized alongside a comprehensive economic analysis of treatment methods for vapor-dominated systems.

This study advances academic knowledge and practical applications through five key objectives: developing a comprehensive scale removal methodology using broaching, assessing economic viability, optimizing techniques for specific wells conditions, establishing treatment guidelines, and creating monitoring frameworks. These contributions aim to enhance

geothermal well maintenance efficiency, offering cost-effective solutions while advancing sustainable geothermal resource management.

2. Geothermal System and Tectonic Setting of Kamojang Field

The Kamojang geothermal field, operating since 1983, is located approximately 40 km south of Bandung in West Java, Indonesia. The temperatures range from 15 to 20 ◦C with the annual rainfall reaching 2885 mm (Prasetyo et al., 2021). As Indonesia's first geothermal exploitation site, Kamojang began with a 0.25 MW Monoblock turbine generator at well KMJ-6 in 1978, followed by the first commercial unit of 30 MWe in 1982. The field demonstrates remarkable potential with a current installed capacity of 235 MW across five generating units utilizing a single-flash system (Suryadarma et al., 2010). The power generation is distributed among multiple operators: PT. Indonesia Power manages Units 1, 2, and 3 (with capacities of 30 MW and 55 MW, respectively), while PT. Pertamina Geothermal Energy operates Units 4 and 5 (60 MW and 35 MW). Additionally, the Agency for the Assessment and Application of Technology Indonesia (BPPT) operates a pilot-scale facility (Suryadarma et al., 2010). The reservoir characteristics are distinctive, with temperatures, ranging from 230 to 245 ◦C, and pressures of 30–37 bar, causing geothermal fluid to fluctuate between compressed liquid and superheated states along the saturation line (Pambudi, 2018). In this single-flash system, wellhead fluid exists as a saturated liquid before entering a separator where pressure reduction leads to phase separation, maintaining constant enthalpy while increasing entropy (Ameri & Shamshirgaran, 2006). Despite being traditionally considered less prone to scaling compared to liquid-dominated systems, recent studies have revealed significant scaling problems that potentially affect long-term production sustainability (Sofyan, 2023b).

Located within the western Indonesian archipelago, the Kamojang geothermal system emerges from the dynamic convergence between the Indian–Australian Ocean Plate and the Eurasian Continental Plate (Pena-Castellnou et al., 2019).

The tectonic evolution of the region since the Eocene has resulted in unique structural patterns throughout Indonesia's principal islands. Sumatra exhibits oblique subduction accompanied by a corresponding fault system (Sieh & Natawidjaja, 2000). Java, on the other hand, has a perpendicular subduction pattern that has created unique east–west trending physiographic zones (Ahnaf et al., 2018; Gunnlaugsson et al., 2014; Haryanto, 2020). The

tectonic architecture of Java demonstrates distinctive structural patterns (A. & Martodjojo, 1994) characterized by three primary lineament systems: the Meratus Pattern (northeast–southwest), Sunda Pattern (north–south), and Java Pattern (east–west). These structural elements have shaped the development of an extensive magmatic belt from the Late Eocene to Quaternary periods. This belt features diverse magmatic compositions ranging from tholeiitic series to calc-alkaline and shoshonitic varieties (Soeria-Atmadja et al., 1994).

One of the forty identified geothermal prospects in the region is the Kamojang geothermal field, which is situated within the quaternary volcanic belt of West Java (Setijadji, 2010). Geothermal activity in the region is primarily concentrated in two main zones: the salak corridor and the Galunggung–Tangkuban Prahu belt (Figure 33). Within the Pleistocene age of the Pangkalan caldera structure, Kamojang, along with the Darajat and Wayang Windu systems, comprise the Kendang volcanic complex (Rejeki et al., 2004).

An east–west trending volcanic chain defines the local geology, encompassing several volcanic edifices: Mt. Rakutak, Ciharus Lake, Pangkalan Lake, Mt. Gandapura, Mt. Guntur, and Mt. Masigit. Volcanic activity in the region spans from 1.2 to 0.452 Ma, as determined by radiometric dating (Rejeki et al., 2004). The volcanic sequences predominantly consist of basaltic to andesitic compositions (Yudiantoro et al., 2013), with the main thermal up-flow zone centered in the Kamojang area (Yudiantoro et al., 2013).

The hydrothermal system of the field exhibits complicating alteration patterns indicative of both acidic and neutral pH environments (A. R. Utami et al., 2025; P. Utami, 2000). A specific vertical zonation pattern encompasses argillic and propylitic domains (Y. D. Tavip & Kamah, 2023). The distribution of clay minerals in the argillic zone is governed by temperature. Kaolin is produced below 120 ◦C, smectite forms below 150 ◦C, and smectite–illite assemblages develop beyond 200 ◦C. Various forms of silica, particularly quartz, are present in various regions. This indicates the presence of active silica transport pathways, which may lead to scaling problems throughout production.

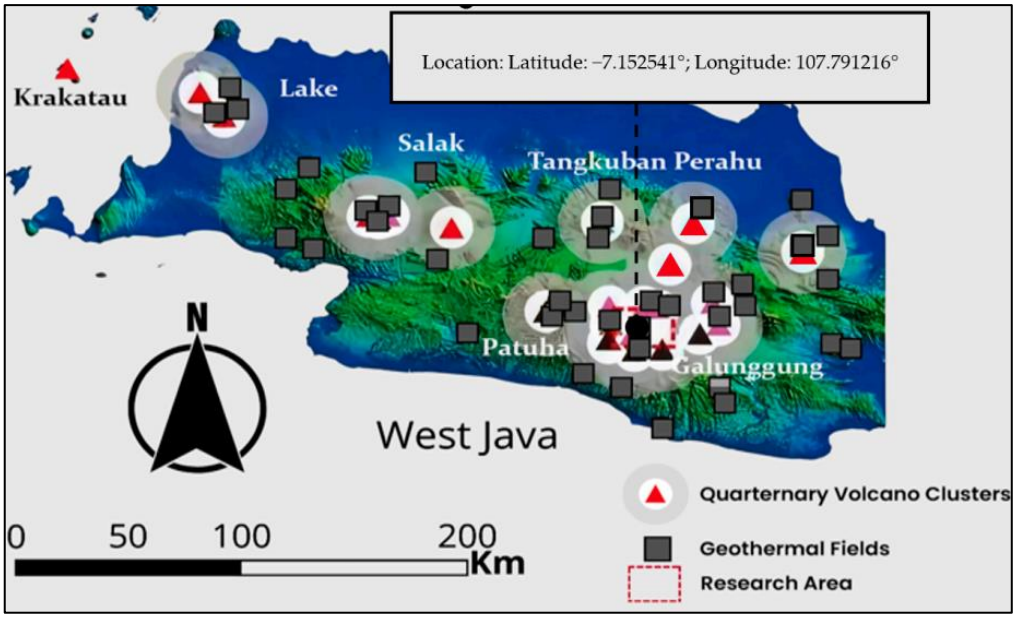

Figure 20. Distribution of the Quaternary volcano segment's boundary zone in West, Central, and East Java Island (Latitude: −7.152541°; Longitude: 107.791216°) (Modified from [2].

3. Material and Methods

This chapter outlines the scientific framework utilized to examine scaling issues in geothermal wells, specifically concentrating on Well X in PT. Pertamina Geothermal Energy Area Kamojang. The research technique includes methodical approaches to data collecting, analysis, and assessment, offering a thorough understanding of scaling phenomena and associated treatment choices in geothermal well operations

3.1. Research and Location

The research was conducted at PT. Pertamina Geothermal Energy Area Kamojang, situated in Laksana, Ibun, Bandung, West Java (Figure 34). This site was strategically selected because of its substantial scale formation challenges and its exemplification of vapor-dominated geothermal systems. This study included field data gathering under diverse operating settings and enabled a comprehensive understanding of scaling phenomena in geothermal well operations.

Among the production wells studied in this field, Well X, as shown in Figure 3, is classified as a big hole type. The well is situated at an elevation of 1,483 meters above sea level and reaches a measured depth (MD) of 2,501 meters, with a true vertical depth (TVD) of

2,225.26 meters. The reservoir conditions indicate a pressure of 26.5 bar and a temperature of 230°C. These specifications characterize Well X as a significant production asset in the geothermal field, providing essential baseline parameters for analyzing its performance and scaling issues.

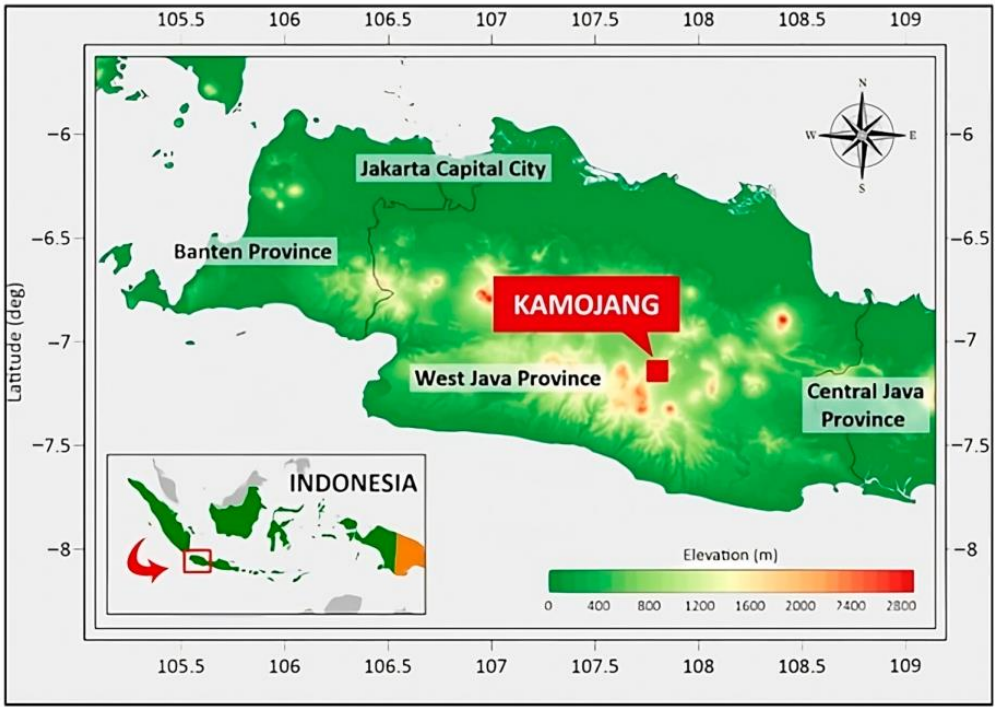

Figure 21. Location of Kamojang Geothermal Field.

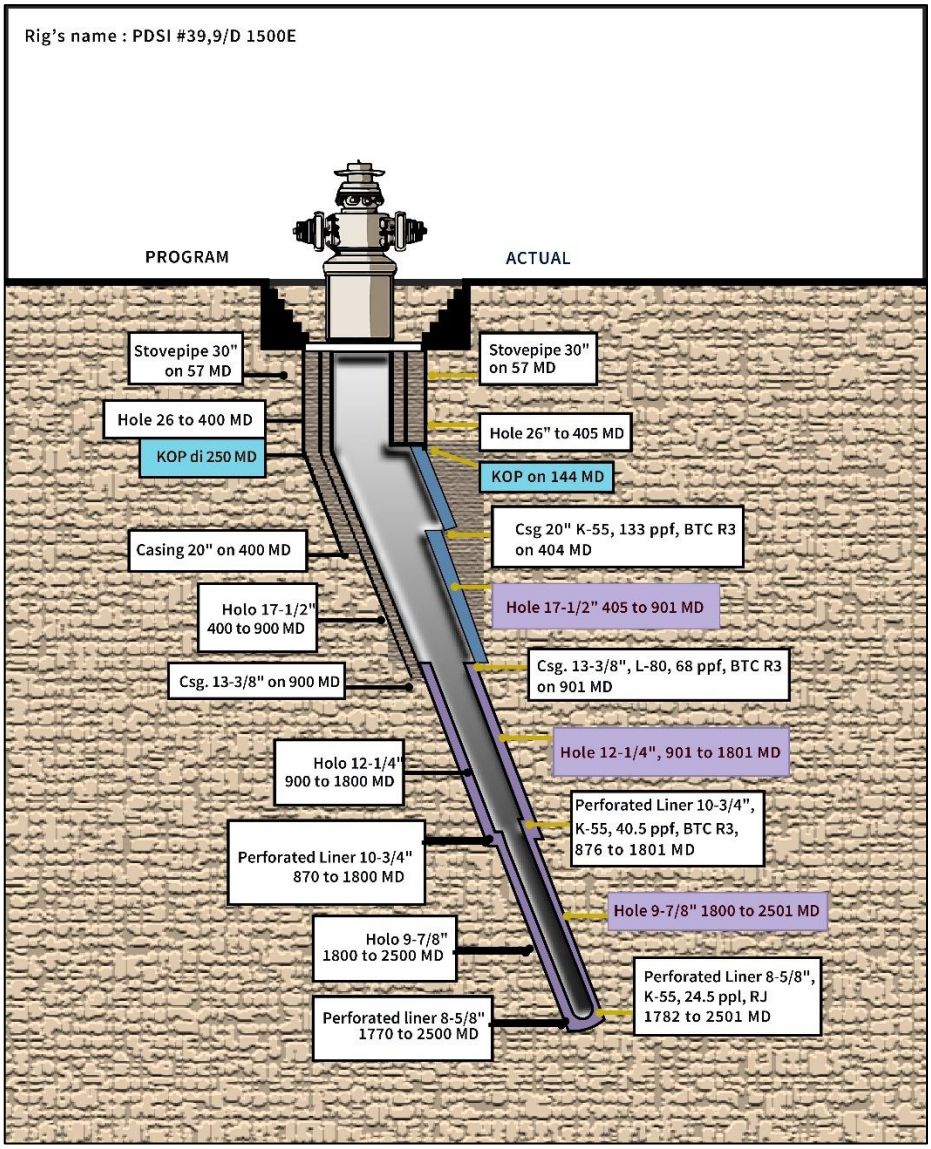

Figure 22. Well X Profile.

3.2. Research Methods

This study implemented an integrated methodological approach integrating quantitative data evaluation, laboratory analysis, and field observations. Direct field measurements, well integrity testing, scale sample collecting, and geochemical fluid sampling were the primary data-collecting procedures (Arnórsson et al., 2006). Secondary data from past treatment records, historical well performance records, and relevant technical specifications were added to these main data sources. This holistic methodology guaranteed data validity through several verification techniques and allowed a thorough study of scaling issues.

Figure 36 illustrates the systematic progression of the research, which commenced with an initial assessment and literature review to establish foundational knowledge on geothermal scaling mechanisms. This was followed by field data collection, including well integrity testing through Go-Devil operations and sample catcher deployments to retrieve scale samples at precise depths (900.74 m). Subsequent phases focused on laboratory analysis, where scale samples underwent geochemical characterization, XRD analysis, and scale type determination to identify silica (quartz) as the primary deposit. These analytical outcomes informed the treatment method selection, where the broaching method was validated as optimal based on technical feasibility, economic viability (USD 42,690 vs. conventional methods), and compatibility with the well's 30◦ inclination. The final stages involved broaching method design, tailored to the casing geometry and scale thickness 252.7 mm (9.95 inches), and implementation planning to ensure operational safety and efficiency.

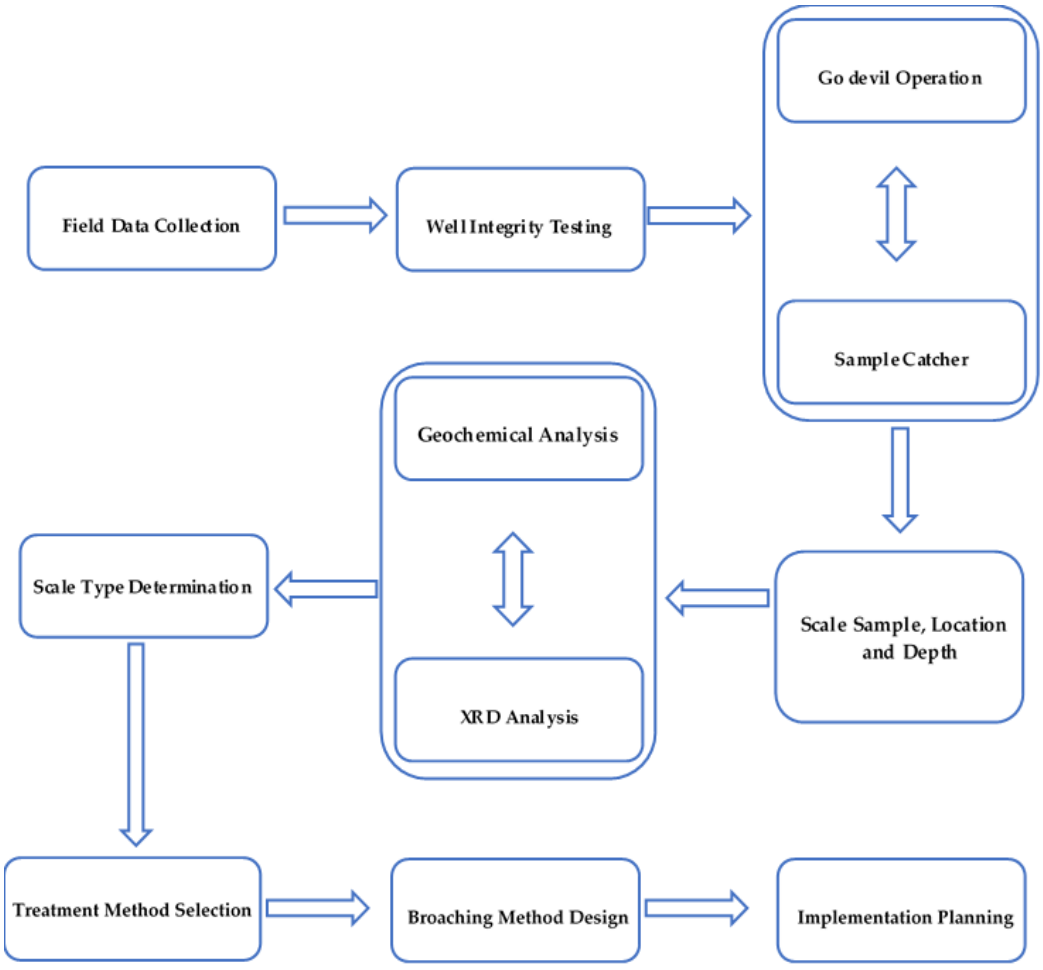

Figure 23. Research flow diagram

3.2.1. Geochemical Sampling

Steam from production wells serves as the primary resource for power generation at this geothermal facility (Sofyan et al., 2021). The wells produce high-quality single-phase steam with 98.9% dryness, essential for efficient power generation (T.-L. Li et al., 2022). PGE Kamojang's laboratory conducts regular steam sampling and analysis using four main testing methods to maintain optimal performance. The comprehensive analysis includes cation measurement using ICP and AAS instruments, anion testing through Ion Chromatography (with titration as an alternative for high chloride samples), gas content analysis via Gas Chromatography or acid titration, and CO_2 base analysis using spectrophotometry with a focus on ammonia content (Bragulla et al., 2023)bragb. This systematic testing protocol ensures the steam meets quality standards necessary for efficient power generation and equipment protection.

At the Kamojang geothermal field, a comprehensive sampling protocol encompasses steam and gas collection from production wells. Steam sampling is conducted during well operation, with the single-phase dry Total Flow Steam (TFS) collected directly from the steam pipeline and condensed into polyethylene bottles (ASTM, 2004; Muravyev, 2022) This approach is tailored to the unique characteristic of Kamojang, which produces exclusively single-phase dry steam.

Gas sampling occurs concurrently with well operation, employing a direct collection method without separation. The procedure utilizes a T-rod assembly directly linked to the side valve or connected via specific sampling points along the steam pipeline. The gas is directed into collection vessels containing a 35% sodium hydroxide (NaOH) solution, which ensures effective capture and preservation of gas components for subsequent analysis as shown in Figure 37 (Rahayudin et al., 2020).

Figure 24. Gas sampling collection

All sampling procedures follow ASTM D1066-97 standard methodology, ensuring consistency and reliability in sample collection and analysis. This standardized approach enables accurate steam quality assessment and maintains proper quality control protocols (ASTM, 2004).

These regular quality checks help maintain optimal operating conditions, prevent equipment damage, and ensure consistent power generation performance. The testing program provides essential data for daily operations and long-term maintenance planning, ultimately supporting sustainable geothermal power production.

3.2.2. Scale Analysis Methods

Scale analysis encompassed multiple analytical approaches to characterize the scaling phenomena comprehensively. Mineral composition was identified through XRD analysis, while formation mechanisms were assessed through the correlation of operational parameters and geochemical data. The severity of scaling was evaluated through well performance indicators and physical measurements, enabling quantitative assessment of scale impact on well productivity. Production data

analysis included a detailed examination of well performance trends, pressure and flow rate correlations, and decline curve analysis, providing crucial insights into the scale formation patterns and their operational impacts. In addition to this method, water samples were analyzed for cations (K, Na, Mg, Ca, Li, B) using Inductively Coupled Plasma–Optical Emission Spectrometry (ICP-OES) and for anions (SO_4, F, Cl, NO_3) using ion chromatography. Gas samples were analyzed using gas chromatography for unreactive gasses (H_2, Ar, N_2, CH_4) and titration methods for reactive gasses (CO_2, NH_3, H_2S). Besides that, the analytical methodology involved non-chemical sample preparation through agate mortar grinding and oven drying, followed by bulk XRD analysis of materials collected via the 5.5″ sample catcher in well "X" locations in the Kamojang geothermal field. The samples were analyzed using a Rigaku MiniFlex II (Cu Kα radiation, λ = 1.5418 Å, operating at 30 kV and 15 mA). Diffraction patterns were collected over a 2θ range of 5–80° with a step size of 0.02° and a scan speed of 0.5°/min. The data were analyzed using Jade® 9.0, and mineral identification was performed using the COD-Inorg 2023.12.05 (Crystallography Open Database). Quantitative phase analysis (QPA) was conducted via the Rietveld refinement method to determine the weight percentages of crystalline phases.

3.2.3. PHREEQC Analysis

The chemical water samples were used for chemical thermodynamic modeling with PHREEQC 3.7.3.15968. The PHREEQC software simulation provided saturation index (SI) values for various minerals that might form in the brine samples. These SI values show how saturated different minerals are in the brine, which helps us understand the potential for scaling. The SI values come from the geochemical field data we collected earlier. This analysis gives us a more detailed look at which minerals in the brine might cause scaling problems.

3.3. Data Collection and Analysis Procedures

Treatment method selection followed a systematic evaluation process incorporating multiple criteria. Technical feasibility was assessed based on well conditions and scale

characteristics, while economic considerations encompassed immediate implementation costs and long-term operational implications.

4. Results and Discussion

4.1. Scale Formation Indicators in Well X

4.1.1. Analysis of Wellhead Pressure (WHP) Decline Indicators

Initial evidence of scaling in Well X was identified through the systematic monitoring of wellhead pressure decline over specific periods. This pressure reduction can be attributed to wellbore diameter constriction and increased frictional resistance caused by scale deposition. This analysis outlines the WHP patterns recorded in Well X during three successive monitoring periods, illustrating the temporal progression of pressure decrease characteristics. The pressure monitoring data provides crucial diagnostic information for evaluating the progression of scale formation within the wellbore system.

The evolution of wellhead pressure data, as shown in Figure 38, reveals a notable declining trend beginning in 2021. This pressure reduction may be attributed to scaling formation or other well integrity issues. The observed WHP decline could stem from multiple factors such as reservoir depletion, wellbore integrity issue, scale formation, etc. However, comprehensive well integrity testing was conducted, to definitively attribute this pressure reduction to scale formation (Bedrikovetsky et al., 2009).

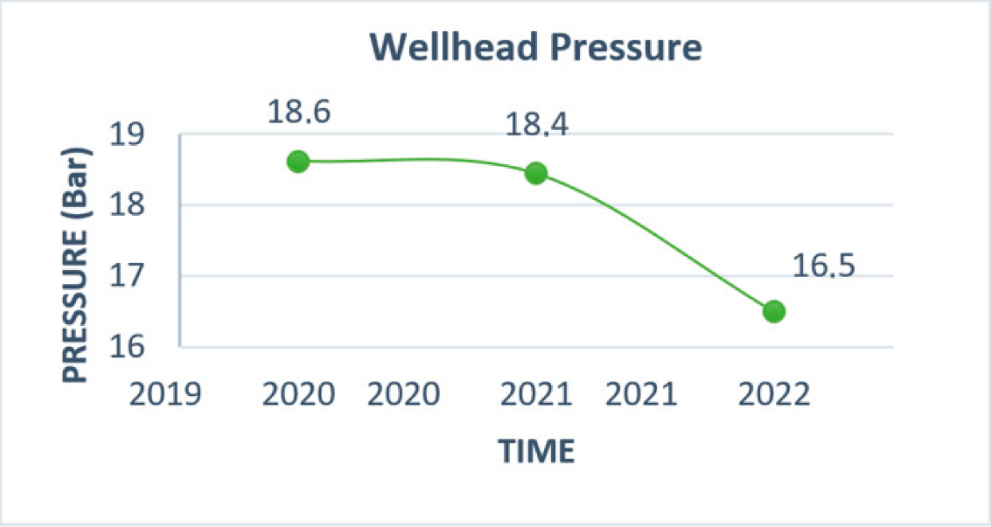

Figure 25. Evolution of wellhead pressure trends in Well X in the last 3 years.

4.1.2. Analysis of Production Decline Characteristics

Figure 39 illustrates the correlation study between steam flow rate and wellhead pressure trends. The plotted data reveals that while steam production rates showed a moderate decline of approximately 8.9% over three years, a notable reduction in wellhead pressure was observed in 2022. The small decrease in production at Well X creates an uncertain diagnostic situation. The existing production data alone provides no conclusive evidence to ascribe the performance decline, especially to scaling phenomena. Consequently, thorough well integrity testing was considered essential to validate the root cause of the observed changes and conclusively determine the presence and effects of scale formation (Bedrikovetsky et al., 2009).

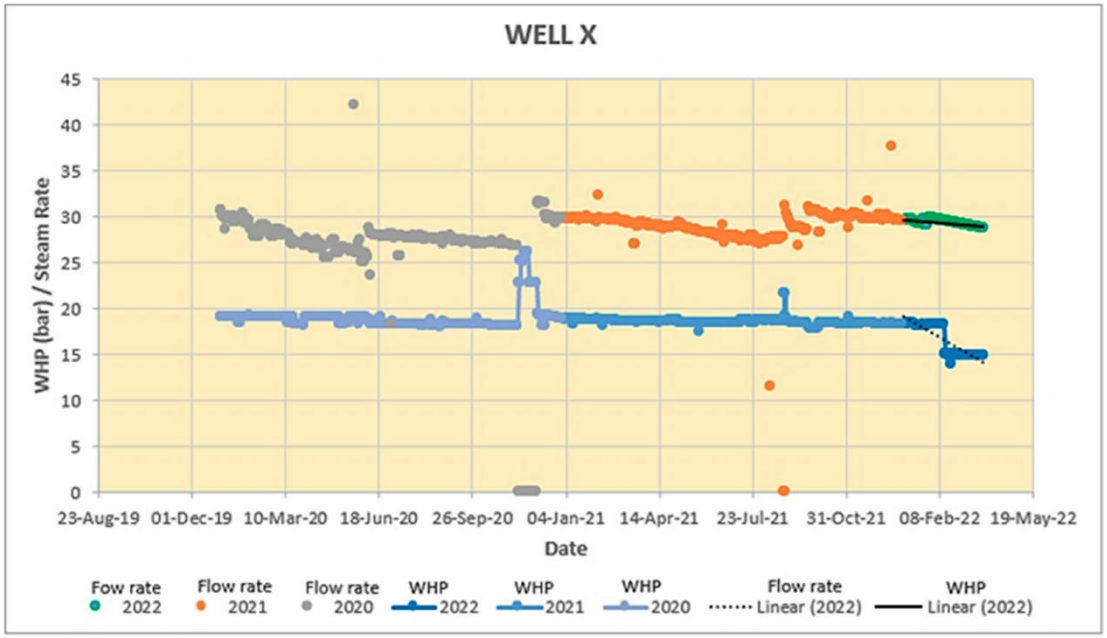

Figure 26. Production decline trends in Well X.

4.2. Scale Formation Assessment Through Well Integrity Testing: Go-Devil and Sample Catcher Analysis

Well integrity testing was conducted to verify scaling issues in Well X, determine the precise depth of scale deposits, and obtain physical samples for laboratory analysis of scale composition (Y. Li et al., 2020). The investigation was conducted on Well X, which features a well architecture comprising multiple casing strings: a 762 mm (30

inches) conductor casing extending from the surface to 30 MD, 508 mm (20 inches) surface casing reaching 390 MD, and a 339.7 mm (13-3/8 inches) production casing that extends to 901 MD. The lower section consists of a 273.05 mm (10 3/4 inches) liner extending from 901 to 1800 MD, and a 219.075 mm (8 5/8-inches) liner from 1800 to 2500 MD, culminating in a total measured depth of 2500 MD (true vertical depth of 2225.26 MD). The kick-off point of the well is located at 250 MD. The well integrity assessment program employed a 203.2 mm (8 inches) go-devil tool, chosen following the existing casing dimensions. The investigation focused on the complete wellbore length of 2500 MD, with measurements taken over a duration of approximately two hours during a shut-in period. This evaluation offered diagnostic data on scale accumulation and physical samples for further laboratory analysis (Cheng et al., 2021).

4.2.1. Analysis of Go-Devil Measurement Results

Go-devil operations were implemented as a diagnostic tool to identify wellbore diameter anomalies and constrictions by analyzing tool movement and sticking points at various depths (Othman et al., 2022) as shown in Figure 40. The initial setting depth of the tool serves as a primary indicator of wellbore constriction zones. The diagnostic assembly consisted of multiple components carefully selected for optimal performance and reliable data collection. The tool string configuration included a 45 cm go-devil tool (5.40 kg), a 200 cm jar assembly (7.25 kg), a 10 cm socket (0.40 kg), a 45 cm extension sinker (1.95 kg), and a 20 cm bull nose (0.90 kg) (Figure 40). The operation utilized a slickline with specifications of 23.37 mm (0.92 inches) and 2.74 mm (0.108 inches) diameters, rated for maximum tensions of 640 kg and 930 kg, respectively, ensuring operational safety and measurement accuracy.

Figure 27. Well integrity assessment using go-devil.

The well integrity assessment utilized a carefully designed tool assembly measuring 3.2 m in total length. This assembly integrated five essential components: a 45 cm go-devil tool, 200 cm jars, a 10 cm socket, a 45 cm extension, and a 20 cm bull nose. The complete assembly weighed 15.00 kg, with weight distribution across components as follows: go-devil tool (5.40 kg), jars (7.25 kg), socket (0.40 kg), extension (1.95 kg), and bull nose (0.90 kg).

The initial diagnostic operation took place from 02:00 to 03:30 GMT, utilizing a 203.2 mm (8 inches) go-devil tool. In the initial Run-In-Hole (RIH) phase, the tool descended smoothly to a maximum depth of 900.04 m, encountering no obstacles. However, the Pull-Out-Of-Hole (POOH) phase demonstrated notable wellbore constrictions. The tool was immobilized at a depth of 900.04 m, necessitating several jar-up operations for its retrieval. A second obstruction was encountered at 369.07 m, which was similarly addressed through repeated jarring operations. Upon overcoming these obstacles, the tool was successfully retrieved to the surface without additional incidents.

A subsequent operation was performed from 16:10 to 17:10 WIB using a 63.5 mm (2.5 inches) sinker. This procedure achieved a slightly deeper penetration to 901.00 m and, notably, encountered no obstructions during either the descent or retrieval phases. The scale in the well depth illustrated in Figure 41 provides crucial data points for mapping the

scale formation zones and characterizing the extent of wellbore constrictions, essential information for planning future well intervention strategies (Pudyaksa et al., 2019).

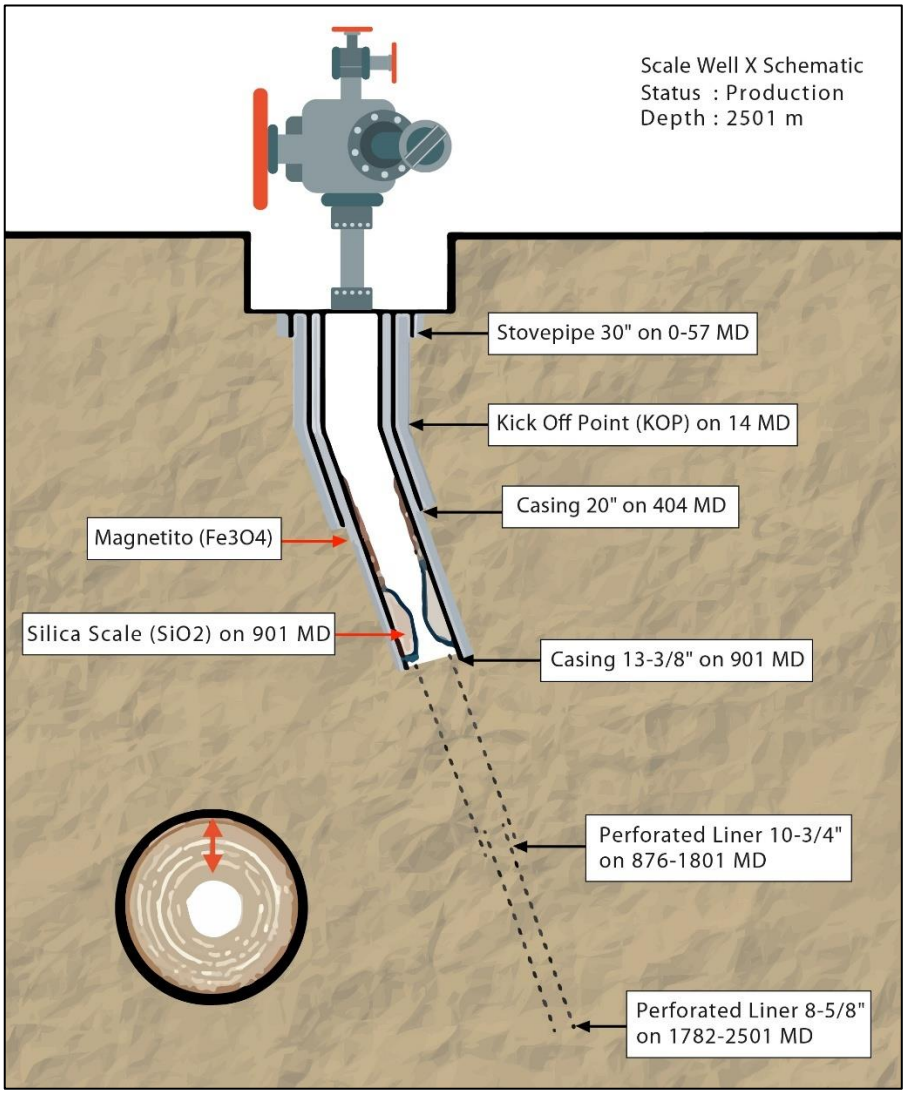

Figure 28. Scale Well X schematic.

4.2.2. Analysis of Sample Catcher Measurement Results

After identifying scale deposit anomalies at 900.74 m, a systematic sampling operation was conducted utilizing two distinct sample catcher configurations. The initial sample collection employed a 139.7 mm (5.5 inches) sample catcher, targeting the scale formation at 900.04 m. This was followed by a second sampling phase

using an 88.9 mm (3.5 inches) sample catcher, specifically designed to collect samples at 900.74 m. The sampling procedure was conducted over approximately four hours to ensure comprehensive sample collection and tool manipulation at both target depths.

A comprehensive scale sampling operation was conducted utilizing two distinct tool configurations to ensure thorough sample collection at the identified scale formation depth. As shown in Table 15 and Figure 42, the initial deployment employed a 139.7 mm (5.5 inches) scale catcher assembly, engineered with a total length of 3.35 m and comprising five integrated components: a 60 cm scale catcher (3.50 kg), 200 cm jars (7.25 kg), a 10 cm socket (0.40 kg), a 45 cm extension (1.95 kg), and a 20 cm bull nose (0.90 kg), yielding a total assembly weight of 13.1 kg.

Figure 29. Sample catcher 5.5″ and 3.5″.

Table 15. Data tool scale catcher.

Data Tools Sample Catcher SC		
Tools	**Length**	**Weight**
Scale Catcher 5.5”	60 cm	3.50 kg
Scale Catcher 3.5”	60 cm	2.00 kg
Jars	200 cm	7.25 kg
Socket	10 cm	0.40 kg
Extention sinkers	45 cm	1.95 kg
Bull Nose	20 cm	0.90 kg
Slickline 0.92”. Max Tension 640 kg 0.108”. Max 930 kg		

The first sampling operation, conducted from 04:30 to 05:45 GMT, successfully reached the target depth of 900.74 m, retrieving both solid scale deposits and fluid

samples. During the retrieval phase, the tool encountered significant resistance at two distinct points: 900.04 m and 369.07 m, necessitating repeated jarring operations to overcome these obstacles. A subsequent operation utilizing an 88.9 mm (3.5 inches) scale catcher (Figure 43) assembly of identical length but reduced weight (12.5 kg) was performed from 13:50 to 15:10 WIB, targeting the same depth. While this second run encountered similar obstruction points during retrieval, it did not yield additional samples.

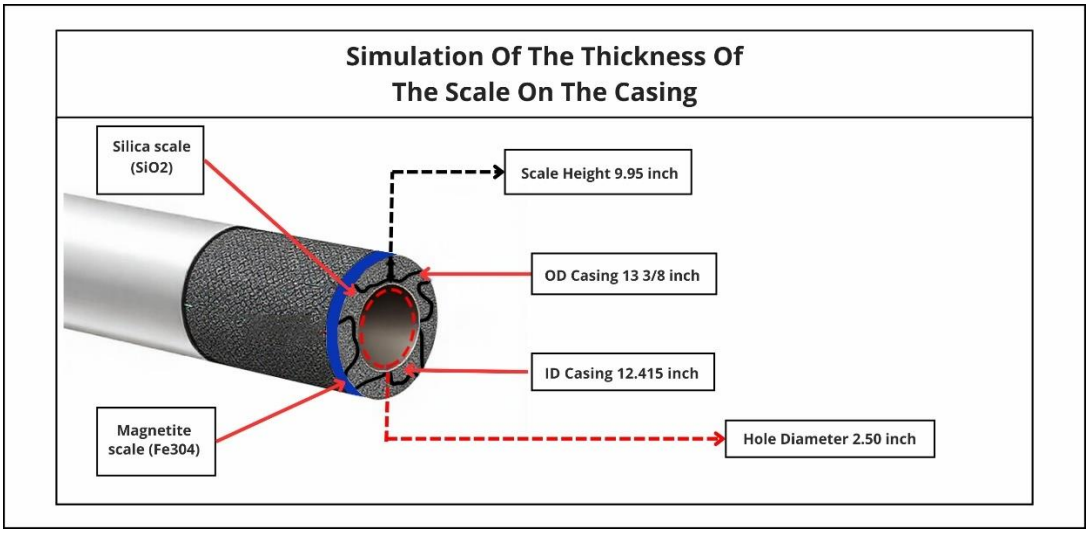

Figure 30. Scale thickness simulation analysis in Well X production casing.

The physical analysis of the retrieved samples indicated the presence of distinctive white layered scale deposits, approximately 1 cm in size, collected from an environment with a wellhead pressure of 24.9 bar and a temperature of 205.17 °C. The fluid observed in the 139.7 mm (5.5 inches) tool samples was linked to wellbore condensation processes, as recorded by PGE Kamojang, offering a further understanding of the downhole environmental conditions. The findings, along with the consistent depth of mechanical obstacles encountered during both runs, support the existence and characteristics of scale formation at the specified depths.

4.2.3. Well Schematic Analysis of Scale Deposition Points Based on Well Integrity (Go-Devil) Measurements

The comprehensive well integrity assessment conducted on Well X revealed detailed characteristics of scale deposition through systematic diagnostic operations.

The initial deployment of a 203.2 mm (8 inches) go-devil tool identified a significant restriction at 900.74 m, which was subsequently confirmed through successful scale sample retrieval at the identical depth, definitively establishing the upper boundary of scale formation. A secondary diagnostic run utilizing a 63.5 mm (2.5 inches) go-devil tool penetrated marginally deeper to 901.00 m, effectively delineating the lower boundary of the scale accumulation zone and providing crucial vertical profiling of the deposition pattern.

An analysis of the production casing configuration ((339.7 mm (13-3/8 inches) L-80, 68 ppf, BTC R3) and scale formation characteristics indicated significant internal diameter reduction. The casing specifications disclose an outer diameter of 339.7 mm (13.375 inches) and an inner diameter of 315.3 mm (12.415 inches). The remaining effective internal diameter was determined to be 251.8 mm (9.915 inches) through a precise calculation methodology that included go-devil measurement data and casing specifications, indicating a significant scale thickness of 251.8 mm (9.915 inches). The scale deposits were identified primarily as silica-based formations, aligning with the geothermal well environment and its operational history.

This detailed structural mapping and dimensional analysis, as illustrated in the well schematic (Figure 41) and scale thickness simulation (Figure 43), provides essential technical parameters for future well intervention strategies (Wein et al., 2019). The precise delineation of scale accumulation zones, coupled with quantitative thickness measurements, establishes a robust foundation for designing targeted scale removal operations and implementing effective well-stimulation programs (Davoody et al., 2019). These findings represent critical baseline data for maintaining the well's integrity and optimizing future production performance through informed intervention planning.

4.3. Scale Formation Assessment Through Geochemistry and XRD Analysis

Understanding scale formation in geothermal wells requires a systematic analysis of fluid chemistry and mineral composition. This assessment combines geochemical sampling techniques with advanced X-ray diffraction (XRD) analysis to provide a comprehensive

characterization of scale deposits and their formation mechanisms (Jamero et al., 2018). The integration of these methodologies enables the accurate identification of scale composition and its relationship to well-fluid chemistry, essential for developing effective scale management strategies.

4.3.1. Geochemistry Result and Scaling Prediction

The geochemical evolution observed in the Kamojang geothermal field from July 2019 to November 2021 reveals significant implications for mineral scaling phenomena as shown in Table 16. The decline in pH from 4.75 to 4.04, coupled with fluctuating total dissolved solids (0.69–2.15 mg/L), indicates dynamic reservoir conditions. As shown by Scott et al. (2024), silica polymerization kinetics are influenced by both pH and the degree of supersaturation of the geothermal fluid (Scott et al., 2024).

Table 16. Fluid geochemistry Well X.

Well Name	KMJ-X	KMJ-X	KMJ-X	KMJ-X	KMJ-X	KMJ-X	KMJ-X	KMJ-X
Type of Well	PROD	PROD	PROD	PROD	PROD	PROD	PROD	PROD
Sampling Date	21-Jul-19	27-Aug-19	28-Nov-19	27-Mar-20	08-Dec-20	18-Mar-21	10-Aug-21	09-N0v-21
Conductivity µS/cm	16.60	23.55	24.60	27.00		20.00	21.00	25.00
pH at TEMP 25˚	4.75	4.60	4.51	4.31	3.91	4.41	4.32	4.04
TDS (ppm)	1.28	1.13	0.80	0.82	2.15	1.28	0.96	0.69
Sodium (Na) (ppm)	0.20	0.10	0.04	0.03	0.03	0.08	0.03	0.03
Potassium (K) (ppm)	0.20	0.10	-	-	-	-	-	-
Calcium (Ca) (ppm)	0.05	0.05	-	-	-	-	-	-
Magnesium (Mg) (ppm)	0.05	0.05	0.01	0.01	0.02	0.02	0.02	0.02
Lithium (Li) (ppm)	0.05	0.05	-	-	-	-	-	-
Ammonium (NH_4) (ppm)	1.73	2.16	-	-	-	-	-	-
Iron (Fe) (ppm)	0.01	0.05	0.07	0.01	0.43	0.03	0.02	0.03
Fluor (F) (ppm)	0.21	0.20	0.26	0.20	0.21	0.29	0.30	0.21
Bicarbonate (HCO3) (ppm)	7.44	9.24	-	-	-	-	-	-
Chloride (Cl) (ppm)	0.01	0.14	0.09	0.11	0.04	0.79	0.10	0.05
Sulfate (SO_4) (ppm)	0.67	0.84	0.35	0.52	1.51	0.32	0.45	0.35
Hydrogen Sulfide (H_2S) (ppm)	16.63	26.53	-	-	-	-	-	-
Boron (B) (ppm)	4.76	4.82	4.19	3.97	5.31	4.24	5.21	4.60
Silica (SiO_2) (ppm)	0.05	0.06	0.24	0.14	0.18	0.06	0.41	0.26

Notably, the non-condensable gas composition (Table 16) exhibits predominant CO_2 concentrations (93.96–95.84%) and a substantial hydrogen sulfide content (2.24–3.25%), with total gas concentrations exhibiting an increasing trend from 0.56% to 0.72%. These geochemical transitions potentially exacerbate scaling mechanisms through dual pathways: CO_2 degassing-induced pH perturbations generate localized supersaturation zones conducive to mineral precipitation, while hydrogen sulfide presence facilitates nucleation sites for scale formation (Clark et al., 2020).

Table 17. NCG composition in Well X

Date	**CO_2**	**H_2S**	**NH_3**	**Ar**	**N_2**	**CH_4**	**H_2**	**Air Cont**	**Total NCG**
	% moles								(% wt)
28/11/2019	93.96	3.25	0.03	0.01	0.93	0.13	1.69	-	0.56
27/02/2020	95.02	3.06	0.06	0.00	0.54	0.11	1.21	-	0.61
08/12/2020	95.84	2.54	0.05	0.00	0.55	0.08	0.93	0.01	0.71
19/03/2021	95.06	3.00	0.05	0.01	0.59	0.09	1.20	0.00	0.65
10/08/2021	95.57	2.24	0.05	0.00	0.71	0.12	1.31	0.01	0.72

Based on Table 17, the analysis results indicate that the brine samples in the surface have the potential to form several minerals, as calculated by PHREEQC software using its available mineral database. Although many types of minerals were analyzed, only a few have saturation index (SI) values above zero, indicating potential for scaling formation. The minerals with SI values above zero in the brine samples are Goethite and Hematite.

Table 18. PHREEQC analysis.

Phase	SI	**log lAP**	**log K{443 K, S atm)**	
Anhydrite	-4,85	-11,15	-6,30	CaS04
Aragonite	-7,30	-17,80	-10,50	CaC03
Ca lcite	-6,42	-17,80	-11,38	CaC03
CH4(g)	-62,12	-64,96	-2,84	CH4
Cha lcedony	-3,66	-6,08	-2,42	Si02
Chrysotile	-20,73	-0,80	19,93	Mg3Si205(0H)4
C02(g)	-1,84	-3,92	-2,08	C02
Dolomite	-12,37	-35,39	-23,02	CaMg(C03)2
Fe(OH)3(a)	-5,52	-0,63	4,89	Fe(OH)3
FeS(ppt)	-60,27	-64,19	-3,91	FeS
Fluorite	-6,03	-16,26	-10,23	CaF2
Gypsum	-5,80	-11,15	-5,35	CaS04:2H20
H2(g)	-18,16	-21,07	-2,92	H2

H20(g)	0,88	0,00	-0,88	H20
H2S(g)	-57,15	-65,51	-8,36	H2S
Halite	-13,27	-11,62	1,65	NaCl
Jarosite-K	-15,17	-31,89	-16,72	KFe3(S04)2(0H)6
Mackinawite	-59,54	-64,19	-4,65	FeS
Melanterite	-11,91	-13,41	-1,50	FeS04:7H20
02(g)	-15,77	-18,75	-2,98	02
Pyrite	-96,43	-112,19	-15,77	FeS2
Quartz	-3,54	-6,08	-2,54	Si02
Sepiolite	-23,87	-10,67	13,20	Mg2Si307,50H:3H20
Sepiolite(d)	-29,32	-10,67	18,65	Mg2Si307,50H:3H20
Siderite	-8,58	-20,06	-11,48	FeC03
Si02(a)	-4,17	-6,08	-1,91	Si02
Smithsonite	-7,92	-18,96	-11,04	ZnC03
Sphalerite	-53,45	-63,09	-9,64	ZnS
Sulfur	-43,81	-41,21	2,60	s
Sylvite	-13,24	-11,85	1,39	KCI
Talc	-23,25	-12,96	10,29	Mg3Si4010(0H)2
Willemite	-8,57	-1,24	7,33	Zn2Si04
Zn(OH)2(e)	-9,08	2,42	11,50	Zn(OH)2

a. Goethite (FeO(OH))

Goethite is an iron mineral that can form under certain conditions in water or brine containing iron. Goethite tends to precipitate at specific pH levels, especially in environments with relatively high oxygen contents.

b. Hematite (Fe2O3):

Hematite is an iron oxide mineral that can also form in brine with high iron concentrations under specific conditions. Hematite is commonly found in oxidizing environments and has the potential to form scales on pipe surfaces or equipment.

Based on the analysis showing that both minerals have SI > 1, this indicates that these minerals could precipitate from the brine solution if the environmental conditions support it (e.g., temperature, pressure, and brine chemical composition). The formation of goethite and hematite in the system could lead to scaling, which in turn could affect fluid flow, process efficiency, and the lifespan of the equipment used.

4.3.2. XRD Analysis and Result

X-ray diffraction (XRD) analysis was employed to characterize scale deposits in Well X, utilizing a systematic analytical protocol comprising mechanical pulverization and digital diffractogram interpretation (Clark et al., 2020; Khanfar & Sitepu, 2021). The investigated scale specimens retrieved from the production casing at 900.74 m depth under specific thermodynamic conditions (24.9 barg, 205.17 °C), exhibited distinctive morphological features: predominantly white coloration with brownish-black sections and laminar structure approximately 1 cm in dimension.

XRD analysis of scale samples from Well X (sample code LB21017-1) definitively identified two distinct mineral phases: quartz (SiO_2) and magnetite (Fe_3O_4) as shown in Figure 44. The diffraction patterns, as illustrated in the analytical curve, confirmed the presence of these crystalline phases, with characteristic peaks corresponding to both minerals. Based on the mineralogical distribution analysis, the predominant scale type in Well X is classified as silica scale, primarily due to the presence of quartz, a principal silica mineral. The co-occurrence of magnetite (Fe_3O_4) suggests a complex scaling mechanism involving both siliceous and ferrous components. This silica scaling phenomenon typically occurs due to pressure and temperature changes during fluid ascent in the wellbore, where the solubility of silica decreases significantly as the geothermal fluid cools and depressurizes. The process is further enhanced when fluid temperature drops below 340 °F (171.1 °C), causing dissolved silica to precipitate as amorphous silica, which eventually crystallizes into quartz (Clark et al., 2020; Jamero et al., 2018). The presence of magnetite suggests concurrent iron oxide precipitation, possibly due to oxidation reactions in the production system. This mineralogical assemblage indicates that the scaling mechanism is primarily driven by thermodynamic changes in the wellbore (Hajirezaie et al., 2019; Sojková et al., 2024), requiring careful consideration of pressure and temperature management for effective scale prevention strategies.

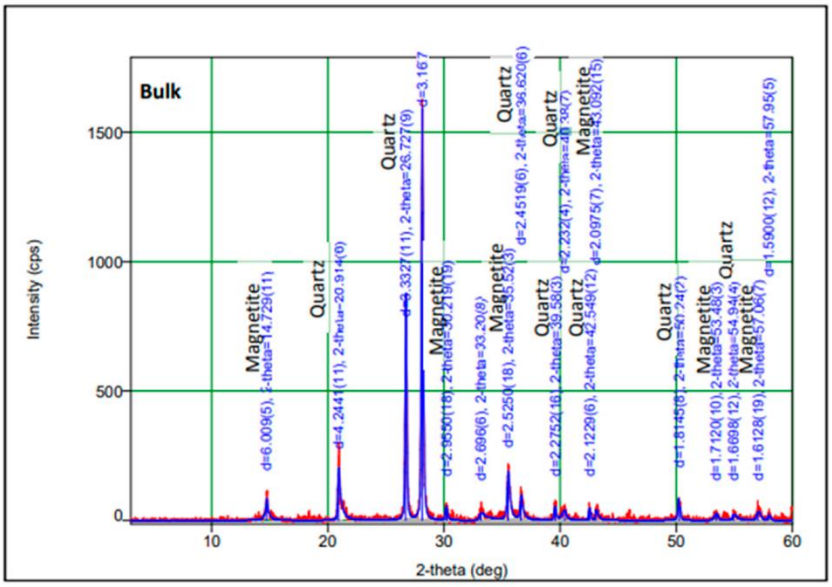

Figure 31. XRD mineral scale result

The result is that the geothermal operation at Well X in the Kamojang field is characterized by a dynamic interplay of geochemical, thermodynamic, and environmental factors, where silica (quartz) scaling predominates at a depth of 900.74 m within the 339.7 mm (13-3/8 inches) production casing, driven by the rapid reduction in pressure from 26.5 bar in the reservoir to 16.49 bar at the wellhead, and cooling from reservoir temperatures of 230–245 °C to a surface temperature of 199 °C as the fluid ascends. These conditions significantly reduce silica solubility, triggering its precipitation as quartz deposits in the wellbore. Meanwhile, discrepancies between the downhole XRD results, which identify silica (quartz) and magnetite (Fe_3O_4) as the dominant scale components, and the surface-based PHREEQC predictions, which indicate potential precipitation of goethite (FeO(OH)) and hematite (Fe_2O_3), underscore the influence of differing environmental conditions: reducing conditions at depth favor the formation of magnetite, while oxidizing conditions at the surface, combined with oxygen exposure during sampling and the chemical evolution of the brine, promote the precipitation of ferric iron minerals such as goethite and hematite.

4.4. Determination of Scale Cleaning Stimulation Methods

The selection of appropriate well-scale cleaning methods in geothermal operations is a complex process that necessitates careful consideration of several critical

factors. Various cleaning techniques are employed, including reaming, high-pressure water injection (roto jet), acidizing, and broaching, each with specific applications depending on the operational context (Yenice & Dünya, 2007). Extensive field experience, particularly in the Kamojang geothermal field, has identified three primary factors that significantly influence the selection of these methods.

The first factor is the type and hardness of the scale present. Different scales, such as ammonium bicarbonate, silica, and calcite, exhibit varying hardness levels and thicknesses, which dictate the choice of cleaning method (Davoody et al., 2019). For instance, chemical cleaning is effective for removing ammonium bicarbonate scales, while silica and calcite scales can be addressed through methods such as broaching, roto jets, mechanical reaming, coiled tubing, or acidizing. In cases of particularly hard scales, mechanical methods such as reaming are preferred (Guo et al., 2015; Mavredaki et al., 2007; Wilson et al., 2015). This evidence observed in the use of abrasive water jet (AWJ) technology has been shown to significantly reduce the time required for reaming compared to conventional methods, as demonstrated in the Gonghe geothermal well (Guo et al., 2015). For example, in Well X, which has a silica scale (Quartz SiO_2) with a column height below 1 m and a thickness of approximately 228.6 mm (9 inches), the broaching method has been deemed suitable based on these physical characteristics.

The second critical factor is the well deviation and the location of the scale deposits. Directional wells with high deviation angles present unique challenges for stimulation methods that involve string assemblies (Wilson et al., 2015). Such assemblies may encounter maneuverability issues at the kick-off point (KOP), increasing the risk of collisions and casing leakage. Field experience has shown that broaching operations should be avoided in wells with a deviation exceeding 50 degrees, as the operational risks become significantly increased (Elwan et al., 2024).

The third and arguably most crucial factor is the operational costs associated with the cleaning methods as seen in Table 19 and Table 20. The economic viability of the broaching method is demonstrated through comparative revenue analysis. With an initial investment of USD 42,690, the intervention restored Well X's steam production from 28.71 to 31.50 tons/hour. Assuming a plant availability factor of 35% (accounting for operational downtime and maintenance), the daily revenue increased by USD 431.22

(steam price: USD 18.40/ton). This results in a monthly revenue gain of USD 12,936.63, yielding a payback period of 3.3 months. In contrast, conventional methods (USD 628,147–USD 1,195,339) would require 4–10 years for cost recovery under similar conditions. Broaching's rapid return on investment, coupled with reduced downtime, establishes it as the optimal scale treatment solution for Well X. The economic efficiency of these methods plays a pivotal role in decision-making processes. It is essential to balance the cost of implementation against the potential production improvements that result from the cleaning operations. Expensive methods that yield low success rates or minimal production enhancements can severely strain company resources (Jarrahian et al., 2024). Therefore, a thorough evaluation of the cost structures of various cleaning methods and their expected outcomes is necessary to ensure economic viability (Jamero et al., 2018).

Table 19. Scale stimulation cost comparison (Flores Armenta et al., 2015; Wilson et al., 2015).

Stimulation Method	**Cost**
Drilling equipment	US$. 1,195,339
Coiled Tubing Hole cleaning	US$. 866,181
Bull heading	US$. 628 147
Broaching	US$. 42,690

Table 20. Cost prediction breakdown for the broaching method.

Cost Component	**Cost (US$)**	**Details**
Broaching Tools	5,000	Single-use tools (3.5"–5.5", as specified in Table 9).
Slickline unit Mobilization	15,000	1 day of rig time at $15,000/day.
Labor	8,000	2 technicians × 2 days × $2,000/day.
Fluid Circulation	2,000	Brine or water used for debris flushing during operation.
Well Downtime	12,690	1 day of lost production: 689 tons/day × $18.40/ton (steam price).
Total Cost	**42,690**	Sum of all components.

4.5. Planning for Broaching Scale in Well X

Scale broaching planning in Well X is conducted to evaluate the method's feasibility and establish operational guidelines for future company implementations. The effectiveness of this

method relies on three critical operational parameters that require continuous monitoring. The first parameter is wireline speed (ft/min), which must be precisely controlled during descent and ascent operations to prevent line failure due to excessive or insufficient velocity. The second parameter is depth (ft), which requires constant surveillance to track the broaching tool's position and identify scale locations within the wellbore. The third and most crucial parameter is tension (lbs), which measures the stress experienced by the wireline (Wilson et al., 2015). Tension typically increases proportionally with depth but exhibits a characteristic of decreases when the tool encounters scale deposits. During jarring operations, tension displays a distinctive oscillating pattern. The definitive indicator of scale detection is a decrease in tension, signifying the broaching tool's contact with scale deposits, at which point jarring operations are immediately initiated to remove the obstruction.

4.5.1. Requirements for Broaching Operations to Be Used in a Well

The feasibility of broaching operations is determined by three critical factors: scale composition, scale thickness within the casing, and well deviation. In terms of scale composition, broaching can effectively remove calcite and silica deposits, although operational difficulty increases with scale hardness and thickness (Wilson et al., 2015). In Well X's case, the scale characteristics fall within acceptable parameters for broaching implementation. Regarding scale thickness within the casing, Well X exhibits a constriction that reduces the internal diameter to approximately Broaching 63.5 mm (2.5 inches), which remains within operational limits for various broaching tool sizes, making the mechanical scale removal viable. Well X's deviation represents another crucial consideration, as highly deviated or horizontal wells significantly complicate broaching operations and reduce their effectiveness. Well X's deviation angle and kick-off point (KOP) are within acceptable limits for successful broaching operations. The aforementioned factors suggest that broaching is an appropriate method for scale removal in Well X.

4.5.2. Determination of Broaching Based on Well X's Deviation Angle

The deviation analysis of Well X demonstrates optimal geometric conditions for broaching operations. As shown in Figure 45 (a) and (b), the well's architecture begins its deviation at a Kick-Off Point (KOP) of 144 MD, extending to a total depth of 2501 MD. The deviated section length, calculated as the difference between total depth and KOP (2501—144

MD), yields 2357 MD. Through trigonometric analysis using the cosine relationship (cos 30° = TVD/2357), the true vertical depth is determined to be 2041 MD, derived from the equation TVD = 2357 × ½√3. The well's primary deviation parameter, characterized by an inclination angle (α) of 30 degrees, falls significantly below the critical threshold of 50 degrees, the maximum allowable deviation for effective broaching operations (Elwan et al., 2024).

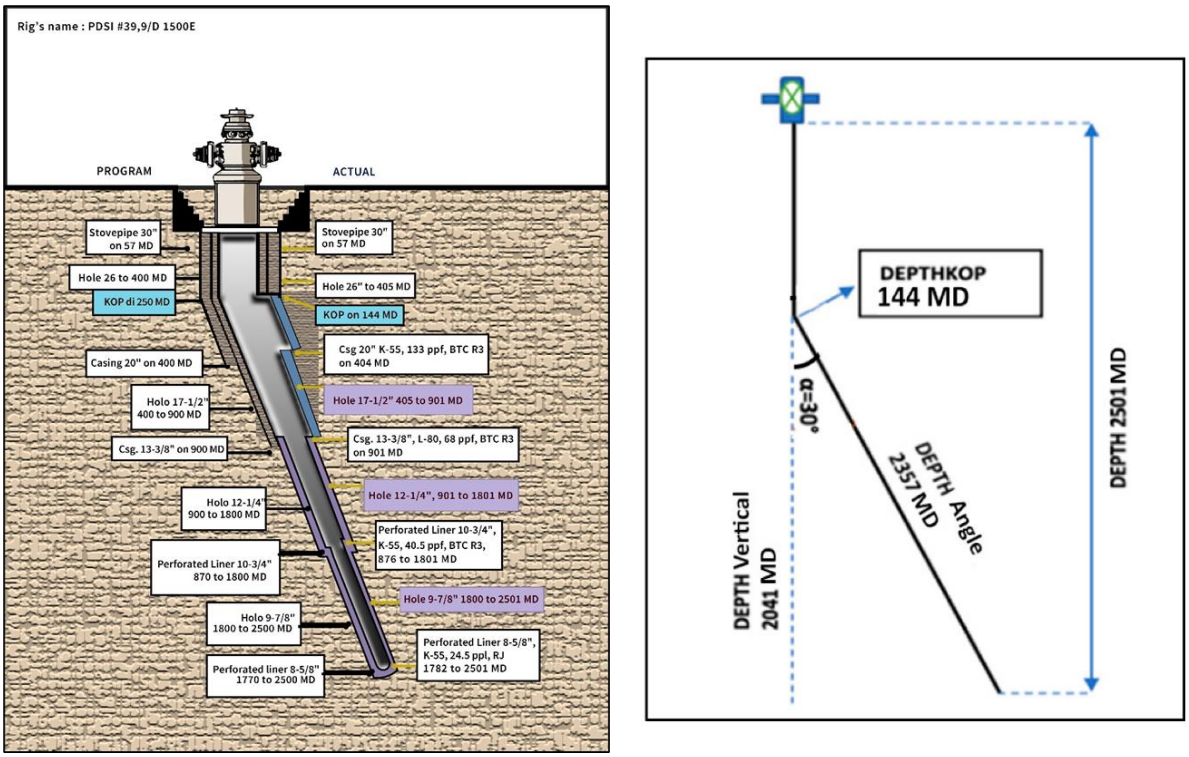

(a) (**b**)

Figure 32. (a) Well X profile; (b) Well X's deviation angle (KOP).

This geometric configuration, which maintains a 20-degree margin below the operational limit, facilitates optimal conditions for broaching tool deployment, scale removal efficiency, and overall operational success. The moderate deviation angle of the well facilitates effective tool weight transfer and mechanical advantage for scale removal while reducing the risks of tool binding and uneven load distribution.

4.5.3. Pre-Job Planning

Successful broaching operations require comprehensive well data analysis before execution. Essential documentation includes casing records, downhole surveys, PTS logs for flashpoints, wellhead schematics, and identification of problematic zones, including casing

damage or debris (Aka et al., 2020; Wilson et al., 2015). Critical operational parameters such as flow rates and wellhead pressures must also be established. The success of the intervention heavily depends on effective communication and data sharing, between steamfield operators and slickline personnel, as this collaboration minimizes operational risks associated with the uncertain data.

4.5.4. Determination of Broaching Target Depths Based on Well Schematic Review

The well's schematic analysis provides critical guidance for broaching operations by precisely identifying scale formation zones within specific casing sections. As illustrated in Figure 46, a detailed examination of scale deposition patterns against casing architecture enables accurate targeting of intervention depths. This systematic evaluation maps the scale accumulation location, facilitating proper tool selection and operational planning while accounting for casing specifications and potential mechanical constraints. The well schematic serves as the primary reference document, ensuring precise depth correlation and optimal execution of broaching operations.

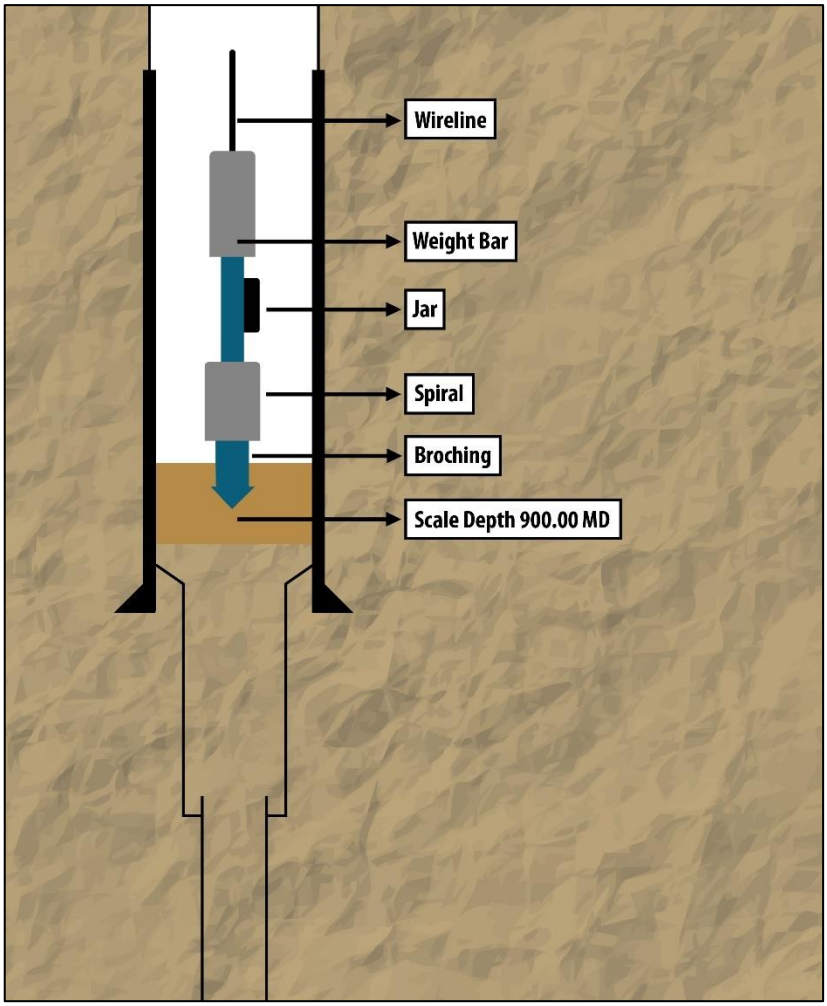

Figure 33. Broaching scale target points in Well X.

4.5.5. Broaching Tools

Broaching equipment is categorized into two groups: surface and subsurface equipment, where surface equipment connects to subsurface equipment through wireline cable as shown in Table 21 and Table 22, and Figure 47 and Figure 48.

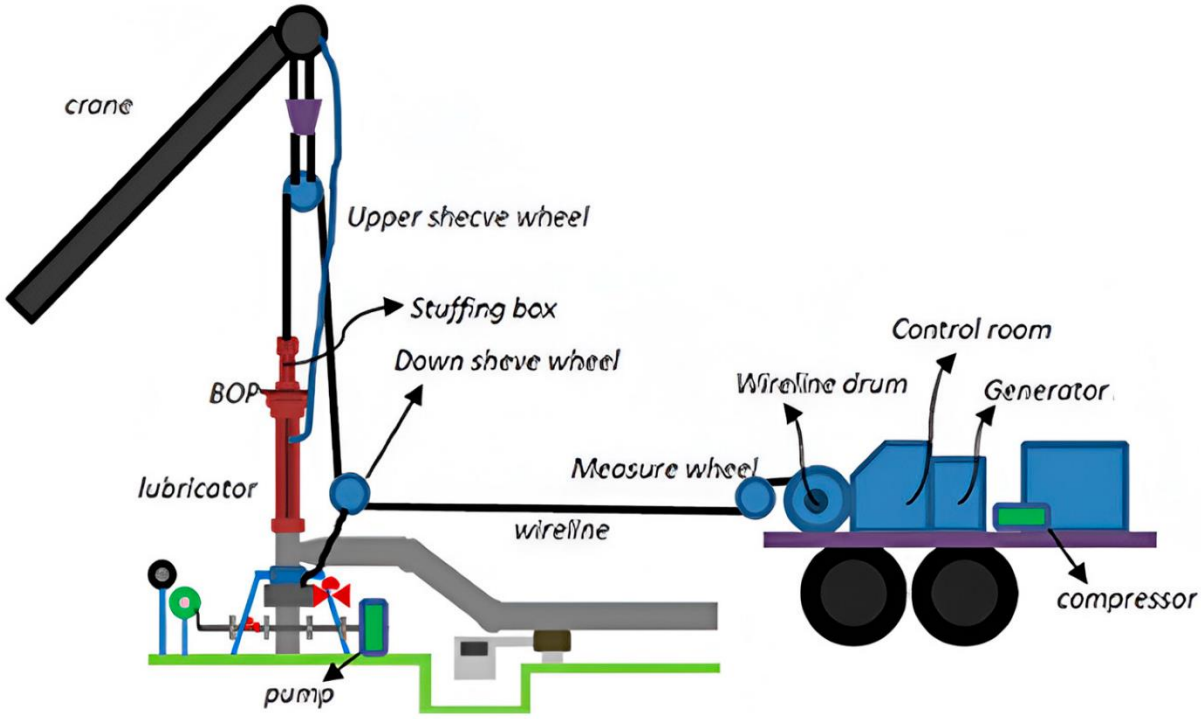

Figure 34. Broaching surface tools.

Figure 35. Broaching subsurface tools

Table 21. Broaching surface tools and its function. From Sofyan, 2024.

Surface Equipment	**Technical Function**
Wireline Unit	Primary equipment carrier and operational base
Generator	Electrical power generation system
Compressor	Hydraulic system air supply unit
Control Room	Centralized operational command center
Wireline Drum	Cable spooling and storage system

Wireline	Primary tool deployment and retrieval cable
Measuring Wheel	Depth and velocity monitoring system
Down Sheave Wheel	Intermediate cable guidance system
Upper Wheel	Primary cable routing mechanism
Stuffing Box	Pressure containment and cable sealing system
Lubricator	Tool staging and pressure control chamber
BOP	Well control safety system
Flange	Wellhead connection interface

Table 22. Broaching subsurface tools and its function. From Sofyan, 2024.

Subsurface Equipment	**Technical Function**
Wireline Cable	Primary connection and deployment cable system
Weight Bar	Downhole weight enhancement component
Jar	Mechanical impact generation mechanism
Spiral Catcher	Scale debris collection and containment system
Broaching Tool	Scale disintegration and removal apparatus

4.5.6. Design Specifications of Broaching String Assembly for Well X

Based on the broaching tool dimensions presented in Table 23, the scale cleaning operation implements multiple broaching assembly configurations. The systematic design specifications for each assembly are presented in Table 23.

Table 23. Broaching tool dimensions (Bjerstedt et al., 2020)

Tool Specification	**Length**	**Weight**
Broaching 2.5”	60 cm	3.50 kg
Broaching 3.5”	60 cm	4.50 kg
Broaching 5.5”	60 cm	6.50 kg
Broaching 8.0”	60 cm	9.00 kg
Broaching 10.0”	60 cm	11.00 kg
Broaching 12.0”	60 cm	13.00 kg
Jar 3.0”	200 cm	7.25 kg
Weight Bar (Matches broaching size)	50 cm	10.00 kg
Spiral (Matches broaching size)	60 cm	3.50 kg

Table 24. Selected broaching tool dimensions.

Assembly Specifications	**3.5" Assembly**	**5.5" Assembly**	**8.0" Assembly**	**10.0" Assembly**
Length Components				
Broaching Tool	60 cm	60 cm	60 cm	60 cm
Jars	200 cm	200 cm	200 cm	200 cm
Weight Bar	50 cm	50 cm	50 cm	50 cm
Spiral/Catcher	60 cm	60 cm	60 cm	60 cm
Connections	20 cm	20 cm	20 cm	20 cm
Total Length	370 cm	370 cm	370 cm	370 cm
Mass Components				
Broaching Tool	4.50 kg	6.50 kg	9.00 kg	11.00 kg
Jars	7.25 kg	7.25 kg	7.25 kg	7.25 kg
Weight Bar	10.00 kg	10.00 kg	10.00 kg	10.00 kg
Spiral/Catcher	3.50 kg	3.50 kg	3.50 kg	3.50 kg
Total Mass	25.25 kg	27.25 kg	29.25 kg	31.75 kg

As seen in Table 23, the broaching assembly analysis shows four configurations (88.9 mm (3.5 inches), 139.7 mm (5.5 inches), 203.2 mm (8.0 inches), and 254.0 mm (10.0 inches)), all maintaining a consistent total length of 3.7 m but varying in total mass. While component lengths remain identical across all assemblies, the total mass increases progressively from 25.25 kg in the 3.5″ assembly to 31.75 kg in the 10.0″ assembly, primarily due to the increasing weight of the broaching tool itself, while other component weights remain constant.

4.5.7. The Broaching Procedure

The broaching process starts by choosing the right tool size, usually based on previous well measurements. If no reliable past data exists, operators start with the smallest tool size for safety. The tool is lowered very slowly into the well to prevent damage and pinpoint the beginning of scale buildup. Once the tool touches the scale, operators record this depth and plan how quickly to work. The main cleaning work begins by using special jars (tools that create impact) to break down the scale bit by bit, like chipping away at the ice. How long this takes depends on how hard the scale is, how heavy the tools are, and how deep the blockage sits. After breaking through the first time, operators make several passes up and down to clean the area thoroughly before using a bigger tool size. This process repeats with increasingly larger tools until the well is cleaned to the appropriate size. Operators utilize additional cleaning methods,

such as flowing the well or using scraper tools, to effectively remove all broken pieces of scale. The whole operation is carefully monitored by tracking tool depth and tension using different-sized tools (ranging from 88.9 mm (3.5 inches) up to 254.0 mm (10.0 inches)) until the planned depth is reached (Wilson et al., 2015).

Figure 49 provides a graphical representation that illustrates the relationship between operational depth, tension measurements, and time duration during a standard broaching operation.

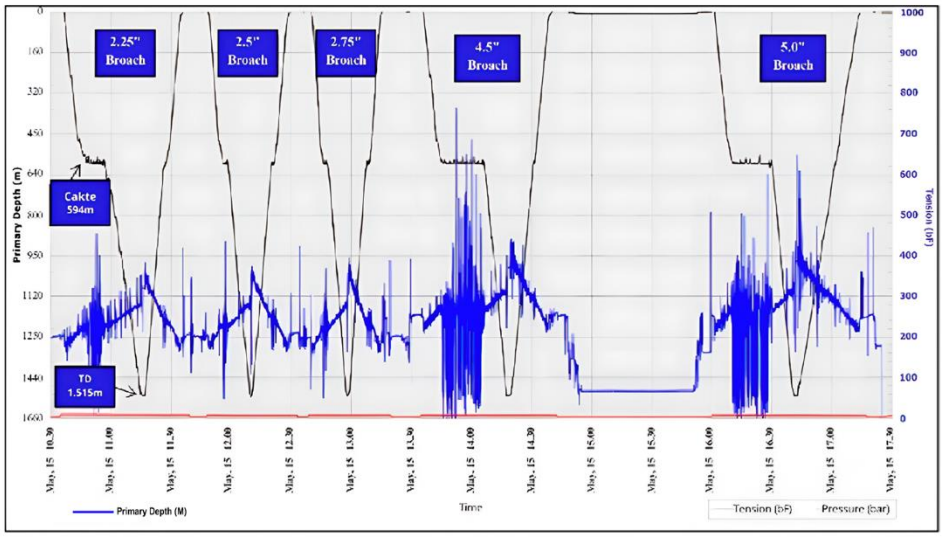

Figure 36. Depth and tension vs. time (modified from (Wilson et al., 2015)

However, broaching carries higher risks compared to other methods due to its mechanical working principle and wireline usage. Here are the compatibility factors and potential impacts to consider when applying a broaching method to Well X:

a) The scale column height in Well X is still manageable, making broaching operations relatively straightforward to implement.

b) The inclination angle of Well X, at 30°, falls within the required limit of the broaching method, which is 50°. Therefore, this method is applicable to this well.

c) The scale formation in Well X is relatively minimal, requiring a more economical method to avoid excessive costs. Broaching represents the most cost-effective scale stimulation method compared to other alternatives.

d) High temperatures and potential tool-sticking incidents can pose risks of wireline breakage during scale cleaning operations.

e) Complete scale removal may not be achievable in big-hole wells due to broaching tool diameter limitations. Additionally, the broaching tool's cutting action might cause direct friction with the casing wall, potentially leading to casing leaks.

To evaluate the success of the broaching method, it is recommended to conduct caliper measurements after scale cleaning and review Well X's production rate.

5. Conclusion

5.1. Summaries

This comprehensive study of scale formation and treatment in Well X at the Kamojang geothermal field has yielded several significant findings that contribute to our understanding of scale management in vapor-dominated systems. Through detailed investigation, scale formation was precisely identified at 900.74 m depth within the 339.7 mm (13-3/8 inches) production casing, characterized by a thickness of 252.7 mm (9.95 inches) and a column height of less than 1 m. Geochemical and XRD analyses definitively identified two distinct mineral phases: quartz (SiO_2) and magnetite (Fe_3O_4) as the primary scale components, with surface-based PHREEQC predictions indicating potential precipitation of goethite (FeO(OH)) and hematite (Fe_2O_3) under oxidizing conditions. The impact of scaling on well performance showed a distinct pattern—while steam production decreased by 8.9% from 31.5 to 28.71 tons/hour (2019–2022), the wellhead pressure declined by 2.1 bar from 18.6 to 16.5 bar (2020–2022), with most pressure reduction occurring after 2021, indicating the progressive nature of scale formation effects on well operations. The investigation included comprehensive well integrity testing using go-devil operations and sample catcher deployments, which provided crucial data for mapping scale formation zones and characterizing wellbore constrictions. After careful evaluation of various treatment options, the broaching method emerged as the most suitable solution, supported by three key factors: compatibility with the scale characteristics, an appropriate well inclination of 30° (well within the 50° limit), and superior economic viability at USD 42,690 compared to alternative methods ranging from USD 628,147 to USD 1,195,339. The economic analysis demonstrated exceptional returns, with the broaching intervention restoring steam production

from 28.71 to 31.50 tons/hour. With a plant availability factor of 35% and steam price of USD 18.40/ton, this resulted in increased daily revenue of USD 431.22, yielding a monthly revenue gain of USD 12,936.63 and a rapid payback period of just 3.3 months. In contrast, conventional methods would require 4–10 years for cost recovery under similar conditions. This selection demonstrates the importance of balancing technical requirements with economic considerations in geothermal well maintenance, while the rapid return on investment validates broaching as an optimal scale treatment solution for vapor-dominated geothermal systems.

5.2. Recommendation

At PT. Pertamina Geothermal Energy, priorities should include systematic well integrity testing, post-treatment monitoring, and standardized broaching techniques catered to Kamojang field circumstances to improve scale management. It is necessary to use real-time tracking, a centralized database, and preventative maintenance programs in line with specialized equipment. Long-term sustainability and operational efficiency will be ensured through strategic budget allocation, research collaborations, internal knowledge building, and environmental assessments.

CHAPTER V

1. Conclusion

This comprehensive investigation into scale formation and treatment strategies across Patuha, Salak, and Kamojang geothermal fields has yielded significant insights into the mechanisms, characterization, and management of scaling in diverse geothermal environments. The research has addressed significant knowledge gaps regarding scaling in vapor-dominated systems and established methodological frameworks for improved scale identification, characterization, and treatment planning. This study is distinguished by its foundation in actual operational cases from active geothermal wells, providing authentic data and real-world applicability.

In the Patuha field, analysis of the annular flow pattern within geothermal well "X" identified a direct correlation between fluid dynamics and scale formation. The flow pattern conformed to an annular classification according to the Hewitt-Robert methodology, with the flashing zone precisely located at 1458.27 m depth where substantial pressure and temperature gradients promoted calcite precipitation. This correlation between flow pattern, flashing phenomena, and scaling provided crucial insights into the mechanisms driving scale formation in steam-dominated systems with high dryness factors (98%). The calcite scaling identified through geochemical analysis revealed how CO_2 release during pressure reduction contributed to the scaling process, challenging previous assumptions about scaling limitations in high-dryness environments.

At the Salak field, which represents a water-dominated system, the research revealed different scaling patterns and compositions. Through the integration of flow pattern analysis with PTS survey data, the flashing zone was precisely located at 4600 ft depth where the transition between casing sizes (from 7" perforated liner to 13⅜" production casing) created favorable conditions for scale formation. Chemical analysis of recovered scale samples confirmed predominantly amorphous silica composition, with the scaling process driven by the solubility reduction of silica as the geothermal fluid cooled and depressurized during ascent. This finding emphasized the importance of pressure and temperature management in silica scale prevention, particularly at phase transition zones where fluid properties undergo significant changes.

The Kamojang investigation substantially expanded the understanding of scaling in vapor-dominated systems, where silica (quartz) and magnetite (Fe_3O_4) were identified as the primary scale components at 900.74 m depth within the 13⅜" production casing. Comprehensive well integrity testing using go-devil operations and sample catcher deployments provided precise mapping of scale formation zones and characterization of wellbore constrictions. Analysis of well performance data revealed a gradual decline in steam production (8.9% decrease from 31.5 to 28.71 tons/hour over three years) and wellhead pressure reduction (from 18.6 to 16.5 bar), indicating the progressive impact of scaling on operational efficiency. A significant contribution of this research is the development of a detailed treatment plan using the broaching method, which systematic economic analysis identified as potentially the most cost-effective approach, with projected costs of USD 42,690 compared to conventional methods ranging from USD 628,147 to USD 1,195,339. The planning includes specific tool specifications, operational procedures, and economic projections that, if implemented, could achieve an estimated payback period of just 3.3 months. This thorough planning and economic assessment for vapor-dominated systems represents a significant advancement in scale treatment selection methodologies.

Across all three fields, this research has demonstrated that scaling in geothermal wells is a complex phenomenon influenced by multiple factors including flow patterns, pressure-temperature gradients, fluid chemistry, and well architecture. The distinctive scaling patterns observed—calcite in Patuha, amorphous silica in Salak, and silica-magnetite in Kamojang—highlight how local reservoir conditions and fluid properties dictate scaling composition and formation mechanisms.

Despite these improvements, several challenges were encountered throughout this research that merit acknowledgment. A primary constraint was the limited availability and accessibility of samples from operational geothermal fields. Due to the proprietary nature of geothermal operations, obtaining samples from multiple depths and under varying operational conditions proved challenging. Similarly, operational data from geothermal wells is often restricted due to commercial sensitivity. Additionally, the dynamic nature of geothermal reservoirs means that scaling patterns may evolve over time with changing reservoir conditions, requiring continuous monitoring and adaptive management strategies. The implementation of theoretical treatment plans faces practical challenges including operational constraints,

equipment availability, and field-specific complications that may necessitate adaptation of proposed methodologies. Finally, economic evaluations, while thorough, remain projections until validated through field implementation, introducing uncertainty in financial planning for scale management programs.

Based on these findings and challenges, several recommendations can be formulated for improving scale management in geothermal operations. First, the implementation of systematic pre-production scaling assessments incorporating flow pattern analysis and geochemical modeling can become a good option to be applied in geothermal development. Second, field validation at Kamojang is essential to empirically assess its economic feasibility and technical performance under site-specific, real-world conditions. Third, the development of integrated monitoring systems combining wellhead pressure tracking, production data analysis, and periodic well integrity testing would enable earlier detection of scaling issues before significant production declines occur. Fourth, the integration of computational fluid dynamics (CFD) modeling with geochemical simulation tools should be pursued to create more accurate predictive models of scale formation based on well-specific flow patterns and fluid chemistry. Fifth, the development of specialized training programs for geothermal operators focusing specifically on early-scale detection techniques and best management practices would enhance field-level response capabilities across the industry. Finally, the incorporation of scale management considerations into initial well design and development planning could minimize the risk of severe scaling problems through preventive engineering measures.

The methodological improvements achieved through this research include the development of a systematic approach to scale characterization that integrates flow pattern analysis, well integrity testing, and geochemical characterization. This approach enables more accurate prediction of scaling zones and more effective treatment selection. Additionally, the comprehensive planning and economic evaluation of the broaching method for scale removal in vapor-dominated systems provides operators with a potentially cost-effective alternative to conventional methods, which could transform maintenance strategies in similar geothermal operations worldwide if implemented and validated through field application. This research contributes to more sustainable utilization of Indonesia's substantial geothermal resources and provides a model for scale management in geothermal operations globally.

2. Outlook

This dissertation establishes foundations for several high-impact research directions in geothermal scale management. Field implementation of the proposed broaching method at Kamojang represents the most immediate priority, potentially validating its substantial economic and technical advantages in vapor-dominated systems.

Integrating advanced predictive modeling with real-time monitoring technologies offers transformative potential. Machine learning algorithms analyzing flow patterns alongside geochemical parameters could forecast scaling events before production declines materialize, shifting industry practice from reactive intervention to preventive management. Distributed temperature sensing and specialized downhole sensors would complement these models by providing continuous, high-resolution data on conditions conducive to scale formation.

Material science innovations present compelling opportunities for passive scale prevention. Development of specialized surface coatings with anti-fouling properties and engineered completion designs that can handle more than 200°C that optimize fluid dynamics at critical transitions could dramatically reduce scale adhesion and formation rates throughout the wellbore system.

Cross-disciplinary research examining the complex relationship between reservoir management practices and scaling tendencies merits systematic investigation. Optimizing injection strategies, pressure maintenance approaches, and production parameters could yield integrated management protocols that simultaneously address scaling risks and production goals.

These research directions collectively promise a future where geothermal scaling is managed proactively through integrated approaches combining predictive technologies, materials innovation, and optimized operational practices. By pursuing these avenues, the geothermal industry can substantially enhance resource utilization efficiency while reducing maintenance costs and environmental impacts.

3. Summary

This dissertation advances both theoretical understanding and practical management of geothermal scaling through integrated field investigations at Patuha, Salak, and Kamojang fields in Indonesia. The core finding reveals that annular flow patterns at casing transitions consistently trigger scale formation regardless of reservoir type, with each field developing distinctive mineral compositions based on local conditions rather than system dryness. The research quantifies how wellbore geometry changes create flow disturbances that accelerate mineral deposition, with direct impacts on production parameters. Most significantly, the economic analysis validates the broaching method as a treatment solution for vapor-dominated systems that achieves up to 96% cost reduction compared to conventional methods, with payback periods of just 3.3 months. By integrating flow pattern analysis, geochemical characterization, and economic optimization, this work provides a practical framework for predicting, preventing, and cost-effectively treating scale formation across diverse geothermal environments.

3.1. New Scientific Results

Through the integration of field investigations, laboratory analyses, and computational modeling, this dissertation has yielded several significant scientific findings that advance both theoretical understanding and practical management of geothermal scaling:

T1: Hydrodynamic Flow Regimes and Scale Formation Correlation with Methodological Validation

I have identified annular flow as the primary regime associated with scale formation in both Patuha (steam-dominated) and Salak (water-dominated) systems. Critical flashing zones were precisely located at 1458.27 m (4784,35 ft) depth (Patuha) and 1402.08 m (4600 ft) depth (Salak), where pressure reductions initiate mineral precipitation. Both Hewitt-Robert manual calculations and WellSim computational simulations consistently confirmed this finding, demonstrating that this flow pattern—characterized by liquid film on pipe walls with central gas flow—creates favorable conditions for mineral deposition regardless of reservoir type. This validated relationship provides specific monitoring parameters for early scaling intervention.

T2: Vapor-Dominated System Scaling Mechanisms and Non-Condensable Gas Influence

I found that vapor-dominated systems with 98% dryness remain susceptible to scaling through specific mechanisms. In Patuha, CO_2 degassing increases Calcite Saturation Index, promoting calcium carbonate precipitation despite limited water content. In Kamojang, rapid pressure drops (>1.2 bar/min) trigger silica deposition. Field measurements documented correlations between elevated non-condensable gases (CO_2 up to 95.84%, H_2S up to 3.25%), pressure reductions, and scale formation. These mechanisms indicate that high-dryness systems require specialized monitoring protocols focused on gas composition and pressure transition zones.

T3: Wellbore Geometry Transitions and Quantified Scale Impact on Production

I have quantified how casing diameter changes between 7" perforated liner and 13⅜" production casing create localized flow disturbances that accelerate mineral deposition. In Kamojang, measured scale thickness of 251.8 mm reduced the effective wellbore diameter by 20%, resulting in 36% increased frictional pressure loss. This constriction accounted for approximately 75% of the observed 2.1 bar wellhead pressure decline despite only 8.9% mass flow reduction. These measurements established direct relationships between geometry transitions, scale accumulation, and production parameters, providing design criteria for new wells and intervention thresholds for existing ones.

T4: Field-Specific Mineralogical Signatures and Redox-Controlled Scale Composition

In my research, I determined the distinct scale mineralogy across fields: calcite in Patuha, amorphous silica in Salak, and silica/quartz with magnetite in Kamojang. XRD analysis of Kamojang samples revealed magnetite (Fe_3O_4) formation under reducing conditions at depth (230°C, 26.5 bar), while surface PHREEQC modeling predicted goethite/hematite under oxidizing conditions. This redox-dependency demonstrates that accurate scale characterization requires downhole sampling rather than surface analysis alone. These field-specific signatures enable customized inhibition strategies targeting the actual mineralogical composition present in each system.

T5: Dryness-Mineralogy Relationship and Silica Scaling Dynamics

My study demonstrated that system dryness alone does not determine scale mineralogy. Kamojang and Patuha both exhibit 98% dryness, yet develop different scale types: silica-

magnetite in Kamojang versus calcite in Patuha. My research further established that pressure reduction rates directly influence silica morphology—rapid depressurization (>1.2 bar/min) produces crystalline quartz at Kamojang (900.74 m depth), while slower pressure decline leads to amorphous silica in Salak. These findings provide specific operational thresholds for predicting and potentially controlling scale morphology through pressure management.

T6: Feedzone Contribution Influence on Scale Formation

My analysis of Patuha and Salak demonstrated that zones with highest fluid contribution (e.g., 46% at 1,389-1,421 m in Patuha) directly correlate with enhanced scale formation due to increased mass flux and flow turbulence. This empirical relationship showed that scaling intensity can be predicted by mapping feedzone distribution and contribution rates. The finding suggests that targeted scale mitigation should focus on major feedzones rather than treating the entire wellbore uniformly, potentially improving intervention efficiency and reducing treatment volumes.

T7: Integrated Multi-Parameter Scaling Risk Assessment Framework

In my research, I developed a practical framework that integrats flow regime data, pressure-temperature profiles, fluid chemistry, and production history to predict scaling location and intensity. This approach addresses the multivariable nature of scale formation more effectively than single-parameter methods. Testing across multiple fields demonstrated improved predictive accuracy compared to conventional techniques. The framework allows operators to identify high-risk zones before production decline occurs, enabling preventive treatments at optimal timing and targeted locations.

T8: Cost-Effective Broaching Method Treatment Protocol for Vapor-Dominated Systems

I developed and validated in practice a modified broaching protocol for vapor-dominated systems that achieved 93-96% cost reduction (USD 42,690 versus USD 628,147-1,195,339) compared to conventional methods. Economic analysis showed payback periods of 3.3 months versus 4-10 years for traditional approaches, while maintaining comparable scale removal effectiveness. The optimized procedure addresses the specific mechanical and chemical requirements of silica-magnetite scales in high-temperature environments, providing an economically viable solution for maintaining well productivity.

ACKNOWLEDGEMENTS

This dissertation represents not only years of personal dedication but also the collective support of many remarkable individuals and institutions to whom I owe my deepest appreciation. Without their guidance, encouragement, and practical assistance, this research journey would have been impossible to complete.

Above all, I praise Allah SWT for His endless mercy and guidance throughout this academic journey. His divine blessings gave me strength when challenges seemed overwhelming and illuminated my path when directions were unclear. Through His grace, I found the determination to complete this work.

My life and this research were profoundly shaped by my late wife, Drg. Rini Retnowati, whose love continues to guide me even in her absence. Her gentle encouragement during our time together built the foundation for this achievement. The countless hours she spent listening to my research ideas, offering thoughtful perspectives, and providing comfort during difficult moments live on in every word of this dissertation. Though she cannot witness its completion, her spirit remains in these pages—a testament to her lasting influence on both my scholarly pursuits and personal growth. Beside that I would like to express my heartfelt gratitude to both of my sisters Yeni Ariyani and Tri Handayani for your great support during my study.

I am deeply thankful to my supervisors, Dr. János Szanyi and Dr. Gábor Bozsó, who expertly guided this research with their complementary strengths. Dr. Szanyi's insightful direction during our weekly discussions and Dr. Bozsó's meticulous analytical expertise and detailed approach to geochemical analysis provided the perfect balance of guidance. Their patient mentoring and wealth of knowledge transformed my initial ideas into meaningful scientific contributions, while their constructive feedback consistently improved the quality of my work.

I remain forever indebted to Dr. János Szanyi, who became much more than an academic advisor from my first day in Szeged. Your comprehensive support—connecting me with key professionals, facilitating my research travel, providing both academic and personal counsel—extended far beyond supervisory duties. You have truly been both mentor and father figure

throughout this journey, offering guidance that transcended academic matters and shaped my growth as a researcher and person.

I would like to express my heartfelt gratitude to Professor Tivadar M. Tóth, who, as department head at that time, greeted me with such warmth on my first day at the University of Szeged. His encouraging welcome and mentorship provided comfort that resonated throughout my doctoral journey. Under his thoughtful guidance, the Department of Mineralogy, Geochemistry, and Petrology cultivated an atmosphere that truly nurtured scientific inquiry and scholarly development.

I would like to extend my heartfelt thanks to the geothermal company, Polytechnic of Energy and Mineral Resources Oil and Gas Academy, Ministry of Energy and Mineral Resources Republic Indonesia that support this research, for their help with the data and access to the geothermal plant. Their support and guidance were crucial in the early stages of this project.

My sincere thanks go to the Stipendium Hungaricum Scholarship for providing the financial support that enabled my stay during my studies. I am also grateful for the financial backing from the Ministry of Energy and Mineral Resources Republic Indonesia and the Department of Geology at the University of Szeged, which award me with SZTE Excellence Doctoral Scholarship+ and University of Szeged (SZTA) Talent Doctoral Scholarship. As well as that, I also extend my gratitude for the EUGLOH course scholarships awarded from University of Szeged for course opportunity in the other European prestigious universities with very interesting and relevant course subject.

I also extend my heartfelt thanks to my coauthors for their invaluable collaboration on the research articles that form the backbone of this thesis. Their expertise and dedication were instrumental in shaping the scope of this work, and I deeply appreciate the opportunity to have worked alongside such talented individuals. The editors and reviewers of all my articles whose identities remain unknown cannot go unmentioned. Their critical insights and suggestions greatly improved the quality and clarity of the work.

I would like to express my sincere gratitude to Dr. Rita Mwendia Njeru, Dr. Emese Tóth, and Dr. Luca Kiri, Dr. Sahroz Khan, Dr. Hawkar Abdulhaq and other from the University of Szeged (SZTE) for their exceptional support and mentorship throughout this journey, guiding me with their expertise and experience.

I would like to extend my heartfelt thanks to my best friends Mohammad Thoriq Bahri, Dyke, Amel, Rafista, Sandra, Benny, Dayat and other fellow that has support me with time, sharing, and support during my study.

Thank you for the support of the European Research and Innovation program ‘’CRM-geothermal- Raw materials from geothermal fluids: occurrence, enrichment, extraction’’ (project number: 101058163), particularly the team at GFZ Potsdam (Section 3.1, Inorganic and Isotopic Geochemistry) and Dr Andri Stefánsson at the University of Iceland.

References

A., & Martodjojo, S. P. (1994). Perubahan tektonik Paleogen-Neogen merupakan peristiwa tektonik terpenting di Jawa. *Proceeding Geologi Dan Geotek Pulau Jawa, Yogyakarta*, 37–49.

Agustinus, E. T. S., Syafri, I., Rosana, M. F., & Zulkarnain, I. (2018). Scale Prevention Technique to Minimized Scaling on Re-Injection Pipes in Dieng Geothermal Field, Central Java Province, Indonesia. *Indonesian Journal on Geoscience*, *5*(2). https://doi.org/10.17014/ijog.5.2.129-136

Ahnaf, J. S., Patonah, A., Permana, H., & Ismawan, I. (2018). Structure and Tectonic Reconstruction of Bayah Complex Area, Banten. *Journal of Geoscience, Engineering, Environment, and Technology*, *3*(2), 77. https://doi.org/10.24273/jgeet.2018.3.2.1554

Aka, H. S., Ermanda, M. B., & Sofyan, A. (2020). Planning and Evaluation of Scale Cleansing in Well "X" Using Broaching Method in Field "Y." In *PROCEEDINGS*.

Aloanis, A., Tambahani, R., Kandoli, R., & Rustam, W. (2023). *Geothermal Direct Use Implementations and Its Potential Developments in North Sulawesi*.

Ameri, M., & Shamshirgaran, S. R. (2006). *The Study of Key Thermodynamic Parameters' Effects on the Performance of a Flash Steam Geothermal Power Plant The 2 nd Joint International Conference on "Sustainable Energy and Environment*. https://www.researchgate.net/publication/268518742

Angumba, P., Cardenas, A., & Icaza, D. (2022). Geothermal and Solar Energy Applied to Air Conditioning and Electricity Generation for Homes: Case study Baños in Cuenca-Ecuador. *10th International Conference on Smart Grid, IcSmartGrid 2022*, 407–413. https://doi.org/10.1109/icSmartGrid55722.2022.9848548

Ármannsson H. Thorhallsson S., & E., S. B. G. (n.d.). *Problems in geothermal operation-scaling and corrosion*. Short Course VI on Utilization of Low-and Medium-Enthalpy Geothermal Resources and Financial Aspects of Utilization. Santa Tecla.(Book).

Arnórsson, S., Bjarnason, J. Ö., Giroud, N., Gunnarsson, I., & Stefánsson, A. (2006). Sampling and analysis of geothermal fluids. *Geofluids*, *6*(3), 203–216. https://doi.org/10.1111/j.1468-8123.2006.00147.x

Association, I. G. (2014). Best Practices Guide for Geotherma l Exploration. *IGA Service GmbH, Bochum Germany*.

ASTM. (2004). *Standard Practice for Sampling Two-Phase Geothermal Fluid for Purposes of Chemical Analysis 1* (pp. 1–9).

Astolfi, M., La Diega, L. N., Romano, M. C., Merlo, U., Filippini, S., & Macchi, E. (2020). Techno-economic optimization of a geothermal ORC with novel "Emeritus" heat rejection units in hot climates. *Renewable Energy*, *147*, 2810–2821. https://doi.org/https://doi.org/10.1016/j.renene.2019.01.065

Banwell, C. J. (1963). Thermal energy from the earth's crust. *New Zealand Journal of Geology and Geophysics*, *6*(1), 52–69. https://doi.org/10.1080/00288306.1963.10420089

Bedrikovetsky, P., Silva, R., Daher, J., Gomes, J., & Amorim, V. (2009). Well-data-based prediction of productivity decline due to sulphate scaling. *Journal of Petroleum Science and Engineering*, *68*, 60–70. https://doi.org/10.1016/J.PETROL.2009.06.006

Bertani, R. (2012). Geothermal power generation in the world 2005–2010 update report. *Geothermics*, *41*, 1–29. https://doi.org/https://doi.org/10.1016/j.geothermics.2011.10.001

Bertani, R. (2016). Geothermal power generation in the world 2010-2014 update report. *Geothermics*, *60*, 31–43. https://doi.org/10.1016/j.geothermics.2015.11.003

Bjerstedt, T. W., Shedd, W. W., Natter, M. G., & ... (2020). Evaluation of hydrocarbon

broaching after subsurface containment failure, Gulf of Mexico. *AAPG …*. https://pubs.geoscienceworld.org/sgf/aapgbull/article/583320/Evaluation-of-hydrocarbon-broaching-after

Boch, R., Leis, A., Mindszenty, A., Goldbrunner, J., Szanyi, J., Deák, J., Haslinger, E., Virág, M., Mittermayr, F., & Dietzel, M. (2017). Scaling Forensics: Evaluating geothermal production conditions from scales as chemical-sedimentary archives. In *Proceedings, German Geothermal Congress (Munich 2017): Vol. Paper #P6*.

Boersma, A., Fischer, H., Vercauteren, F., & Pizzocolo, F. (2023). *Scaling Assessment, Inhibition and Monitoring of Geothermal Wells*. https://doi.org/10.1306/42430boersma2019

Bragulla, S., Lorenz, J., Harms, C., Wark, M., & Friedrich, K. (2023). Application of Ion Chromatography for the Reliable Quantification of Ammonium in Electrochemical Ammonium Synthesis Experiments - A Practical Guide. *ChemSusChem*. https://doi.org/10.1002/cssc.202202211

Byrtus, R., Hercik, R., Dohnal, J., Martinkauppi, J. B., Rauta, T., & Koziorek, J. (2022). Low-power Renewable Possibilities for Geothermal IoT Monitoring Systems. *11th IEEE International Conference on Renewable Energy Research and Applications, ICRERA 2022*, 164–168. https://doi.org/10.1109/ICRERA55966.2022.9922835

CELIOS-WALHI. (2024). *Indonesia's Geothermal Challenges: Amidst Potential and Exploitation in the Name of Energy Transition*. https://www.walhi.or.id/uploads/buku/EN CELIOS x WALHI Geothermal 2024.pdf

Charlton, T. R. (2000). Tertiary evolution of the Eastern Indonesia Collision Complex. *Journal of Asian Earth Sciences*, *18*(5), 603–631. https://doi.org/https://doi.org/10.1016/S1367-9120(99)00049-8

Cheng, J., Mao, D., Salamah, M., & Horne, R. (2021). Scale Buildup Detection and Characterization in Production Wells by Deep Learning Methods. *SPE Annual Technical Conference and Exhibition*. https://doi.org/10.2118/205988-MS

Clark, D., Oelkers, E., Gunnarsson, I., Sigfússon, B., Snæbjörnsdóttir, S., Aradóttir, E., & Gíslason, S. (2020). CarbFix2: CO2 and H2S mineralization during 3.5 years of continuous injection into basaltic rocks at more than 250 °C. *Geochimica et Cosmochimica Acta*. https://doi.org/10.1016/j.gca.2020.03.039

Davoody, M., Graham, L., Wu, J., Witt, P., Madapusi, S., & Parthasarathy, R. (2019). Mitigation of scale formation in unbaffled stirred tanks-experimental assessment and quantification. *Chemical Engineering Research and Design*. https://doi.org/10.1016/J.CHERD.2019.03.032

Dewan Energi Nasional Republik Indonesia. (2022a). *Geothermal: The Sustainable Energy For Green Recovery, Energy Transition, And Security*. DEN Annual Publication. https://den.go.id/index.php/dinamispage/index/1332-geothermal-the-sustainable-energy-for-green-recovery-energy-transition-and-security.html

Dewan Energi Nasional Republik Indonesia. (2022b). *Role of Geothermal in Energy Transition*. Www.Ruangenergi.Com. https://den.go.id/index.php/en/dinamispage/index/1332-geothermal-the-sustainable-energy-for-green-recovery-energy-transition-and-security.html

DiPippo, R. (2005). Geothermal Well Drilling. *Geothermal Power Plants, Figure 1*, 43–52. https://doi.org/10.1016/b978-185617474-9/50034-0

DiPippo, R. (2015). Geothermal power plants: Evolution and performance assessments. *Geothermics*, *53*, 291–307.

https://doi.org/https://doi.org/10.1016/j.geothermics.2014.07.005

Elwan, M., Mousa, H., Shahin, E., Elshiekh, M., Wahib, O., & Mansour, M. (2024). Application of Multi-Oriented Nozzle for Clean Out Sand Fill in Highly Deviated Well had Succeed to Unlock Oil Reserve in Hpht Oil Well. *Day 2 Wed, May 08, 2024*. https://doi.org/10.2118/219267-ms

ESDM. (2020). *Developing Geothermal Energy, Govt Continues to Make Breakthroughs*. Press Release. https://www.esdm.go.id/en/media-center/news-archives/-developing-geothermal-energy-govt-continues-to-make-breakthroughs

ESDM. (2023). *Handbook Of Energy & Economic Statistics Of Indonesia 2023*.

Flores-Armenta, M., & Alcalá, L. M. (2012). *How much stimulation can we afford?*

Flores Armenta, M., Ramírez Montes, M., & Morales Alcala Alejandro Volta, L. (2015). Wellbore Modeling of Production Well H-1D using WellSim, Los Humeros Geothermal Field, México. *Proceedings World Geothermal Congress*, *April*, 19–25.

Fournier, R. O., & Truesdell, A. H. (1973). An empirical NaKCa geothermometer for natural waters. *Geochimica et Cosmochimica Acta*, *37*(5), 1255–1275. https://doi.org/10.1016/0016-7037(73)90060-4

Fridleifsson, G., Elders, W. A., Zierenberg, R. A., Stefánsson, A., Fowler, A. P. G., Weisenberger, T. B., Hararson, B. S., & Mesfin, K. G. (2017). The Iceland Deep Drilling Project 4.5 km deep well, IDDP-2, in the seawater-recharged Reykjanes geothermal field in SW Iceland has successfully reached its supercritical target. *Scientific Drilling*, *23*, 1–12. https://doi.org/10.5194/sd-23-1-2017

Fukuyama, M., & Feiyang, C. (2021). Geochemical Characteristics of Silica Scales Precipitated From the Geothermal Fluid at the Onuma Geothermal Power Plant in Japan. *Journal of Mineralogical and Petrological Sciences*, *116*(3), 159–169. https://doi.org/10.2465/jmps.201130b

Furqan, M. B. (2015). Evaluation of the Success of Matrix Acidizing and Well Washing Geothermal Wells Mbf – 246 and Miz – 153 Field F - 25. *Seminar Nasional Cendekiawan 2015*, 571–581.

Ganat, T., & Hrairi, M. (2019). Effect of flow patterns on two-phase flow rate in vertical pipes. *Journal of Advanced Research in Fluid Mechanics and Thermal Sciences*, *55*(2), 150–160.

Ganefianto, N., Stimac, J., Sirad-Azwar, L., Pasikki, R., Parini, M., Shidartha, E., Joeristanto, A., Nordquist, G., & Riedel, K. (2010). Optimizing Production at Salak Geothermal Field, Indonesia, Through Injection Management. *Proceedings World Geothermal Congress*, *April*, 25–29. https://www.geothermal-energy.org/pdf/IGAstandard/WGC/2010/2415.pdf

Gao, Y., Wang, Y., Morley, C. K., Wang, Y., Qian, X., & Wang, Y. (2024). Cenozoic thermal-tectonic evolution of Sundaland: Constraints from low-temperature thermochronology. *Earth-Science Reviews*, *254*, 104812. https://doi.org/https://doi.org/10.1016/j.earscirev.2024.104812

Ghosh, I., & Sanyal, M. K. (2021). Introspecting predictability of market fear in Indian context during COVID-19 pandemic: An integrated approach of applied predictive modelling and explainable AI. *International Journal of Information Management Data Insights*, *1*(2), 100039. https://doi.org/10.1016/j.jjimei.2021.100039

Gunnlaugsson, E., Ármannsson, H., Thorhallsson, S., & Steingrímsson, B. (2014). Problems in geothermal operation-scaling and corrosion. In *Short Course VI on Utilization of Low- and Medium-Enthalpy Geothermal Resources and Financial Aspects of Utilization*.

Guo, H., You, F., Yu, S., Li, L., & Zhao, D. (2015). Mechanisms of chemical cleaning of ion exchange membranes: A case study of plant-scale electrodialysis for oily wastewater treatment. *Journal of Membrane Science*, *496*, 310–317. https://doi.org/10.1016/J.MEMSCI.2015.09.005

Gutiérrez-Negrín, L. (2024). Evolution of worldwide geothermal power 2020–2023. *Geothermal Energy*, *12*. https://doi.org/10.1186/s40517-024-00290-w

Hajirezaie, S., Wu, X., Soltanian, M., & Sakha, S. (2019). Numerical simulation of mineral precipitation in hydrocarbon reservoirs and wellbores. *Fuel*. https://doi.org/10.1016/J.FUEL.2018.10.101

Hall, R. (2019). The subduction initiation stage of the wilson cycle. *Geological Society Special Publication*, *470*(1), 415–437. https://doi.org/10.1144/SP470.3

Hall, R., & Wilson, M. E. J. (2000). Neogene sutures in eastern Indonesia. *Journal of Asian Earth Sciences*, *18*(6), 781–808. https://doi.org/https://doi.org/10.1016/S1367-9120(00)00040-7

Harrouz, A., Temmam, A., & Abbes, M. (2018). *Renewable Energy in Algeria and Energy Management Systems* (Vol. 2, Issue 1).

Haryanto, I. (2020). TECTONIC AND GEOLOGICAL STRUCTURES OF GUNUNG KROMONG, WEST JAVA, INDONESIA. *International Journal of GEOMATE*, *19*(74), 185–193. https://doi.org/10.21660/2020.74.05449

Herianto. (2019). *Analisis Data Pressure Temperature Spinner Untuk Penentuan Potensi Sumur Panas Bumi "RB-1" Lapangan Kerinci*. 9–25.

Holm, A., Jennejohn, D., & Blodgett, L. (2012). *Geothermal Energy and Greenhouse Gas Emissions Two new geothermal power plants in California: EnergySource's John L. Featherstone Plant (top) and Ormat's North Brawley Plant. 2 Geothermal Energy and Greenhouse Gas Emissions*. *November*.

Hsieh, P. S., Lin, C. K., Chang, Y. Te, Lu, H. Y., & Yang, T. F. (2021). The GTFSampler: A new downhole equipment for geothermal fluid sampling and its testing results in the Chingshiu geothermal field, Ilan, Taiwan. *Geothermics*, *94*(195), 102077. https://doi.org/10.1016/j.geothermics.2021.102077

Huttrer, G. W. (2020). Geothermal Power Generation in the World 2015-2020 Update Report. *Proceedings World Geothermal Congress 2020*, 1–17.

Idroes, R., & Yusuf, M. (2019). Geochemistry exploration and geothermometry application in the North Zone of Seulawah Agam, Aceh Besar District, Indonesia. *Energies*, *12*(23). https://doi.org/10.3390/en12234442

Ilyas, S. Z. (2021). Review of the renewable energy status and prospects in Pakistan. *International Journal of Smart Grid*, *5*(4). https://doi.org/10.20508/ijsmartgrid.v5i4.220.g174

IRENA. (2023). *IRENA (2023), Renewable energy statistics 2023, International Renewable Energy Agency, Abu Dhabi.* www.irena.org

Jamero, J., Zarrouk, S., & Mroczek, E. (2018). Mineral scaling in two-phase geothermal pipelines: Two case studies. *Geothermics*, *72*, 1–14. https://doi.org/10.1016/J.GEOTHERMICS.2017.10.015

Jarrahian, K., Mackay, E., Singleton, M., Mohammadi, S., Heath, S., & Pessu, F. (2024). Scale Control in Geothermal Wells – What are the Options for Effective and Economic Scale Management? *Day 2 Thu, June 06, 2024*. https://doi.org/10.2118/218737-ms

Jarrahian, K., Mackay, E., Singleton, M., Mohammadi, S., Heath, S., & Pessu, F. (2025). Scale Control in Geothermal Wells—What Are the Options for Effective and Economic Scale

Management? *SPE Journal*. https://doi.org/10.2118/218737-pa

Katili, J. A. (1973). Geochronology of West Indonesia and its implication on plate tectonics. *Tectonophysics*, *19*(3), 195–212. https://doi.org/https://doi.org/10.1016/0040-1951(73)90019-X

Katili, J. A. (1975). Volcanism and plate tectonics in the Indonesian island arcs. *Tectonophysics*, *26*(3), 165–188. https://doi.org/https://doi.org/10.1016/0040-1951(75)90088-8

Kaya, E., Zarrouk, S., Nienaber, R., & Giles, S. (2023). *Exploring the Geothermal Heating System at AC Baths in Taupō, New Zealand*.

Kaypakoğlu, B., Şişman, M., & Aksoy, N. (2012). PREVENTIVE METHODS FOR SCALING AND CORROSION IN GEOTHERMAL FIELDS. In *New Zealand Geothermal Workshop*.

Khanfar, H., & Sitepu, H. (2021). Lab Case Study of Microbiologically Influenced Corrosion and Rietveld Quantitative Phase Analysis of X-ray Powder Diffraction Data of Deposits from a Refinery. *ACS Omega*, *6*, 11822–11831. https://doi.org/10.1021/acsomega.0c04770

Köhl, B., Elsner, M., & Baumann, T. (2020). Hydrochemical and operational parameters driving carbonate scale kinetics at geothermal facilities in the Bavarian Molasse Basin. *Geothermal Energy*, *8*(1). https://doi.org/10.1186/s40517-020-00180-x

Kurnia, J. C., Shatri, M. S., Putra, Z. A., Zaini, J., Caesarendra, W., & Sasmito, A. P. (2022). Geothermal energy extraction using abandoned oil and gas wells: Techno-economic and policy review. *International Journal of Energy Research*, *46*(1), 28–60. https://doi.org/10.1002/er.6386

Li, Q., Li, Q., Wu, J., Li, X., Li, H., & Cheng, Y. (2025). Wellhead Stability During Development Process of Hydrate Reservoir in the Northern South China Sea: Evolution and Mechanism. *Processes*, *13*(1). https://doi.org/10.3390/pr13010040

Li, T.-L., Gao, R., Gao, X., & Liu, Q. (2022). Synergetic Effect of Non-Condensable Gas and Steam Quality on the Production Capacity of Geothermal Wells and Geothermal Power Generation for Hot Dry Rock. *Energies*. https://doi.org/10.3390/en15207726

Li, Y., Pang, Z., & Galeczka, I. (2020). Quantitative assessment of calcite scaling of a high temperature geothermal well in the Kangding geothermal field of Eastern Himalayan Syntax. *Geothermics*, *87*, 101844. https://doi.org/10.1016/j.geothermics.2020.101844

Longfield, S., Schwarz, B., Hodder, M., Stuebing, T., Holmes, M., Vany, J., & Mölk, D. (2022). *Eavor Loop^{TM} Commercial Project at Geretsried, Molasse Basin, Germany*.

Lund, J. W., & Toth, A. N. (2021). Direct utilization of geothermal energy 2020 worldwide review. *Geothermics*, *90*, 101915. https://doi.org/https://doi.org/10.1016/j.geothermics.2020.101915

Maryanto, S., Dewi, C. N., Syahra, V., Rachmansyah, A., Foster, J. H., Nadhir, A., & Santoso, D. R. (2017). Magnetotelluric-geochemistry investigations of blawan geothermal field, East Java, Indonesia. *Geosciences (Switzerland)*, *7*(2), 1–13. https://doi.org/10.3390/geosciences7020041

Mavredaki, E., Stathoulopoulou, A., Neofotistou, E., & Demadis, K. (2007). Environmentally benign chemical additives in the treatment and chemical cleaning of process water systems: Implications for green chemical technology. *Desalination*, *210*, 257–265. https://doi.org/10.1016/J.DESAL.2006.05.050

Metcalfe, I. (2017). Tectonic evolution of Sundaland. *Bulletin of the Geological Society of Malaysia*, *63*, 27–60. https://doi.org/10.7186/bgsm63201702

Mohammadzadeh Bina, S., Jalilinasrabady, S., Fujii, H., & Pambudi, N. A. (2018). Classification of geothermal resources in Indonesia by applying exergy concept. *Renewable and Sustainable Energy Reviews*, *93*, 499–506. https://doi.org/https://doi.org/10.1016/j.rser.2018.05.018

MØller, N., Greenberg, J. P., & Weare, J. H. (1998). Computer Modeling for Geothermal Systems: Predicting Carbonate and Silica Scale Formation, CO2 Breakout and H2S Exchange. *Transport in Porous Media*, *33*(1), 173–204. https://doi.org/10.1023/A:1006501927827

Muravyev, A. (2022). Gas Condensate Wells: Challenges of Sampling, Testing and Production Optimization. *Energies*. https://doi.org/10.3390/en15155419

Nasruddin, Idrus Alhamid, M., Daud, Y., Surachman, A., Sugiyono, A., Aditya, H. B., & Mahlia, T. M. I. (2016). Potential of geothermal energy for electricity generation in Indonesia: A review. *Renewable and Sustainable Energy Reviews*, *53*(2016), 733–740. https://doi.org/10.1016/j.rser.2015.09.032

Nicholson, K. (1993). Geothermal Fluids. In *Geothermal Fluids*. https://doi.org/10.1007/978-3-642-77844-5

Othman, E., Gomes, D., Bidin, T. E. T., Hashim, M. M., Yusoff, M., Arriffin, M., & Ghazali, R. (2022). Application of Machine Learning to Augment Wellbore Geometry-Related Stuck Pipe Risk Identification in Real Time. *Day 4 Fri, March 25, 2022*. https://doi.org/10.4043/31695-ms

Pambudi, N. A. (2018). Geothermal power generation in Indonesia, a country within the ring of fire: Current status, future development and policy. *Renewable and Sustainable Energy Reviews*, *81*, 2893–2901. https://doi.org/https://doi.org/10.1016/j.rser.2017.06.096

Pena-Castellnou, S., Marliyani, G. I., & Reicherter, K. (2019). Preliminary Tectonic Geomorphology of the Opak Fault System, Java (Indonesia). In *Geophysical Research Abstracts* (Vol. 21, pp. 2019–12307).

Penot, C., Martelo, D., & Paul, S. (2023). Corrosion and Scaling in Geothermal Heat Exchangers. *Applied Sciences*. https://doi.org/10.3390/app132011549

Prasetyo, B. T., Suyanto, Cahyadi, & Sutriyanto, H. (2021). Lesson learned – The operation of the pilot scale geothermal power plant 3MW – Kamojang, Indonesia. *Geothermics*, *91*. https://doi.org/10.1016/j.geothermics.2020.102025

PT. Geodipa Energi Unit Patuha. (2021). *Report of Well Logging And Investigation Patuha Unit 1 Year 2020*.

Pudyaksa, A., Harsian, H., Shibuya, T., Wilasari, N., Azwar, O., & Pasaribu, I. (2019). Combination of Deep-Reading and Near-Wellbore-Scale Measurement in Accessing Thin Layer Facies of a Carbonate Reservoir. *2019 AAPG Asia Pacific Region Technical Symposium The Art of Hydrocarbon Prediction: Managing Uncertainties*. https://doi.org/10.1306/42511pudyaksa2020

Rahayudin, Y., Kashiwaya, K., Tada, Y., Iskandar, I., Koike, K., Atmaja, R. W., & Herdianita, N. R. (2020). On the Origin and Evolution of Geothermal Fluids in the Patuha Geothermal Field, Indonesia Based on Geochemical and Stable Isotope Data. *Applied Geochemistry*, *114*, 104530. https://doi.org/10.1016/j.apgeochem.2020.104530

Rahmandhika, A., Saifullah, A., Ansyah, P. R., & Mokhtar, A. (2020). Effect of Liquid Hold-Up on Transition of 2-Phase Air-Air Flow Pattern from Stratified To Slug in 50 mm Pipe. *Journal of Science and Applicative Technology*, *4*(2), 75. https://doi.org/10.35472/jsat.v4i2.279

Rejeki, S., Hadi, J., & Suhayati, I. (2004). *Porosity Study for Detail Reservoir Characterization in Darajat Geothermal Field , West Java , Indonesia*. https://api.semanticscholar.org/CorpusID:196591232

Richter, A. (2017a). *Indonesia launches geothermal risk mitigation scheme to boost development*. Think Geoenergy. https://www.thinkgeoenergy.com/indonesia-launches-geothermal-risk-mitigation-scheme-to-boost-development/

Richter, A. (2017b). *Small-scale geothermal plant technology explored for Indonesia's remote areas*. Think Geoenergy. https://www.thinkgeoenergy.com/small-scale-geothermal-plant-technology-explored-for-indonesias-remote-areas/

Rubio-Maya, C., Ambríz Díaz, V. M., Pastor Martínez, E., & Belman-Flores, J. M. (2015). Cascade utilization of low and medium enthalpy geothermal resources − A review. *Renewable and Sustainable Energy Reviews*, *52*, 689–716. https://doi.org/https://doi.org/10.1016/j.rser.2015.07.162

Saptadji, N. M. (2001). *Teknik panasbumi*. ITB University Press.

Sapto, C., & Salvius, P. (2001). *Evaluasi Potensi Silica Scaling Pada Pipa Produksi Lapangan Panasbumi Lahendong – Sulawesi Utara*. Yogyakarta.

Sarjiya, Putranto, L. M., Irnawan, R., & Budi, R. F. S. (2022). Assessing Potential Scenarios for Achieving New and Renewable Energy Targets in Java-Bali Power System, Indonesia. *International Journal of Energy Economics and Policy*, *12*(2), 502–515. https://doi.org/10.32479/ijeep.12852

Scott, S., Galeczka, I. M., Gunnarsson, I., Arnórsson, S., & Stefánsson, A. (2024). Silica polymerization and nanocolloid nucleation and growth kinetics in aqueous solutions. *Geochimica et Cosmochimica Acta*, *371*, 78–94. https://doi.org/https://doi.org/10.1016/j.gca.2024.02.017

Setiawan, F. A., Rahayuningsih, E., Petrus, H. T. B. M., Nurpratama, M. I., & Perdana, I. (2019). Kinetics of Silica Precipitation in Geothermal Brine With Seeds Addition: Minimizing Silica Scaling in a Cold Re-Injection System. *Geothermal Energy*, *7*(1). https://doi.org/10.1186/s40517-019-0138-3

Setijadji, L. D. (2010). Segmented Volcanic Arc and its Association with Geothermal Fields in Java Island, Indonesia. In *Proceedings World Geothermal Congress* (pp. 25–29).

Shayan, M. E., Najafi, G., & Nazari, A. (2021). *The Biomass Supply Chain Network Auto-Regressive Moving Average Algorithm* (Vol. 5, Issue 1).

Sieh, K., & Natawidjaja, D. (2000). Neotectonics of the Sumatran fault, Indonesia. *Journal of Geophysical Research: Solid Earth*, *105*(B12), 28295–28326. https://doi.org/10.1029/2000jb900120

Sobhi, I., Dobbi, A., & Hachana, O. (2022). Prediction and analysis of penetration rate in drilling operation using deterministic and metaheuristic optimization methods. *Journal of Petroleum Exploration and Production Technology*, *12*(5), 1341–1352. https://doi.org/10.1007/s13202-021-01394-w

Soeria-Atmadja, R., Maury, R. C., Bellon, H., Pringgoprawiro, H., Polve, M., & Priadi, B. (1994). Tertiary magmatic belts in Java. *Journal of Southeast Asian Earth Sciences*, *9*(1–2), 13–27. https://doi.org/10.1016/0743-9547(94)90062-0

Sofyan, A. (2023a). Determination of Scaling Zone and Scaling Type in Slotted Liner Based on the Fluid Flow Pattern in the Geothermal Well "X." In *INTERNATIONAL JOURNAL of RENEWABLE ENERGY RESEARCH A. Sofyan et al* (Vol. 13, Issue 1).

Sofyan, A. (2023b). Determination of Scaling Zone and Scaling Type in Slotted Liner Based on the Fluid Flow Pattern in the Geothermal Well "X." *International Journal of*

Renewable Energy Research, *13*(1), 276–286. https://doi.org/10.20508/ijrer.v13i1.13603.g8681

Sofyan, A., Aka, H. S., Rizaldy, A. M., & Suranta, B. Y. (2021). Development of Indonesian Wellhead Generating Unit (Small Scale) Based on Legal and Regulation of PT. Geo Dipa Dieng: A Case Study. *Proceedings of the 2nd Borobudur International Symposium on Science and Technology (BIS-STE 2020)*. https://doi.org/10.2991/aer.k.210810.013

Sofyan, A., Dwi, Y., Bujang, G., & Dewi, D. C. (2023). Analysis of The Z Well Production Test Using The Horizontal LIP Pressure Method at PT. Pertamina Geothermal Energy Ulubelu Area. *Indonesian Journal of Energy and Mineral*, *3*(1), 40–55.

Sofyan, A., Janos, S., & Sumantri, H. A. (2024). Investigation of Zone and Type of Scaling Based on the Fluid Flow Pattern in the Geothermal Well "X" at the Salak Geothermal Field - Indonesia. *INTERNATIONAL JOURNAL OF RENEWABLE ENERGY RESEARCH*, *14*(1).

Sofyan, A., Jaya, R., Susanto, H., Njeru, R. M., Bozsó, G., & Szanyi, J. (2025). Scale Treatment Planning Using Broaching Method in a Vapor-Dominated Geothermal Well X at Kamojang Geothermal Field. *Eng*, *6*(67), 1–29. https://doi.org/10.3390/eng6040067

Sojková, T., Gröger, R., Poloprudský, J., Kuběna, I., Schneeweiss, O., Sojka, M., Šiška, Z., Pongrácz, J., & Pizúrová, N. (2024). Kinetics of spontaneous phase transitions from wüstite to magnetite in superparamagnetic core-shell nanocubes of iron oxides. *Nanoscale*. https://doi.org/10.1039/d3nr06254f

Solenis. (2021). *Cutting-Edge Scale Control Solutions For Geothermal Power Producers (EMEA And APAC)*. Solenis.Com. https://www.solenis.com/en/resources/events/webinars/cutting-edge-scale-control-solutions-for-geothermal-power-producers-emea-apac

Suryadarma, Dwikorianto, T., Zuhro, A., & Yani, A. (2010). Sustainable development of the Kamojang geothermal field. *Geothermics*, *39*, 391–399. https://doi.org/10.1016/J.GEOTHERMICS.2010.09.006

Tassew, M. (2001). *Effect of solid deposition on geothermal utilization and methods of control*. *13*, 1–20.

Thome, J. R. (2016). *Engineering Data Book III : Enhanced heat transfer design methods for tubular heat exchangers*.

Thome, J. R., & Cioncolini, A. (2015). *Two-Phase Flow Pattern Maps for Microchannels* (Issue October). https://doi.org/10.1142/9789814623216_0020

Tjahjono, Yudha, S. W., & Longhurst. (2022). Unearthing the Dynamics of Indonesia's Geothermal Energy Development. *Energies*, *15*, 5009.

Tolivia, E. (1972). Flow in geothermal wells (An analytical study). *Geothermics*, *1*(4), 141–145. https://doi.org/10.1016/0375-6505(72)90023-5

Tranter, M., Lucia, M. D., & Kühn, M. (2021). Barite Scaling Potential Modelled for Fractured-Porous Geothermal Reservoirs. *Minerals*, *11*(11), 1198. https://doi.org/10.3390/min11111198

Utami, A. R., Widiati, E., Program, M. S., Digital, T., Lokal, P., & Digital, T. (2025). Efektivitas Digital Branding Melalui Platform E-Commerce Dalam Meningkatkan Penjualan Produk Lokal. *Ekonomika*, *8*(2), 294–303.

Utami, P. (2000). *CHARACTERISTICS OF THE KAMOJANG GEOTHERMAL RESERVOIR (WEST JAVA) AS REVEALED BY ITS HYDROTHERMAL ALTERATION MINERALOGY*. http://web01.opencloud.dssdi.ugm.ac.id/wp-content/uploads/sites/395/2012/12/Characteristics-of-the-Kamojang-Geothermal-

Reservoir-2000-Pri-Utami.pdf

Vazquez, O., Mackay, E., & Beteta, A. (2024). Scale Treatment Optimisation in Geothermal Reservoirs. *Day 2 Thu, June 06, 2024*. https://doi.org/10.2118/218724-ms

Wang, Y., Li, B., & Chen, A. (2024). The Geochemical Characteristics and Genesis Mechanisms of the Zaozigou Geothermal Field. *Sustainability (Switzerland)*, *16*(16). https://doi.org/10.3390/su16166790

Wanner, C., Eichinger, F., Jahrfeld, T., & Diamond, L. W. (2017). Causes of abundant calcite scaling in geothermal wells in the Bavarian Molasse Basin, Southern Germany. *Geothermics*, *70*(November 2016), 324–338. https://doi.org/10.1016/j.geothermics.2017.05.001

Wein, F., Dunning, P., & Norato, J. (2019). A review on feature-mapping methods for structural optimization. *Structural and Multidisciplinary Optimization*, *62*, 1597–1638. https://doi.org/10.1007/s00158-020-02649-6

Widodo, E., Akbar, A., & Timur, J. (2015). *Pengaruh Konsentrasi Garam Terhadap Karakterisitik Aliran Dua Fase Gas Dan Air* (Issue 1). Universitas Muhammadiyah Sidoarjo.

Wilson, D. R., Gilliland, J., & Austin, A. (2015). Broaching: An effective method of well intervention for calcite scale removal. *Transactions - Geothermal Resources Council*, *39*, 217–221. https://www.scopus.com/inward/record.uri?eid=2-s2.0-84962840826&partnerID=40&md5=1783744d5541c198bc515c281f9e5eda

Y. D. Tavip, & Kamah, A. Z. A. (2023). Penanggulangan problem geologi dalam operasi pemboran sumur di blok timur area geothermal kamojang jawa barat Indonesia. *Proceedings of 6th Indonesian Geothermal Association*, 175–184.

Yenice, H., & Dünya, H. (2007). Mechanical Cleaning of Calcite Scaling with Rotating Control Head Preventer in a Geothermal Well. *Energy Exploration & Exploitation*, *25*, 451–465. https://doi.org/10.1260/014459807783791827

Yin, Y., Jeong, N.-S., Minjarez, R., Robbins, C., Carlson, K., & Tong, T. (2021). Contrasting Behaviors between Gypsum and Silica Scaling in the Presence of Antiscalants during Membrane Distillation. *Environmental Science & Technology*. https://doi.org/10.1021/acs.est.0c07190

Yudha, D., Sarulla, S., Limited, O., Aprilina, N. V., Satya, D. Y., Rejeki, S., Golla, G., & Waite, M. (2015). Geologic Modeling Workflow for Volcanic Hosted Geothermal Reservoirs: Case Study from Salak Geothermal Field 3D Earth Modeling View project Salak 3D Static Modeling View project Geologic Modeling Workflow for Volcanic Hosted Geothermal Reservoirs: Case St. *Proceedings World Geothermal Congress*, *June 2016*, 19–25. https://www.researchgate.net/publication/304471645

Yudha, S. W., Tjahjono, B., & Longhurst, P. (2022). Unearthing the Dynamics of Indonesia's Geothermal Energy Development. *Energies*, *15*(14). https://doi.org/10.3390/en15145009

Yudiantoro, D. F., Suparka, E., Yuwono, S., Takashima, I., Ishiyama, D., Kamah, Y., & Hutabarat, J. (2013). Interstratified Illite/Montmorillonite in Kamojang Geothermal Field, Indonesia. *Indonesian Journal on Geoscience*, *8*(4), 177–183. https://doi.org/10.17014/ijog.8.4.177-183

Zarrouk, S. J., & Moon, H. (2014). Efficiency of geothermal power plants: A worldwide review. *Geothermics*, *51*, 142–153. https://doi.org/https://doi.org/10.1016/j.geothermics.2013.11.001

Zarrouk, S., Woodhurst, B., & Morris, C. (2014). Silica scaling in geothermal heat exchangers and its impact on pressure drop and performance: Wairakei binary plant, New Zealand.

Geothermics, *51*, 445–459. https://doi.org/10.1016/J.GEOTHERMICS.2014.03.005

Zolfagharroshan, M., & Khamehchi, E. (2020). A rigorous approach to scale formation and deposition modelling in geothermal wellbores. *Geothermics*, *87*(March), 101841. https://doi.org/10.1016/j.geothermics.2020.101841